NOTE TO USERS

The CD is not included in this original manuscript.

This reproduction is the best copy available.

UMI®

University of Alberta

Impact of Climate Change on the Winter Regime of the Peace River

by

Robyn Andrishak 

A thesis submitted to the Faculty of Graduate Studies and Research in partial fulfillment of the requirements for the degree of Master of Science

in

Water Resources Engineering

Department of Civil and Environmental Engineering

Edmonton, Alberta

Spring 2006

Your file Votre référence
ISBN: 978-0-494-13782-6
Our file Notre référence
ISBN: 978-0-494-13782-6

ABSTRACT

The impact of climate change on our environment is not widely understood. Since models indicate above-average warming for northern regions of Canada in the winter months compared to other places in the world, it is important to understand how climate change affects river ice. In places such as the Town of Peace River and Fort McMurray, Alberta, ice-related flooding accounts for some of the highest and most unpredictable flood risk. To better understand this issue, a thermal river ice model has been developed and applied to the Peace River. The results indicate that climate warming over the next half-century could substantially delay freezeup, and to a lesser extent advance breakup. Under the climate change scenario investigated, the initiation of the ice cover was delayed by 30 to 40 days and freezeup at the Town of Peace River was projected to be 40 to 50 days later than the historical norm.

ACKNOWLEDGEMENTS

Funding for this study was provided by the Climate Change Research User's Group (CCRUG) at Alberta Environment as well as the Natural Sciences and Engineering Research Council of Canada (NSERC) through the MAGS (Mackenzie GEWEX Study) Research Network. This support is gratefully acknowledged. I would also like to thank Kim Westcott and Chandra Mahabir of Alberta Environment for their support of this project. Their interest and assistance in this research is truly appreciated.

Thanks are also extended to: Martin Jasek of BC Hydro for supplying historical data; BC Hydro, Glacier Power, and Alberta Environment for their joint monitoring program on the Peace River, which provided the detailed data for 2002/03 and 2003/04; and the MAGS research group for supplying the Coupled Global Climate Model (CGCM2) results used in the climate change analysis. Also appreciated was the help of Gordon Fonstad of Alberta Environment who helped to pull together most of the Peace River from the various sources.

For both selecting this research topic to match my talents and interests and giving me the freedom to explore this subject area independently with my own vision, I am sincerely grateful to my supervisor, Dr. Faye Hicks. Thanks also to Dr. Peter Steffler and Dr. Paul Myers for agreeing to be on the examining committee for my defence. I would also like to acknowledge the software support and user interface development provided by Zhao Yang during the course of this project. Last but not least, thank you to my wife, Lora. Without her support (and tolerance) over the past two-and-a-half years, this work would have been impossible for me to complete.

TABLE OF CONTENTS

LIST OF TABLES

LIST OF FIGURES

LIST OF SYMBOLS

A	Liquid water flow area *(m^2)*
A_f	Suspended frazil ice flow area *(m^2)*
A_i	Solid ice flow area *(m^2)*
A_i'	Flow area of frazil slush and pore water at the surface *(m^2)*
$A'_{i_{new}}$	Cross sectional area of new pans *(m^2)*
B	Top width of channel *(m)*
B_i	Surface ice width or coverage *(m)*
C_f	Suspended frazil ice concentration *(dimensionless)*
C_i	Surface ice concentration *(%)*
C_p	Specific heat of water *(J/kg/°C)*
e_f	Porosity of frazil slush *(dimensionless)*
F	Mass or energy flux *(units vary)*
f_i, f_j	Finite element interpolation functions (linear)
H	Depth of water from bed to free surface *(m)*
h_{wa}	Linear heat transfer coefficient *($W/m^2/°C$)*
K_i	Thermal conductivity of ice *(W/m/°C)*
k_{wa}	Linear heat transfer constant *(W/m^2)*
L_i	Latent heat of ice *(J/kg)*
P_{jux}	Juxtaposition parameter *(dimensionless)*
t	Time *(s)*
T_a	Air temperature *(°C)*
t_f	Thickness of frazil ice layer at the surface *(m)*
t_f'	Initial frazil floe or pan thickness *(m)*

T_i Solid surface ice layer temperature *(°C)*

t_i Thickness of solid ice layer at the surface *(m)*

T_w Water temperature *(°C)*

U Mean water velocity *(m/s)*

U_i Surface ice velocity *(m/s)*

x Longitudinal coordinate along channel centreline *(m)*

X_i Location of ice front *(m)*

α_{iw} Coefficient for turbulent heat exchange between ice and water *($W \cdot s^{0.8}/m^{2.6}/°C$)*

Δt Solution time step *(s)*

Δx Variable element length defined by the input geometry *(m)*

η Frazil rise parameter *(m/s)*

θ numerical implicitness *(dimensionless)*

ρ Density of water *(kg/m^3)*

ρ' Combined density of frazil slush and pore water *(kg/m^3)*

ρ_i Density of ice *(kg/m^3)*

Φ Solution variable of interest *(units vary)*

ϕ_{ia} Net rate of heat exchange per unit area between ice and air *(W/m^2)*

ϕ_{iw} Net rate of heat exchange per unit area between ice and water *(W/m^2)*

ϕ_{wa} Net rate of heat exchange per unit area between water and air *(W/m^2)*

ω Upwinding coefficient *(dimensionless)*

CHAPTER 1 INTRODUCTION

1.1. BACKGROUND INFORMATION

The hydrology of Canada is intertwined with the winter streamflow behaviour of its rivers. Economic development, particularly in Alberta, has put increased pressure on water availability and quality. This demand has strengthened the need to accurately quantify river flows throughout the entire year. The formation of ice on a river can have a significant impact on both flows and water levels and can also make direct measurements of these difficult or impossible. As a result, deterministic hydraulic models that include river ice formation and deterioration processes are required if we are to assess the effects of hydropower operations, downstream water use, and climate change, for example, on water availability during the winter months. It is also important to note that the winter ice cover on most northern rivers plays an important role in ecosystems and water quality (Prowse and Culp, 2003), which further reinforces the need for such models.

Climate change is a complex issue that continues to attract a great deal of attention. Climate model predictions, such as the Coupled Global Climate Model (CGCM2) used in this study, indicate significant warming across Canada, particularly in its northern regions (Intergovernmental Panel on Climate Change (IPCC), 2005). Increased air temperatures will certainly have an impact on river ice regimes, but to what degree and significance is the question that requires investigation. Beltaos and Prowse (2001) suggest that climate warming has the potential to affect the frequency and/or severity of ice jam events. However, another important possible effect of

climate warming on northern life could be the reduced duration of winter river crossings (ice bridges) affecting transportation and animal migration. Since ice bridges are in many cases a significant component of Canada's northern transportation network (Gerard *et al.*, 1992; Kuryk and Domaratzki, 1999), attempting to quantify the effects of climate change on this aspect of a river's ice regime is well worthwhile.

The development of the *River1D* thermal model makes it possible to analyse the response of the river ice regime to climate change.

1.2. STUDY AREA

The study area chosen for this research is the Peace River in northern British Columbia and Alberta. Figure 1.1 provides an overview of the study reach, which covers a total distance of approximately 800 kilometres from Hudson Hope, British Columbia, to Fort Vermilion, Alberta. Some key sites along the 800 km river reach are indicated in Table 1.1. Meteorological stations at Fort St. John, the Town of Peace River, and High Level are also indicated on Figure 1.1. Air temperature data from these three sites was used as input to the river ice model.

The Peace River is a useful subject for the study of the effects of climate change on river ice for a number of reasons. First, it is one of a few sites where an adequate historical database is available from which to assemble the input data required to model thermal river ice processes. More importantly, the present ice regime of the Peace River requires a considerable amount of monitoring by Alberta

Environment to protect, in particular, the Town of Peace River from ice-related flooding. In addition, transportation across the river in places without bridge infrastructure is heavily impacted by the presence of ice on the river. Understanding how climate change could affect the Peace River's ferry and ice bridge operations is an important aspect of this study. The Peace River also falls within one of the global zones that climate change models are predicting significant warming over the next several decades. The above-average winter air temperature warming in the study area means that climate change effects may potentially be more pronounced and therefore important to understand.

1.3. PREVIOUS STUDIES OF THE PEACE RIVER THERMAL ICE REGIME

The earliest efforts to model thermal river ice processes numerically began in the late 1980s and early 1990s. A comprehensive mathematical river ice model, originally named *RICE*, was developed by Lal and Shen (1989) at Clarkson University. That model has undergone continual development over the years, and there is now a version of it specifically adapted to the Peace River, called *PRICE*. The limitation with the *RICE/PRICE* models is the fact that they are proprietary in nature; while reports and papers exist that provide some basic details of the physics employed in the models, only the developers know the specific formulations and solution routines.

Andres (1993) investigated ice formation on the Peace River. In this Alberta Research Council study, he developed and calibrated an ice production algorithm

specifically for the Peace River using an approach that does not explicitly consider ice formation as a two-layer process (i.e. suspended frazil and surface ice), which is drastically different from the *RICE* and *PRICE* models. Each of the physical equations he presents are ordinary differential equations (in the longitudinal coordinate) designed to be solved analytically. The equations developed for the *RICE* and *PRICE* models as well as for the present model are all partial differential equations in the longitudinal coordinate and time. In addition, Andres' (1993) model concentrates on freezeup processes alone; it does not provide for spring melt and ice cover recession, as that was beyond the scope of his study.

1.4. AVAILABLE DATA

Alberta Environment, BC Hydro, and their collaborators have been collecting winter data on the Peace River for more than three decades. The most recent ice seasons, 2002/03 and 2003/04, have the most comprehensive and complete data sets to-date, including water temperatures, surface ice concentrations, and some solar radiation data. There are currently plans to expand the number of sites at which this data is being collected to aid future modeling efforts.

The basic data required to run a thermal river ice simulation consists of air temperatures over the river reach of interest, inflow water temperature, and inflow discharge. There is a lengthy air temperature record at three communities along the river: Fort St. John; the Town of Peace River; and High Level (see Figure 1.1). These three stations can be used to characterise air temperatures along the Peace River. BC Hydro has been recording their discharge rates from the Peace Canyon Dam since it

was installed on the river over twenty years ago; this record provides all of the required inflow discharge data. Water temperature releases from the Peace Canyon dam have also been monitored by BC Hydro quite extensively; however, there are some significant gaps in the record due to instrument placement and malfunction.

1.5. RESEARCH OBJECTIVES

The primary objectives of this research were to develop a public domain, thermal river ice process model that could be used as an analytical tool to assess the potential impacts of climate change on the winter regime of large northern rivers and to demonstrate the model's capabilities by using it to assess the potential effects of climate change on the Peace River. Exhaustive calibration of the model and decisive future climate predictions for the Peace River are beyond the scope of this work, due to the practical limitations in the available data. However, it is hoped that this work will clearly demonstrate the significance of climate warming on the duration and extent of ice cover on the Peace River.

Chapter 2 presents the details of the thermal river ice model developed for this study. In this chapter the physics of river ice formation, the equations developed, and the solution methods implemented within the numerical model are discussed. The available data for model input, calibration, and validation are summarised in Chapter 3. Included in this chapter is some discussion of the data collection challenges and limitations related to river ice modeling and monitoring. Application of the present model to the Peace River using the historical record is covered in Chapter 4. The effects of a standard climate change scenario on the possible future ice regime of the

Peace River are examined in Chapter 5. The final objective of this study was to formulate some conclusions as to the magnitude of the effects of climate change on the ice regime of the Peace River and make some recommendations for future work and improved data collection. These issues are covered in Chapter 6.

Table 1.1 Location of key sites along the Peace River.

Location	Distance from Bennett Dam (km)
Peace Canyon Dam	23
Peace River at Hudson Hope	28
Halfway River confluence	65
Moberly River confluence	103
Peace River at Fort St. John	110
Pine River confluence	120
Peace River at Taylor	121
Beaton River confluence	141
Kiskatinaw River confluence	154
Alces River confluence	164
British Columbia – Alberta border	166
Clear River confluence	186
Peace River at Dunvegan Bridge	296
Shaftesbury ferry / ice bridge	371
Smoky River confluence	388
Heart River confluence	394
Peace River at Peace River	395
Notikewin River confluence	558
Peace River near Carcajou	650
Peace River at Fort Vermilion	829

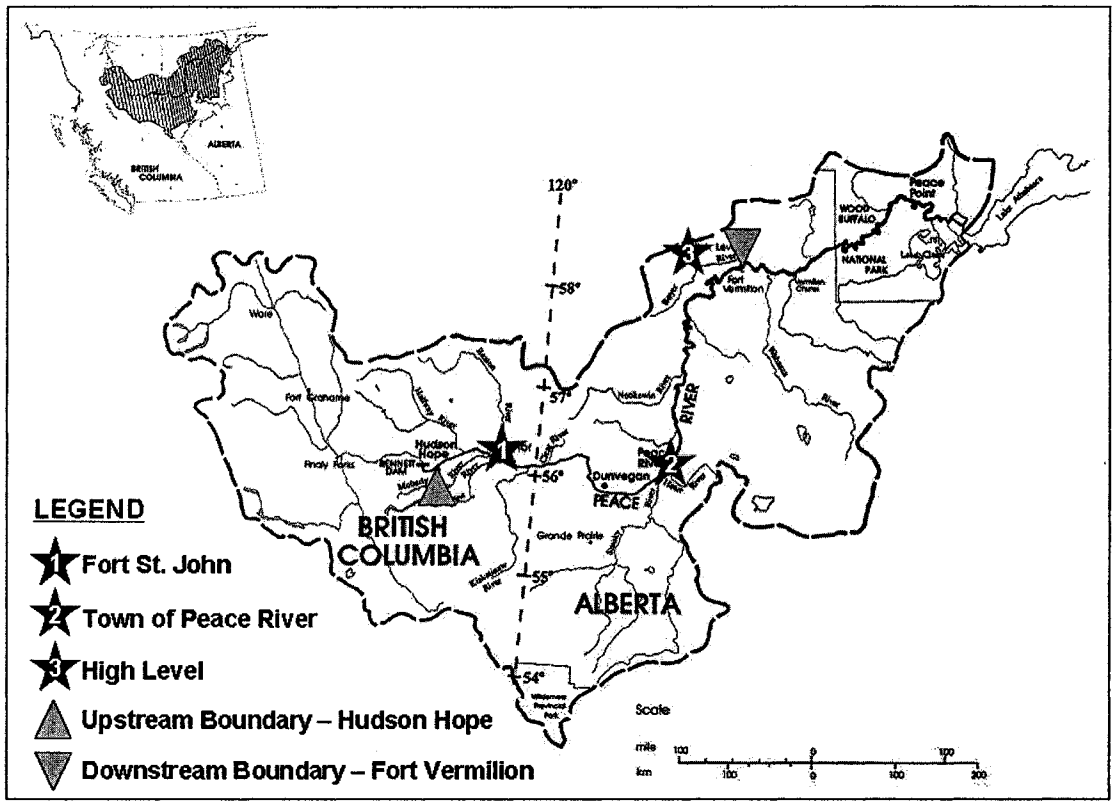

Figure 1.1 **Location map of the Peace River study reach (adapted from Hicks, 1996).**

CHAPTER 2 THERMO-HYDRAULIC RIVER ICE PROCESS MODEL DEVELOPMENT

2.1. INTRODUCTION

2.1.1. Physical Description of Thermal River Ice Processes

Northern rivers go through a process of freezeup and breakup each winter. Throughout the winter season, a typical river ice cover will change and evolve continuously as a wide range of thermal and dynamic river ice processes occur. In addition, the physical properties of the ice cover, such as thickness, roughness, and strength can vary considerably with time and location. These factors make river ice an extremely interesting and challenging modeling subject.

The development of an ice cover on northern rivers begins with the cooling of its waters and the loss of its heat to the atmosphere. This is the beginning of what is termed the freezeup process, shown conceptually in Figure 2.1. The main source of heat loss for a river is convective heat loss from the water surface to colder overlying air. River water temperatures will eventually drop to zero degrees Celsius (0°C), under cold atmospheric conditions. However, before ice can begin to form in the river, supercooling (cooling of the water temperature to at least a few hundredths of a degree below 0°C) must take place (Ashton, 1986).

Near the river banks, where water velocities are much slower than the mean channel flow, supercooling of the river water results in the formation of a thin layer of

skim ice at the water surface. Once in place, it will continue to grow thermally in the vertical direction under cold air conditions. This type of ice cover is termed "border ice". Under supercooled conditions away from the river banks, frazil ice particles, small discs of ice one to three millimetres in diameter, will begin to form. These particles readily adhere and freeze to each other, causing them to agglomerate into clusters of frazil slush or "frazil flocs". Frazil particles can also adhere to large rocks or boulders on the river bed, resulting in an ice formation called "anchor ice".

Frazil flocs eventually reach a size at which buoyant forces overcome the flow turbulence's tendency to keep them in suspension, and they float to the surface. At the surface, the un-submerged portion freezes into the familiar "pancake ice" or frazil pans shown in Figure 2.2. Frazil pans float downstream on the water surface and, as their surface concentration increases, both in time and in the downstream direction, individual pans may freeze together to form "rafts" (Figure 2.3).

When the surface concentration of ice pans and rafts approaches values on the order of 80 to 90%, "bridging" may occur. This is essentially a congestion of ice floes that causes their arrest at a specific site along a river, which may look similar to what is shown in Figure 2.4. The location where bridging takes place is typically a characteristic of the river itself. In other words, bridging tends to occur at the same general location on a given river from year-to-year, often corresponding to, for example, natural or artificial constrictions in river width, tight river bends, bridge crossings, and islands.

Once the initial arrest of the ice cover is complete, incoming ice floes from upstream "juxtapose" or accumulate edge to edge on the water surface at the upstream edge of the ice front (the location along the river that represents the division between stationary ice downstream and moving ice and open water upstream). The resulting, relatively smooth type of ice cover is shown in Figure 2.5. Any water between the frazil pans will freeze, adding strength to the accumulation. Subsequent ice formation first freezes the water in the pores of the slush on the underside of the pans, followed by thermal ice growth, which results in ice cover thickening over the winter. This process can be mitigated by the insulative effects of snow on the ice cover. However, ice cover growth can also be supplemented by the formation of snow ice. Snow ice forms when the river water level rises above the top of the ice cover, flooding it and the snow cover with water that eventually re-freezes.

In the spring, as air temperatures rise, snow on top of the ice cover will melt, followed by deterioration of the ice cover itself, as shown in Figure 2.6. Solar insolation and convective heat transfer from warm overlying air are the main sources of relevant heat energy. Solar energy in particular can penetrate the ice cover, resulting in increased ice porosity and loss of strength. Areas of surface and open waters are particularly important, due to the low surface albedo of water. Water warmed in open leads contributes to ice melt by thinning of the ice cover from the underside. For thermally dominated breakups, an ice front will retreat in the downstream direction as melt progresses, as the photograph in Figure 2.7 illustrates. Eventually, as spring melt continues, the ice front will retreat to the location where bridging initiated the ice cover the previous fall.

In reality, some degree of dynamic activity is a part of every river's breakup. Dynamic breakup processes are complex mechanical phenomena that can be very difficult to predict qualitatively, let alone model quantitatively. For example, water level increases due to large spring runoff events will tend to lift an intact ice cover and create transverse cracks such as those shown in Figure 2.9 or hinge cracks (Figure 2.8) on smaller rivers. Breakup ice jams can also occur, causing water levels to rise and often result in flooding. Figure 2.10 shows a photograph of the 1979 breakup ice jam at the Town of Peace River. These dynamic breakup features are not considered in the present model since on regulated rivers, such as the Peace River, thermal breakup is the dominant process in most years.

2.1.2. Equation Formulation

Existing river ice models (e.g. Shen *et al.*, 1995; Lal and Shen, 1989) use an Eulerian-Lagrangian approach to formulate and model the processes described above. However, for this study, a purely Eulerian frame of reference was used for the development of the governing equations. Since the framework of the present model differs from that of the previous work mentioned above, the physical equations for each of the five primary model components (water temperature, suspended frazil concentration, surface ice concentration, surface frazil ice thickness, and solid surface ice thickness) had to be developed from basic control volume principles. While the Eulerian approach was thus more complex to formulate, it was selected for its straightforward, seamless integration with the *River1D* hydrodynamic model.

Both the base *River1D* hydrodynamic model and the present thermal river ice model are one-dimensional. In other words, the variations of conditions across the width and through the depth of the river are neglected. A schematic representation of the model domain is given in Figure 2.11.

Each primary thermal river ice process equation can be written in the general form:

$$\frac{\partial}{\partial t}(\Phi)+\frac{\partial}{\partial x}(U\Phi)=\Sigma F \qquad [2.1]$$

where x, t = longitudinal *(metres, m)* and temporal *(seconds, s)* coordinates

Φ = the solution variable of interest

U = the applicable mean or surface ice velocity *(m/s)*

ΣF = the sum of the applicable mass or energy fluxes per unit distance in the longitudinal direction

From this form, each equation can be expressed in terms of the finite element method as described in Section 2.4.

Rectangular cross section approximations, shown schematically in Figure 2.12, have been used to characterise the natural channel geometries. This problem simplification is necessary to describe the geometry of the Peace River over the long

reach considered since detailed cross sections are available at too few places along the Peace River to be useful in the present model.

Hicks (1996) showed that rectangular cross sections are sufficient to accurately route river flows but may not always simulate accurate water levels. For the present study, water temperature and ice front simulation results are the basis for model evaluation and climate change analysis; therefore, the precise modeling of water levels is not important. However, if future applications of this model to assess the risk of ice-related flooding are desired, further development of the model to incorporate natural cross section data would be required and water level calibrations and validations would be necessary.

2.2. WATER TEMPERATURE

As mentioned in Section 2.1.1, the preliminary component to river ice formation is water cooling. Accurate water temperature modeling is critical to reliable simulation of all other ice conditions. The heat balance formulation used in the present model has been adapted from Lal and Shen (1989).

The amount of heat energy in the water per metre of river (longitudinally) is equal to $\rho A C_p T_w$, where:

ρ = density of water *(kilograms per cubic metre, kg/m^3)*

A = liquid water flow area *(square metres, m^2)*

C_p = specific heat of water *(Joules per kilogram per degree Celsius, J/kg/°C)*

T_w = water temperature *(degrees Celsius, °C)*

Accordingly, the units multiply out to Joules per metre, *J/m*. To formulate a conservation equation for the heat contained in the river water, one can consider a river cross section with some percentage of surface ice coverage, represented schematically by a continuous segment of ice cover from one side of the channel, as shown in Figure 2.13. In reality this ice is composed of many individual pans and rafts across the river width, but represents the same total mass, cross sectional area, and surface coverage of ice. In the figure, arrows point in the direction of heat transport and:

B = river cross section width *(metres, m)*

B_i = ice covered width of cross section *(m)*

ϕ_{wa} = net rate of heat exchange per unit area between water and air *(Watts per square metre, W/m^2)*

ϕ_{ia} = net rate of heat exchange per unit area between ice and air *(W/m^2)*

ϕ_{iw} = net rate of heat exchange per unit area between ice and water *(W/m^2)*

Three distinct heat fluxes that can affect water temperature are considered for this case: (1) heat exchange with the atmosphere over open water; (2) heat loss to the atmosphere through the ice cover; and (3) heat exchange between warm water and the

ice cover resulting in ice melt. The latter two fluxes are unidirectional, meaning that they can only result in water cooling. This is because warm air over an ice cover will be directed towards ice cover melt before water warming and an ice cover is never warmer than the water beneath it.

The rate of heat exchange between water and air, ϕ_{wa}, can be expressed in a linear form, such as that also used by Lal and Shen (1989):

$$\phi_{wa} = h_{wa}(T_w - T_a) + k_{wa} - \phi_R \qquad [2.2]$$

where h_{wa} = linear heat transfer coefficient *(Watts per square metre per degree Celsius, $W/m^2/°C$)*

T_w = water temperature *(°C)*

T_a = air temperature *(°C)*

k_{wa} = linear heat transfer constant *(W/m^2)*

ϕ_R = net shortwave solar radiation reaching the water surface *(W/m^2)*

Using this result, the rate of heat flux over the open water surface per metre of river (longitudinally) equals $(B - B_i)\phi_{wa}$. The same can be done for water cooling through the ice cover, $B_i\phi_{ia}$, and water cooling due to ice cover melt, $B_i\phi_{iw}$. The models used to calculate ϕ_{ia} and ϕ_{iw} will be explained in Section 2.3.3.

Applying control volume principles, the following partial differential equation can be derived for heat conservation along the length of the river:

$$\frac{\partial}{\partial t}\left(\rho A C_p T_w\right)+\frac{\partial}{\partial x}\left(U\rho A C_p T_w\right)=-\left(B-B_i\right)\phi_{wa}-\underbrace{B_i\phi_{ia}}_{\phi_{ia}>0}-\underbrace{B_i\phi_{iw}}_{\phi_{iw}>0} \qquad [2.3]$$

Note the restrictions on the second and third flux terms, indicating that they are applicable only under water cooling conditions. The density of water is assumed constant and is moved to the right hand side of the equation, resulting in the following:

$$\frac{\partial}{\partial t}\left(A C_p T_w\right)+\frac{\partial}{\partial x}\left(U A C_p T_w\right)=-\frac{\left(B-B_i\right)\phi_{wa}}{\rho}-\underbrace{\frac{B_i\phi_{ia}}{\rho}}_{\phi_{ia}>0}-\underbrace{\frac{B_i\phi_{iw}}{\rho}}_{\phi_{iw}>0} \qquad [2.4]$$

where

A = liquid water flow area *(m^2)*

C_p = specific heat of water *(J/kg/°C)*

T_w = water temperature *(°C)*

U = mean water velocity *(m/s)*

B = top width of channel *(m)*

B_i = surface ice width *(m)*

ϕ_{wa} = net rate of heat exchange per unit area between water and air *(W/m^2)*

ρ = density of water *(kg/m^3)*

ϕ_{ia} = net rate of heat exchange per unit area between ice and air *(W/m^2)*

ϕ_{iw} = net rate of heat exchange per unit area between ice and water (W/m^2)

Longitudinal dispersion of water temperature is neglected in this model formulation, as in the *RICE* model developed by Lal and Shen (1989).

With a solution for AC_pT_w, the hydraulic solution of total water mass and momentum conservation can be used to extract the water temperature from this compound solution variable. In addition, the specific heat of water also varies with water temperature. A quadratic relationship for C_p over a temperature range of 0 to 20°C was derived from accepted values (Chemical Rubber Company, 2004). The resulting equation, shown below, has a coefficient of determination, r^2, equal to 1:

$$C_p = 0.076 \cdot T_w^2 - 3.31 \cdot T_w + 4217.6 \ (J/kg/°C) \qquad [2.5]$$

Known values for A and AC_pT_w leave a cubic equation in T_w to be solved (Equation [2.6]). This equation can be rearranged to the form of Equation [2.7], which can then be solved mathematically.

$$AC_pT_w = A \cdot \left(0.076 \cdot T_w^2 - 3.31 \cdot T_w + 4217.6\right) \cdot T_w \qquad [2.6]$$

$$T_w^3 - \frac{3.31}{0.076} \cdot T_w^2 + \frac{4217.6}{0.076} \cdot T_w - \frac{AC_pT_w}{0.076 \cdot A} = 0 \qquad [2.7]$$

The general form of this equation is:

$$T_w^3 + a_1 \cdot T_w^2 + a_2 \cdot T_w + a_3 = 0 \qquad [2.8]$$

The mathematical solution to this type of equation is described by Press *et al.* (1988) and is based on the three constants: a_1, a_2, and a_3.

First, two new parameters are calculated:

$$Q \equiv \frac{a_1^2 - 3a_2}{9} \qquad [2.9]$$

$$R \equiv \frac{2a_1^3 - 9a_1a_2 + 27a_3}{54} \qquad [2.10]$$

If $Q^3 - R^2 \geq 0$, the equation has three real roots. In this particular case, $Q^3 - R^2$ will always be less than zero for valid values of A and AC_pT_w, and the equation has one real root, given by:

$$T_w = -\mathrm{sgn}(R)\left[\left(\sqrt{R^2 - Q^3} + |R|\right)^{1/3} + \frac{Q}{\left(\sqrt{R^2 - Q^3} + |R|\right)^{1/3}}\right] - \frac{a_1}{3} \qquad [2.11]$$

$$\mathrm{sgn}(R) = \begin{cases} 1, \text{ for } R > 0 \\ 0, \text{ for } R = 0 \\ -1, \text{ for } R < 0 \end{cases} \qquad [2.12]$$

Subsequent ice calculations are dependent on the water temperature reaching 0°C. Numerically, the water temperature solution does not generally reach 0°C or will oscillate slightly around 0°C. To counteract this effect, the model has a threshold water temperature of 0.1°C. Once the water temperature solution at any given location cools to this level, it is assigned a value of 0°C.

2.3. CONSERVATION OF WATER AND ICE MASS

2.3.1. Suspended Frazil

Continued cooling of water below 0°C (i.e. supercooling) leads to the formation of frazil ice suspended in the turbulent river water. As discussed earlier, frazil production actually commences at a few one hundredths of a degree below 0°C (Ashton, 1986). However, for practical purposes this can be taken as 0°C in the model. Two processes can be described that influence the concentration of frazil suspended in the flow: (1) frazil formation due to heat loss (increasing suspended

frazil concentration); and (2) frazil rise due to buoyancy effects (decreasing suspended frazil concentration). In each case, a mass transfer rate can be formulated. Figure 2.14 illustrates the scenario of suspended frazil processes conceptually.

First, only heat loss over open water is considered to lead to suspended frazil formation. The rate of ice formation can thus be tied to the rate of heat loss through the latent heat of ice formation, L_i, and the relative density between ice and water:

$$\frac{\rho}{\rho_i}\frac{(B-B_i)\phi_{wa}}{L_i} \qquad [2.13]$$

The mass conservation equation describing suspended frazil area (within the flow cross section) is then:

$$\frac{\partial A_f}{\partial t}+\frac{\partial UA_f}{\partial x}=\frac{1}{\rho_i}\left[\underbrace{\frac{\rho}{\rho_i}\frac{(B-B_i)\phi_{wa}}{L_i}}_{\substack{\text{frazil formation if}\\ T_w=0}}-\underbrace{\rho_i\eta C_f B}_{\substack{\text{frazil rise if}\\ C_f\geq 0}}\right] \qquad [2.14]$$

where A_f = suspended frazil ice flow area *(m^2)*

U = mean water velocity *(m/s)*

ρ_i = density of ice *(kg/m^3)*

B = top width of channel *(m)*

B_i = surface ice width or coverage *(m)*

ϕ_{wa} = net rate of heat loss per unit area from water to air *(W/m²)*

L_i = latent heat of ice *(J/kg)*

η = frazil rise parameter *(m/s)*

C_f = Suspended frazil ice concentration *(dimensionless)*

Suspended frazil concentration can then be extracted from this area by comparing its magnitude relative to the active flow area:

$$C_f = \frac{A_f}{BH - B_i \frac{\rho_i}{\rho}\{t_i + (1-e_f)t_f\}} \qquad [2.15]$$

where A_f = suspended frazil ice flow area *(m²)*

B = top width of channel *(m)*

H = depth of water from bed to free surface *(m)*

B_i = surface ice width or coverage *(m)*

ρ_i = density of ice *(kg/m³)*

ρ = density of water *(kg/m³)*

t_f = thickness of frazil ice layer at the surface *(m)*

t_i = thickness of solid ice layer at the surface *(m)*

e_f = porosity of frazil slush *(dimensionless)*

2.3.2. Surface Ice Coverage

Once some frazil concentration is present in the flow, surface ice, or pans, will begin to form at the surface and grow in thickness. New pans can be considered to

form over the open water area as shown in Figure 2.15., and an initial frazil pan thickness must be specified to control the rate of change of surface ice coverage. The supply of frazil ice and pore water into this area is dependent solely on slush rising to the surface. Slush deposition at the surface entraps water within its pores; this liquid water mass is removed from the active flow area in proportion to the porosity of newly formed pans. The rate of mass flux forming new pans is:

$$\underbrace{\left(\rho_i + \rho\frac{e_f}{(1-e_f)}\right)\eta C_f (B - B_i)}_{\substack{\text{frazil and pore water deposition if} \\ C_f \geq 0}} \qquad [2.16]$$

Thus, in terms of the cross sectional area of new pans, we have:

$$\frac{\partial A'_{i_{new}}}{\partial t} + \frac{\partial U_i A'_{i_{new}}}{\partial x} = \frac{1}{\rho'}\left[\underbrace{\left(\rho_i + \rho\frac{e_f}{(1-e_f)}\right)\eta C_f (B - B_i)}_{\substack{\text{frazil and pore water deposition if} \\ C_f \geq 0}}\right] \qquad [2.17]$$

where $A'_{i_{new}}$ = cross sectional area of new pans *(m^2)*

U_i = surface ice velocity *(m/s)*

ρ' = combined density of frazil slush and pore water *(kg/m^3)*

ρ_i = density of ice *(kg/m^3)*

ρ = density of water *(kg/m^3)*

e_f = porosity of frazil slush *(dimensionless)*

η = frazil rise parameter *(m/s)*

C_f = Suspended frazil ice concentration *(dimensionless)*

B = top width of channel *(m)*

B_i = surface ice width or coverage *(m)*

The term representing the combined density of frazil slush and pore water arises because Equation [2.17] is actually a merger of two distinct mass conservation equations: one for the frazil ice mass component and the other for the pore water mass component. Thus, the combined density term is given by:

$$\rho' = \rho_i(1 - e_f) + \rho e_f \qquad [2.18]$$

Equation [2.17] will yield the change in surface ice coverage due to frazil rise, but does not handle the incoming transport of ice from upstream. Changing the definition of the area considered in the equation slightly results in a better equation for surface ice coverage that does handle both new pan formation and ice transport. To do this, the conservation area for new pans becomes the initial frazil pan thickness multiplied by ice covered width, as shown in Figure 2.16. This does not affect the solution for overall ice thicknesses, as these are calculated independently as described in Section 2.3.3. Any new frazil slush rising to the surface then extends the new pan area across the river in a manner equivalent to the previous formulation.

Applying the new area definition, the equation becomes:

$$\frac{\partial t'_f B_i}{\partial t} + \frac{\partial U_i t'_f B_i}{\partial x} = \frac{1}{\rho'}\left[\underbrace{\left(\rho_i + \rho\frac{e_f}{(1-e_f)}\right)\eta C_f (B - B_i)}_{\text{frazil and pore water deposition if } C_f \geq 0}\right] \quad [2.19]$$

Dividing this equation by the constant initial frazil floe thickness, t'_f, yields the equation for surface ice coverage:

$$\frac{\partial B_i}{\partial t} + \frac{\partial U_i B_i}{\partial x} = \frac{1}{\rho' t'_f}\left[\underbrace{\left(\rho_i + \rho\frac{e_f}{(1-e_f)}\right)\eta C_f (B - B_i)}_{\text{frazil and pore water deposition if } C_f \geq 0}\right] \quad [2.20]$$

where
B_i = surface ice width or coverage *(m)*
U_i = surface ice velocity *(m/s)*
ρ' = combined density of frazil slush and pore water *(kg/m^3)*
t'_f = initial frazil ice thickness *(m)*
ρ_i = density of ice *(kg/m^3)*
ρ = density of water *(kg/m^3)*
e_f = porosity of frazil slush *(dimensionless)*
η = frazil rise parameter *(m/s)*
C_f = Suspended frazil ice concentration *(dimensionless)*
B = top width of channel *(m)*

The surface ice coverage, B_i, can easily be converted to a concentration, based on the width of the river, B:

$$C_i = \frac{B_i}{B} \times 100\% \qquad [2.21]$$

2.3.3. Surface Ice Thickness

The surface ice layer is split into a frazil slush layer (underside) and a solid ice layer (topside), as shown in Figure 2.17. This type of two-layer model is also used by Lal and Shen (1989). There are several possible mass fluxes that can take place within these layers, depending on the freezing or thawing conditions.

Dealing first with the frazil slush layer, deposition of frazil ice and pore water will increase the thickness of that layer. Since the change in ice coverage is accounted for separately, the total rate of frazil rise over the whole channel width is used to quantify frazil deposition:

$$\underbrace{\left(\rho_i + \rho\frac{e_f}{(1-e_f)}\right)\eta C_f B}_{\text{frazil and pore water deposition if } C_f \geq 0} \qquad [2.22]$$

Next, pore water within the frazil slush layer will freeze due to heat loss through the solid ice cover above, if any is present. This effect is considered by:

$$\underbrace{\frac{\rho'}{\rho_i}\frac{B_i\phi_{ia}}{L_i}}_{\text{pore water freezing if } \phi_{ia}>0} \qquad [2.23]$$

The presence of solid ice above the frazil layer will tend to insulate it from the air above, according to the thermal conductivity of ice, which varies with ice temperature. In the present model, the solid ice temperature is approximated linearly, where the bottom is assumed to be 0°C and the top equal to the air temperature. The thermal conductivity of ice is then taken at the middle of the solid ice layer where the ice temperature would be:

$$T_i = \frac{T_a}{2} \qquad [2.24]$$

The thermal conductivity of ice, also approximated linearly, for a range of ice temperatures between 0 and -30°C based on data from the Chemical Rubber Company (2004) with an r^2 value of 0.98, is:

$$K_i = 2.158 - 0.0118T_i \ \textit{(Watts per metre per degree Celsius, W/m/°C)} \qquad [2.25]$$

With these values, the heat loss through the solid ice layer is (Lal and Shen, 1989):

$$\phi_{ia} = \frac{\phi_{wa}}{\left(1 + \frac{h_{wa} t_i}{K_i}\right)} \qquad [2.26]$$

where ϕ_{ia} = net rate of heat exchange per unit area between ice and air *(W/m²)*

ϕ_{wa} = net rate of heat exchange per unit area between water and air *(W/m²)*

h_{wa} = linear heat transfer coefficient *(W/m²/°C)*

t_i = thickness of solid ice layer at the surface *(m)*

K_i = thermal conductivity of ice *(W/m/°C)*

It should be noted that the heat capacity of the ice cover is neglected in the above ice temperature representation (Equation [2.24]). In reality, as air temperatures change, there is a time lag with respect to the change in ice cover temperature throughout its thickness. Neglecting this response time implies that heat loss through the ice cover could be overestimated during cooling and underestimated during warming. Further refinement of the model to characterise the ice cover in layers, thus accounting for the variation in ice cover temperature and conductivity throughout its thickness, are worthwhile for future study.

The remaining consideration is for melt of the slush layer due to warm water. This is given by:

$$\underbrace{\frac{\rho'}{\rho_i}\frac{B_i\phi_{iw}}{L_i}}_{\text{slush melt if } \phi_{iw}>0} \qquad [2.27]$$

A method for calculating the heat exchange between warm water and a river ice cover was developed by Ashton (1973):

$$\phi_{iw} = \alpha_{iw}\left[\frac{U^{0.8}}{\left(H-\frac{\rho_i}{\rho}\left\{t_i+\left(1-e_f\right)t_f\right\}\right)^{0.2}}\right]T_w \qquad [2.28]$$

where

ϕ_{iw} = net rate of heat exchange per unit area between ice and water *(W/m^2)*

α_{iw} = coefficient for turbulent heat exchange between ice and water *($W{\cdot}s^{0.8}/m^{2.6}/°C$)*

U = mean water velocity *(m/s)*

H = depth of water from bed to free surface *(m)*

ρ_i = density of ice *(kg/m^3)*

ρ = density of water *(kg/m^3)*

t_i = thickness of solid ice layer at the surface *(m)*

e_f = porosity of frazil slush *(dimensionless)*

t_f = thickness of frazil ice layer at the surface *(m)*

T_w = water temperature *(°C)*

Combining these three processes into an equation for slush ice conservation at the surface yields:

$$\frac{\partial A_i'}{\partial t}+\frac{\partial U_i A_i'}{\partial x}=\frac{1}{\rho'}\left[\underbrace{\left(\rho_i+\rho\frac{e_f}{\left(1-e_f\right)}\right)\eta C_f B}_{\substack{\text{frazil and pore water deposition if}\\ C_f\geq 0}}-\underbrace{\frac{\rho'}{\rho_i}\frac{B_i\phi_{ia}}{L_i}}_{\substack{\text{pore water freezing if}\\ \phi_{ia}>0}}-\underbrace{\frac{\rho'}{\rho_i}\frac{B_i\phi_{iw}}{L_i}}_{\substack{\text{slush melt if}\\ \phi_{iw}>0}}\right] \qquad [2.29]$$

where
A_i' = Flow area of frazil slush and pore water at the surface *(m^2)*
U_i = surface ice velocity *(m/s)*
ρ' = combined density of frazil slush and pore water *(kg/m^3)*
ρ_i = density of ice *(kg/m^3)*
ρ = density of water *(kg/m^3)*
e_f = porosity of frazil slush *(dimensionless)*
η = frazil rise parameter *(m/s)*
C_f = Suspended frazil ice concentration *(dimensionless)*
B = top width of channel *(m)*
B_i = surface ice width or coverage *(m)*
ϕ_{ia} = net rate of heat exchange per unit area between ice and air *(W/m^2)*
L_i = latent heat of ice *(J/kg)*
ϕ_{iw} = net rate of heat exchange per unit area between ice and water *(W/m^2)*

With the solution for A_i', the frazil thickness can easily be extracted:

$$t_f = \frac{A_i'}{B_i} \qquad [2.30]$$

The mass fluxes that apply to the solid ice layer depend on whether or not a slush layer is present beneath it. When there is a thickness of frazil below, as in Figure 2.18, pore water freezing or solid ice melt due to the air above are the only possibilities:

$$\frac{\partial A_i}{\partial t} + \frac{\partial U_i A_i}{\partial x} = \frac{1}{\rho_i}\left[\underbrace{\frac{\rho'}{\rho_i}\frac{B_i \phi_{ia}}{L_i}}_{\substack{\text{pore water freezing if} \\ \phi_{ia}>0}} + \underbrace{\frac{\rho}{\rho_i}\frac{B_i \phi_{ia}}{L_i}}_{\substack{\text{solid ice melt if} \\ \phi_{ia}<0}} \right] \qquad [2.31]$$

where

A_i = Solid ice flow area *(m^2)*

U_i = surface ice velocity *(m/s)*

ρ_i = density of ice *(kg/m^3)*

ρ' = combined density of frazil slush and pore water *(kg/m^3)*

B_i = surface ice width or coverage *(m)*

ϕ_{ia} = net rate of heat exchange per unit area between ice and air *(W/m^2)*

L_i = latent heat of ice *(J/kg)*

ρ = density of water *(kg/m^3)*

However, when there is no slush layer underlying the surface ice, as in Figure 2.19, new mass transfer paths are established directly between the solid ice layer and the active water flow. Flux terms for the growth of columnar ice and warm water melt of the solid ice layer now replace the pore water freezing term:

$$\frac{\partial A_i}{\partial t} + \frac{\partial U_i A_i}{\partial x} = \frac{1}{\rho_i}\left[\underbrace{\frac{\rho}{\rho_i}\frac{B_i \phi_{ia}}{L_i}}_{\substack{\text{growth of columnar ice if} \\ \phi_{ia}>0 \\ T_w=0}} + \underbrace{\frac{\rho}{\rho_i}\frac{B_i \phi_{ia}}{L_i}}_{\substack{\text{solid ice melt if} \\ \phi_{ia}<0}} - \underbrace{\frac{\rho}{\rho_i}\frac{B_i \phi_{iw}}{L_i}}_{\substack{\text{solid ice melt to warm water if} \\ \phi_{iw}>0}} \right] \qquad [2.32]$$

where
- A_i = Solid ice flow area (m^2)
- U_i = surface ice velocity (m/s)
- ρ_i = density of ice (kg/m^3)
- ρ = density of water (kg/m^3)
- B_i = surface ice width or coverage (m)
- ϕ_{ia} = net rate of heat exchange per unit area between ice and air (W/m^2)
- L_i = latent heat of ice (J/kg)
- ϕ_{iw} = net rate of heat exchange per unit area between ice and water (W/m^2)

The solution for the solid ice layer provides the solid ice thickness in the same way as for the frazil slush layer:

$$t_i = \frac{A_i}{B_i} \qquad [2.33]$$

2.4. MODEL IMPLEMENTATION

2.4.1. Underlying Hydraulic Model

A reliable hydraulic model that can simulate water mass and momentum conservation is a prerequisite to transient thermal river ice modeling. The core equations presented in Sections 2.2 and 2.3 require a solution for water velocity and depth be known for every cross section and time step. The present thermal river ice model has been built on the *River1D* finite element hydraulic model developed by Hicks and Steffler (1990) and recently applied to the Peace River by Peters and Prowse (2001).

River1D solves a conservation formulation of the St. Venant equations for rectangular channels of varying width. These water mass and momentum conservation equations can be found in Hicks (1996):

$$\frac{\partial A}{\partial t} + \frac{\partial Q}{\partial x} = 0 \qquad [2.34]$$

$$\frac{\partial Q}{\partial t}+\frac{\partial QU}{\partial x}+\frac{\partial}{\partial x}\left(\frac{gAH}{2}\right)-\frac{gAH}{2B}\frac{dB}{dx}=gA\left(S_o-S_f\right) \qquad [2.35]$$

where
A = cross sectional flow area *(m^2)*
Q = discharge *(m^3/s)*
U = cross section average longitudinal velocity *(m/s)*
g = acceleration due to gravity *(m/s^2)*
H = depth of flow *(m)*
B = width of the rectangular cross section *(m)*
S_o = longitudinal channel bed slope *(dimensionless)*
S_f = longitudinal boundary friction slope *(dimensionless)*

This system of equations is solved by the finite element method using the characteristic-dissipative-Galerkin (CDG) scheme (Hicks and Steffler, 1990; Hicks and Steffler, 1992).

2.4.2. Expressing the Thermal River Ice Model Equations in Terms of the Finite Element Method

As mentioned previously, each of the physical equations can be written in the form:

$$\frac{\partial}{\partial t}(\Phi)+\frac{\partial}{\partial x}(U\Phi)=\Sigma F \qquad [2.36]$$

Expression of this general equation in terms of the finite element method occurs by way of the following weak statement for Equation [2.36]:

$$\left[\int_e \left(f_i f_j + \omega \tfrac{U}{|U|}\Delta x \frac{df_i}{dx} f_j\right) dx\right]\left\{\frac{d\Phi}{dt}\right\} - \left[\int_e U\left(\frac{df_i}{dx} f_j + \omega \tfrac{U}{|U|}\Delta x \frac{df_i}{dx}\frac{df_j}{dx}\right) dx\right]\{\Phi\} + [U\Phi]_0^L = \Sigma F \qquad [2.37]$$

where f_i, f_j = finite element interpolation functions (linear)

ω = adjustable upwinding coefficient *(dimensionless)*

U = cross section average longitudinal velocity *(m/s)*

Δx = variable element length defined by the input geometry *(m)*

ΣF = the sum of the applicable mass or energy fluxes per unit distance in the longitudinal direction

On an element level, Equation [2.37] can be written as:

$$\Delta x_j \begin{bmatrix} \frac{1}{3}-\frac{\omega}{2} & \frac{1}{6}-\frac{\omega}{2} \\ \frac{1}{6}+\frac{\omega}{2} & \frac{1}{3}+\frac{\omega}{2} \end{bmatrix} \frac{d}{dt}\begin{Bmatrix} \Phi_{j-1} \\ \Phi_j \end{Bmatrix} - \begin{bmatrix} U_{j-1}\left(-\frac{1}{2}+\omega\right) & U_j\left(-\frac{1}{2}-\omega\right) \\ U_{j-1}\left(\frac{1}{2}-\omega\right) & U_j\left(\frac{1}{2}+\omega\right) \end{bmatrix}\begin{Bmatrix} \Phi_{j-1} \\ \Phi_j \end{Bmatrix} = \Sigma F_j - [U\Phi]_0^L \qquad [2.38]$$

The assembly of all elements for a given problem (depending on the input geometry) yields a global matrix equation of the form:

$$[S]\frac{d}{dt}\{\Phi_j\}+[K]\{\Phi_j\}=\{F\} \qquad [2.39]$$

For which $[S]$, $[K]$, and $\{F\}$ are defined as:

$$[S]=\underset{e=1}{\overset{N_e}{\mathrm{A}}}[S_e]=\underset{e=1}{\overset{N_e}{\mathrm{A}}}\begin{bmatrix}\Delta x_e\left(\frac{1}{3}-\frac{\omega}{2}\right) & \Delta x_e\left(\frac{1}{6}-\frac{\omega}{2}\right)\\ \Delta x_e\left(\frac{1}{6}+\frac{\omega}{2}\right) & \Delta x_e\left(\frac{1}{3}+\frac{\omega}{2}\right)\end{bmatrix} \qquad [2.40]$$

$$[K]=-\underset{e=1}{\overset{N_e}{\mathrm{A}}}[K_e]=\underset{e=1}{\overset{N_e}{\mathrm{A}}}\begin{bmatrix}-U_j\left(-\frac{1}{2}+\omega\right) & -U_j\left(-\frac{1}{2}-\omega\right)\\ -U_j\left(\frac{1}{2}-\omega\right) & -U_j\left(\frac{1}{2}+\omega\right)\end{bmatrix} \qquad [2.41]$$

$$\{F\}=\Sigma F_j-\begin{Bmatrix}-U_o\Phi_o\\ 0\\ \vdots\\ 0\\ U_L\Phi_L\end{Bmatrix} \qquad [2.42]$$

The global equation (Equation [2.39]) can be written in a time-discretized form:

$$[S]\left\{\frac{\Phi_j^{n+1}-\Phi_j^n}{\Delta t}\right\}+\theta[K]^{n+1}\{\Phi_j^{n+1}\}+(1-\theta)[K]^n\{\Phi_j^n\}=\theta\{F\}^{n+1}+(1-\theta)\{F\}^n \qquad [2.43]$$

where θ = numerical implicitness *(dimensionless)*

Rearranging this equation gives:

$$[K']\{\Phi_j^{n+1}\} = \{F'\} \qquad [2.44]$$

where

$$[K'] = \left([S] + \theta\Delta t[K]^{n+1}\right) \qquad [2.45]$$

$$[F'] = \left([S] - (1-\theta)\Delta t[K]^n\right)\{\Phi_j^n\} + \theta\Delta t\{F\}^{n+1} + (1-\theta)\{F\}^n \qquad [2.46]$$

The system of equations represented by Equation [2.46] can be solved iteratively using the Newton-Raphson method. With each iteration, the $\{F\}^{n+1}$ vector is recalculated with the most current solution for ice conditions.

The Newton-Raphson solution routines had previously been built-into the existing *River1D* model (Hicks and Steffler, 1990) and were used to solve the thermal river ice process equations in the same manner as the hydraulic model component.

2.4.3. Solution Sequence

To avoid alteration of the source code for the base hydraulic model and to improve simulation speed and stability, the present thermal river ice model is de-coupled from the hydraulic computations. In addition, the water temperature computation is decoupled from the ice mass conservation computations. This results in a three-stage solution sequence occurring during each time-step in the simulation, shown in Figure 2.20.

At each stage, the finite element system of equations is solved iteratively until an acceptable level of convergence is achieved. The water velocities from the total water mass and momentum solution are used in both the water temperature and ice mass conservation routines. The water temperature solution along the river reach is also necessary in the ice mass conservation routine, as it governs several of the flux terms in that system of equations.

2.5. ICE FRONT PROGRESSION AND RECESSION

In the present version of the model, the time at which bridging occurs at the downstream boundary must be specified. When this time in the simulation is reached, the initial condition for the ice front location is set at the downstream boundary and the approach of ice from upstream leads to the upstream progression of the ice front. A straightforward conservation of surface ice method, inspired by that employed in the *RICEN* model (Shen *et al.*, 1995), is used to track the ice front location:

$$X_i(t+\Delta t) = X_i(t) - \frac{C_i U_i}{P_{jux}} \Delta t \qquad [2.47]$$

where X_i = location of the ice front *(m)*

C_i = surface ice concentration *(% / 100)*

U_i = surface ice velocity *(m/s)*

P_{jux} = juxtaposition parameter *(dimensionless)*

Δt = solution time step *(s)*

The juxtaposition parameter is a calibration parameter that affects the simulated rate of ice cover advance. Its value is intended to empirically account for the reduction of ice velocity as pans arrive at the leading edge of the ice cover as well as any associated crushing, under-turning, or consolidation of floes.

Recession of the ice cover due to melt is handled differently by the model. The ice front location moves node-by-node downstream as the ice thickness at the ice front decreases towards zero. Intermediate ice front locations are not calculated during the melt process as they are during upstream progression. During model development and testing, locating the ice front between nodes during ice cover retreat was attempted with a conservation of energy formulation. However, occasionally small or zero ice thicknesses in the vicinity of the ice front would result in unrealistically rapid recession of the ice front during a single time step. Although this "numerical" issue should be possible to address, this method was abandoned for the simplified approach used in the present study. As the ice front profiles presented in Chapter 4 will demonstrate, the node-by-node approach to ice front recession imposes

no visible limitation on the model's agreement with observations for nodal spacing of one kilometre. However, greater distances between nodes (say ten or 100 kilometre discretization) in other applications could be an important consideration given this feature of the model.

2.6. PRESENT LIMITATIONS OF THE MODEL

There are a number of river ice processes that are not currently considered within the existing model. These processes represent additional levels of complexity that can be added to the river ice model in the future. Below is a qualitative assessment how the thermal simulations could be affected by the processes excluded.

First and foremost, the model does not presently consider ice cover consolidation (ice jamming). As a result, the simulated ice front location may track further upstream than observed, simulated water levels may be low, and ice cover thicknesses where the consolidation event would have occurred would be less than expected. During a consolidation event, the ice cover can collapse and shorten in length to balance the longitudinal forces on it. Consolidated ice covers tend to be rougher than juxtaposed ice covers, and the increased roughness of the ice cover would result in higher water levels than would be simulated assuming a smoother, thermal ice cover.

Border ice formation and bridging are also not included in the present model. Neglecting border ice formation could yield slightly lower surface ice concentration values than those that would be expected. However, in most cases the border ice

formation zone in the natural channel cross section falls outside of the equivalent rectangular cross section (see Figure 2.12). As a result, this effect is probably minimal. Without a proven, deterministic bridging model or criterion, the simulated ice front profiles are subject to the accuracy of the observed or calibrated bridging date.

Snow cover insulation and snow ice formation, which were mentioned in Section 2.1.1, are also neglected at this time. The main implication of this is that simulated ice thicknesses may differ from actual conditions. Excluding snow cover insulation would result in a thicker ice cover while neglecting snow ice formation would have the opposite effect.

Based on advice from Alberta Environment, anchor ice formation is not considered a significant process on the Peace River. For this reason, no provisions for anchor ice have been made in the present model and it is not anticipated that this has any effect on the simulation results in this study.

Finally, dynamic features of breakup, such as hinge and transverse ice cover cracking and breakup ice jam formation are not included in the thermal river ice model. The general implications of this are mainly in regards to the accuracy of the simulated rate of ice cover recession, ice thicknesses, and water levels.

Work is currently underway at the University of Alberta to develop modeling routines capable of handling many of these processes. It is anticipated that the present

limitations of the model will diminish over time as this additional research is completed and verified.

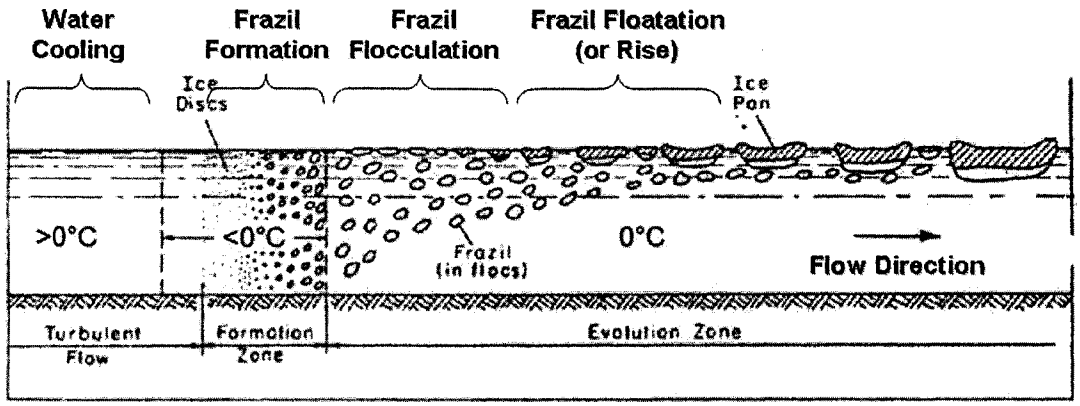

Figure 2.1 **Conceptual diagram of river ice formation processes (adapted from Michel, 1971).**

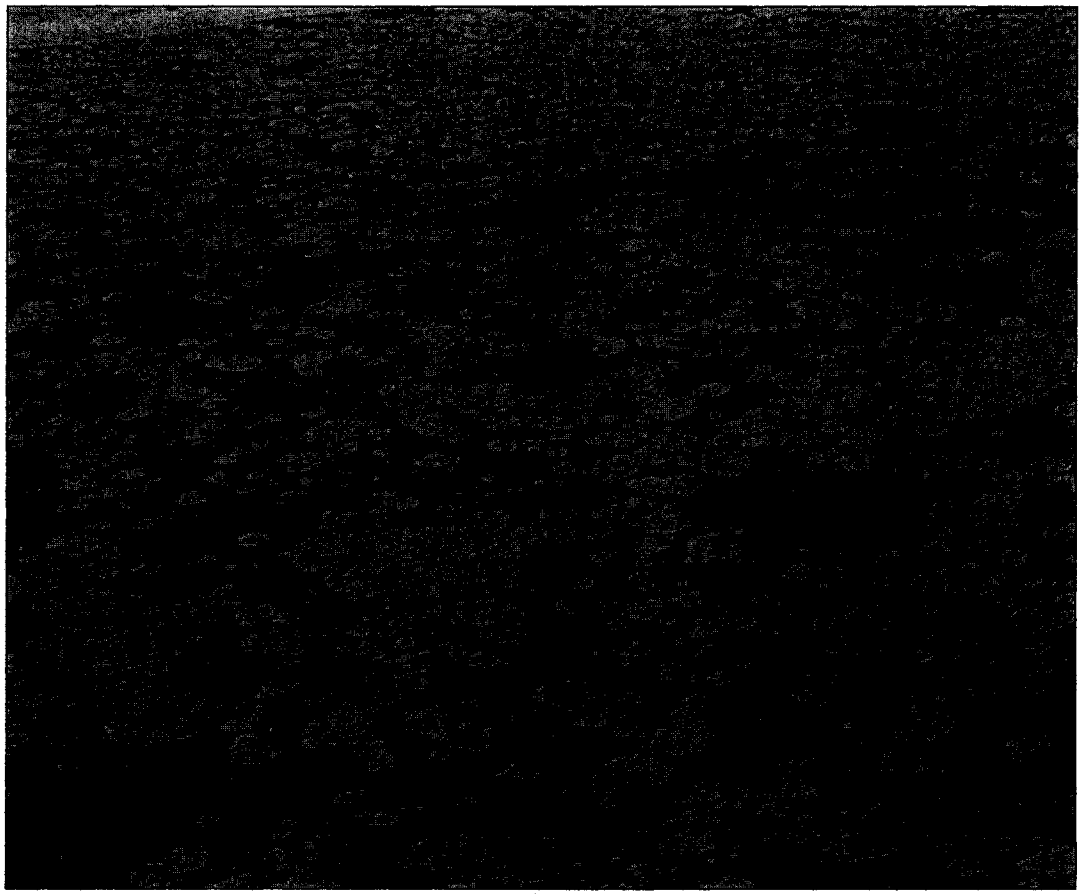

Figure 2.2 **Photograph of frazil pans during freezeup on the Peace River.**

Figure 2.3 Photograph of large rafts during freezeup on the Peace River.

Figure 2.4 Congestion of frazil pans passing through a narrow river reach constricted by border ice growth.

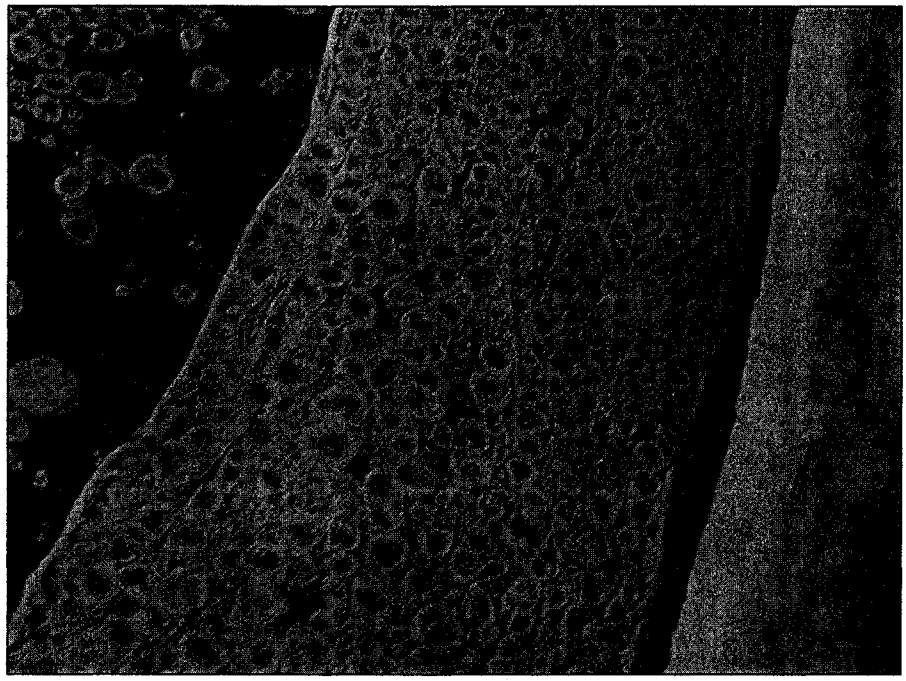

Figure 2.5 **Juxtaposed frazil pans with growth of thermal ice between pan edges.**

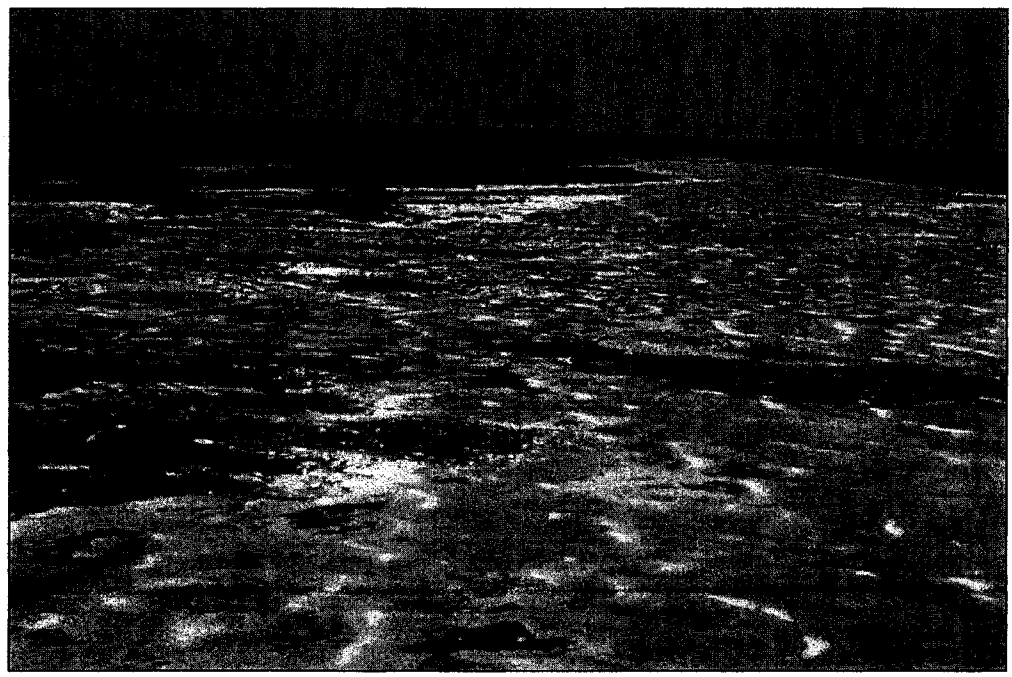

Figure 2.6 **Thermal deterioration of the Mackenzie River ice cover near Fort Providence (photograph used with permission of Faye Hicks).**

Figure 2.7 **Thermal melt and ice front retreat (photograph used with permission of Alberta Environment).**

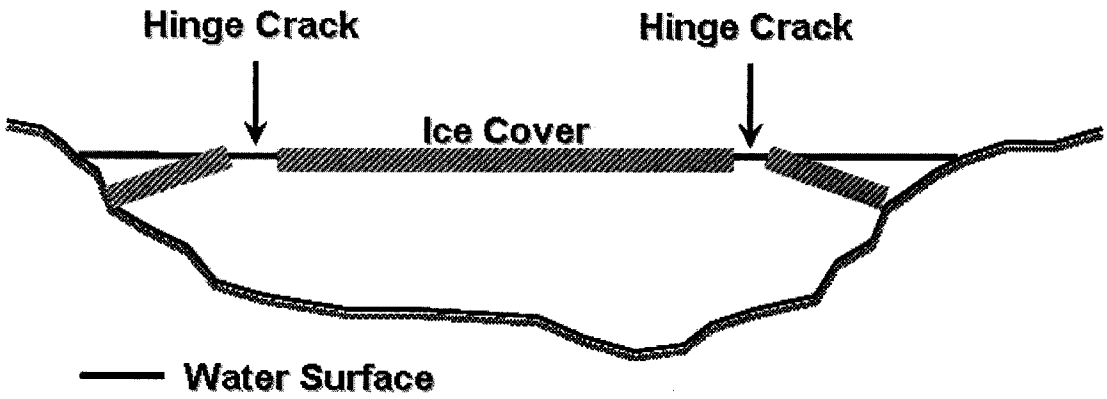

Figure 2.8 **Schematic of hinge crack formation on a river ice cover during breakup.**

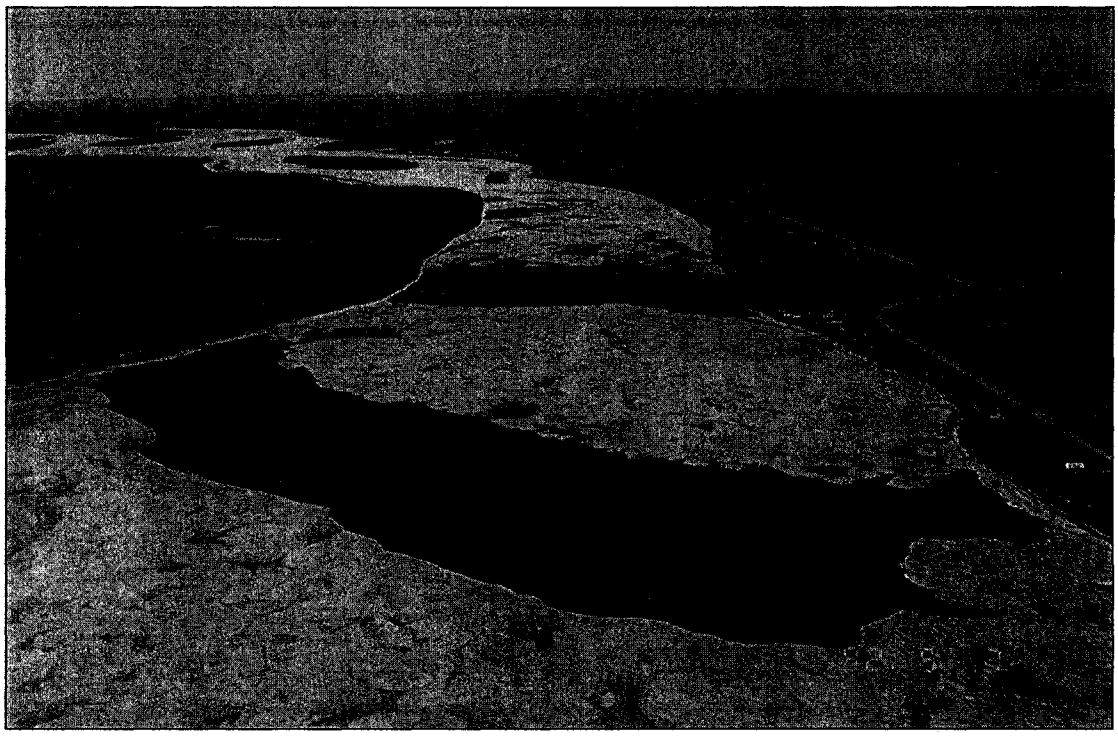

Figure 2.9 **Transverse cracking of the Mackenzie River ice cover near Fort Providence during breakup (photograph used with permission of Faye Hicks).**

Figure 2.10 **Breakup ice jam at the Town of Peace River in April 1979 (photograph used with permission of Alberta Environment).**

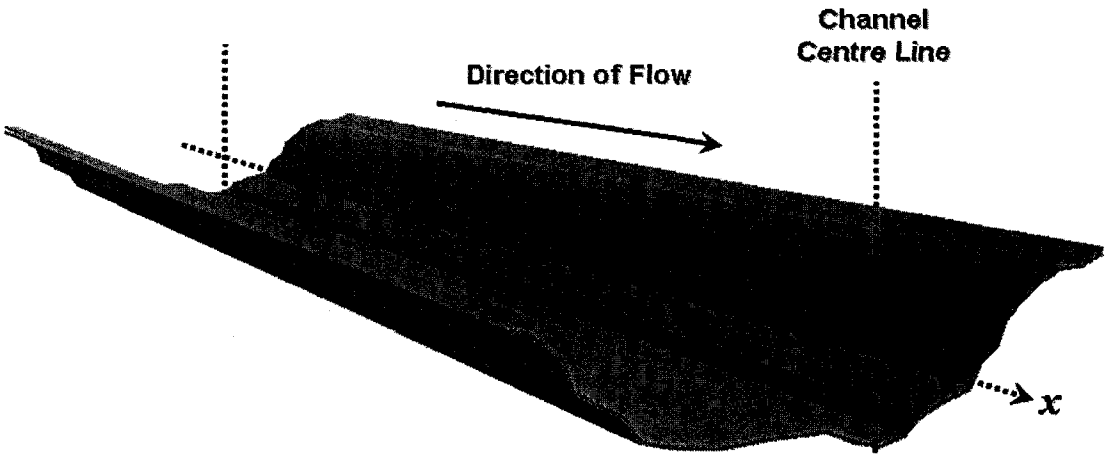

Figure 2.11 **Schematic representation of the problem domain showing the longitudinal coordinate, x, along the channel centre line in the direction of flow.**

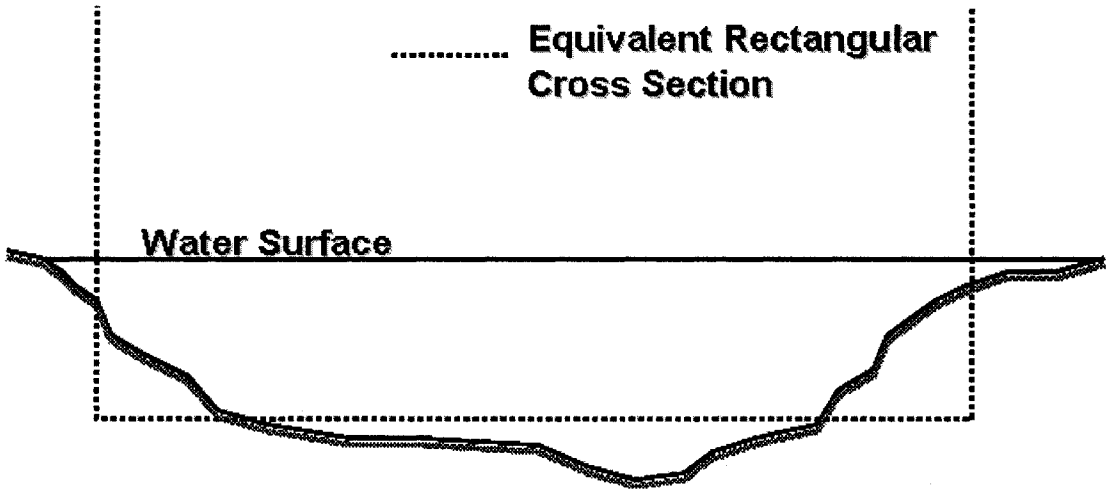

Figure 2.12 **Schematic representation of an equivalent rectangular river cross section.**

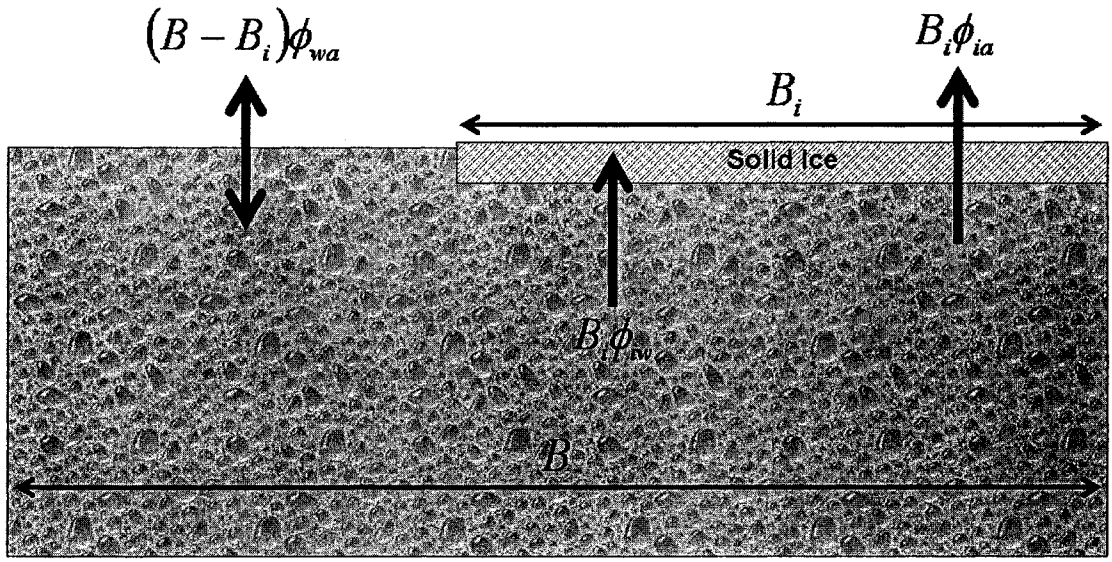

Figure 2.13 **Cross section definition for water temperature formulation with associated energy fluxes identified.**

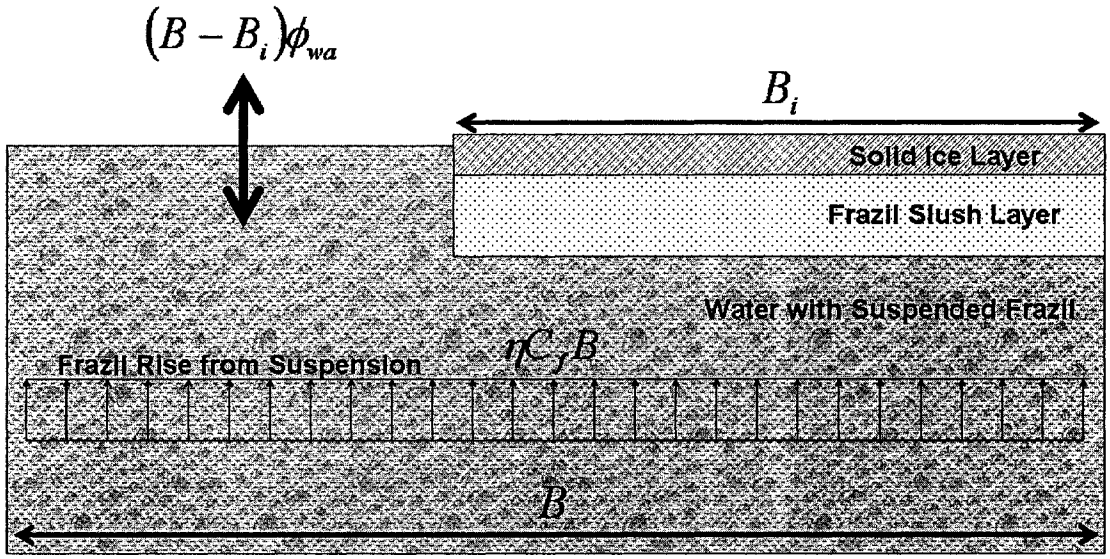

Figure 2.14 **Cross section definition for suspended frazil ice formation with associated mass and energy fluxes identified.**

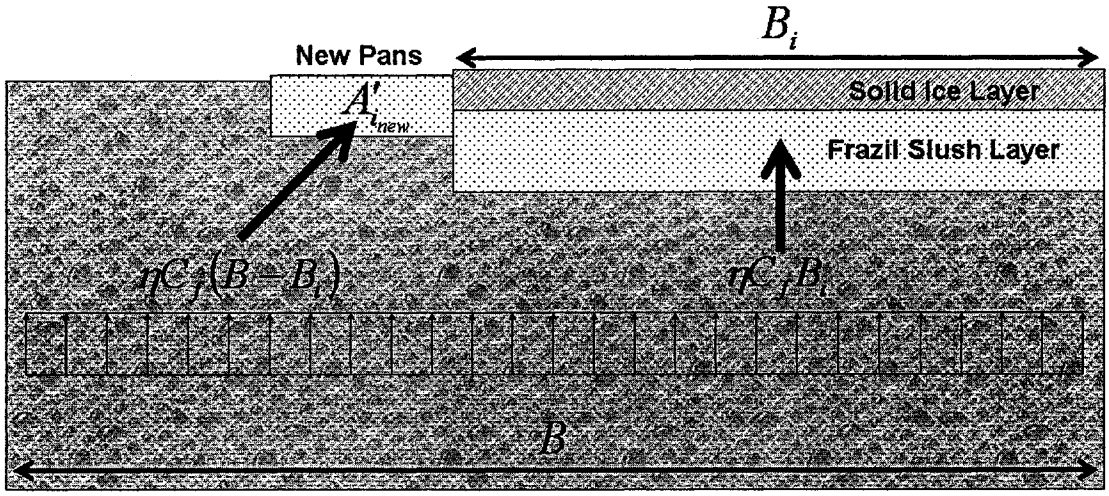

Figure 2.15 **Cross section definition for surface frazil slush layer formation and growth with associated mass fluxes identified.**

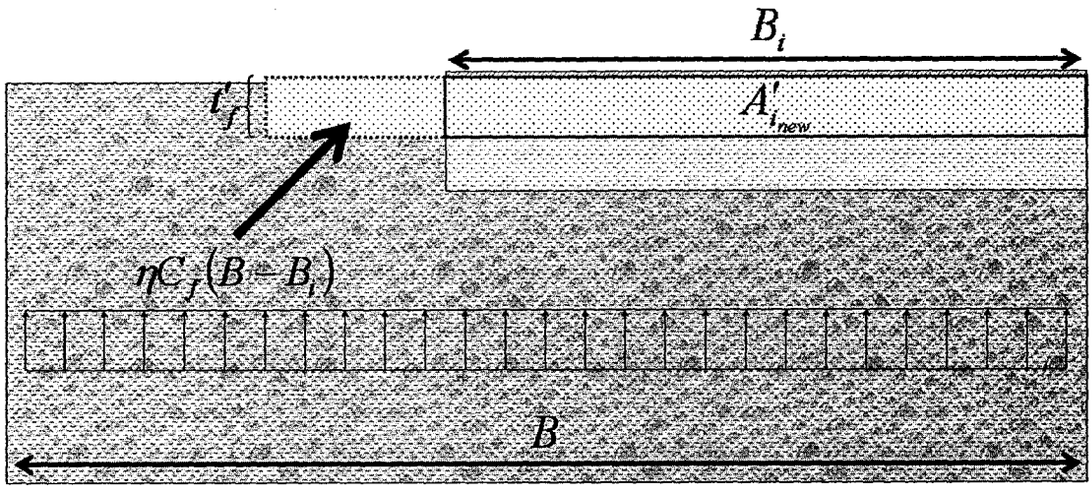

Figure 2.16 Revised cross section definition for new pan formation that leads to formulation of surface ice coverage equation.

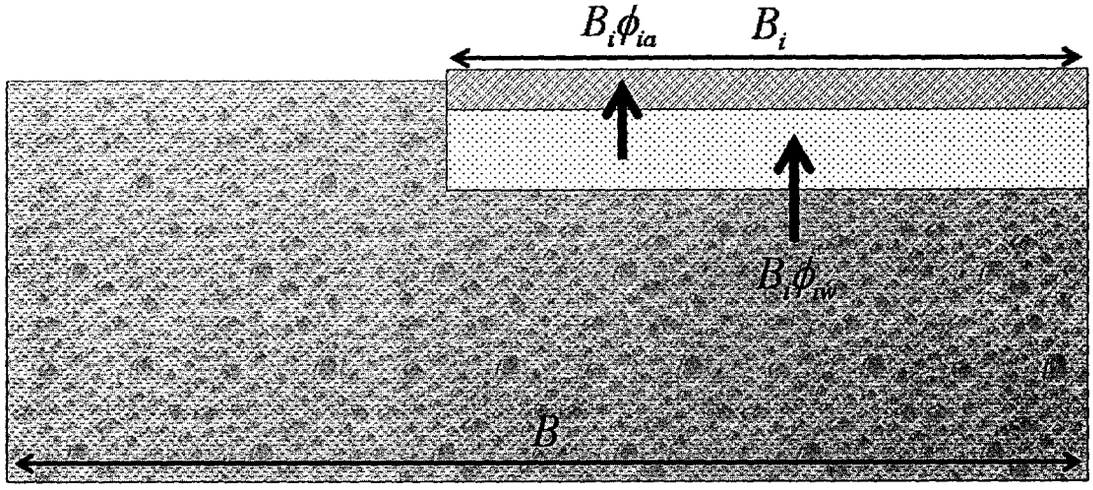

Figure 2.17 Cross section definition for surface frazil slush layer freezing and melt with associated energy fluxes identified.

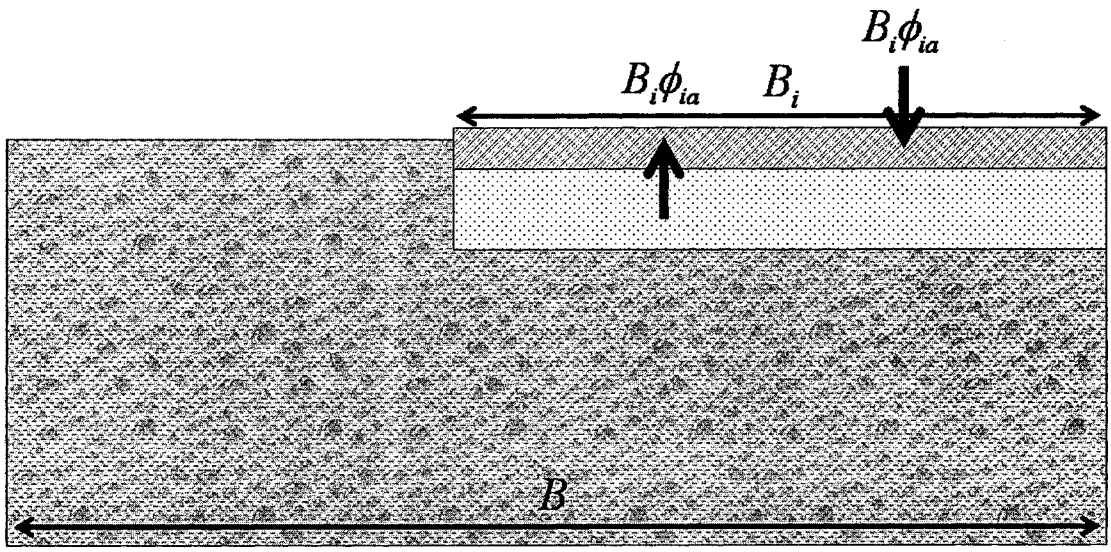

Figure 2.18 **Cross section definition for solid surface ice layer growth and melt with associated energy fluxes identified (when frazil slush layer is present).**

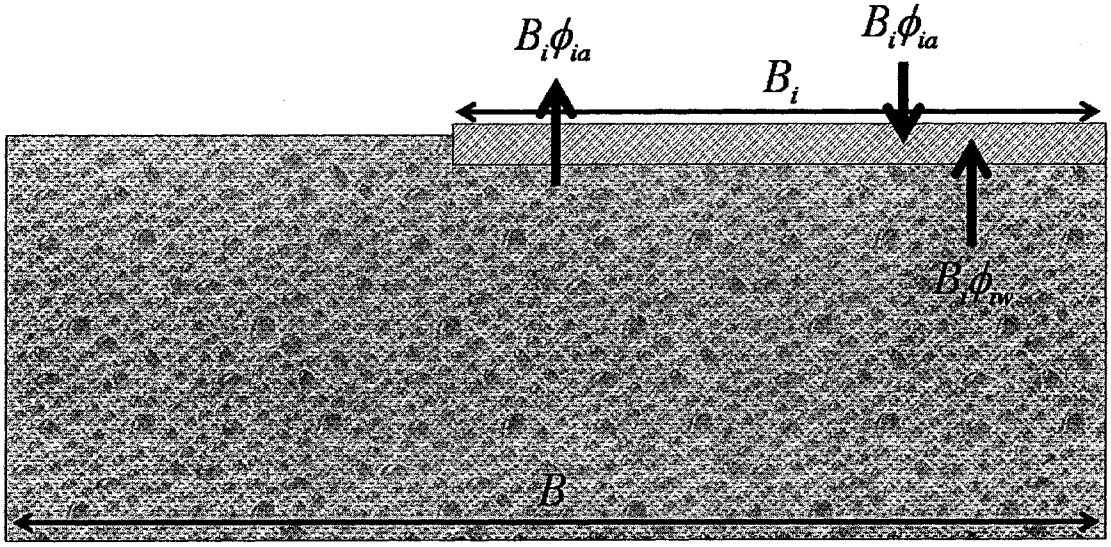

Figure 2.19 **Cross section definition for solid surface ice layer growth and melt with associated energy fluxes identified (when frazil slush layer has frozen through).**

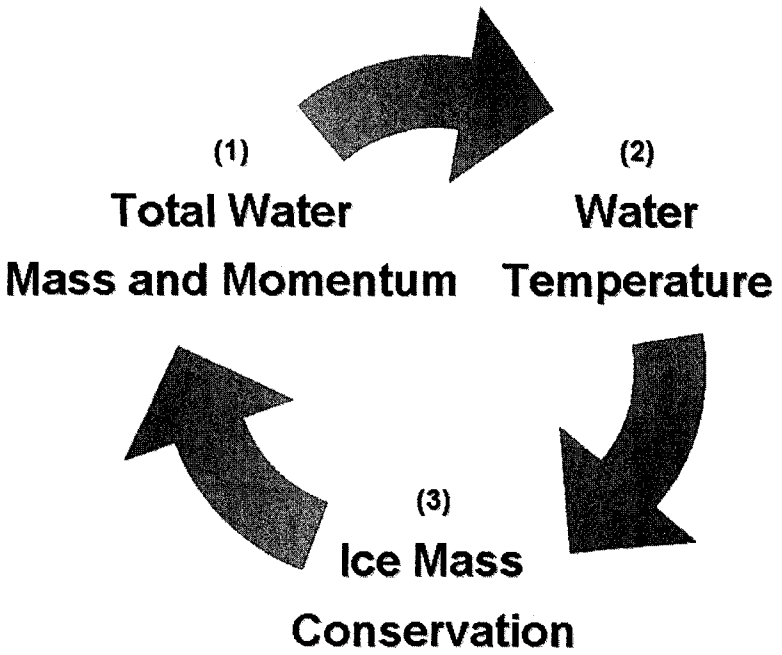

Figure 2.20 **Un-coupled solution sequence employed in the *River1D* thermal river ice process model.**

CHAPTER 3 AVAILABLE DATA ON THE PEACE RIVER

3.1. INTRODUCTION

The Peace River flows in a generally northeasterly direction from Hudson Hope to Lake Athabasca. It is a relatively large river both in terms of width and discharge. Blackburn and Hicks (2002) provide the following technical description of the river based on information by Kellerhals *et al.* (1972):

> *"In the upper portion of the study reach, the river is defined by a straight channel with the occasional island and mid-channel bars where the channel bed is a shallow alluvium of gravel over shale and some sandstone. Near Dunvegan the river becomes slightly sinuous defined by point bars and by Fort Vermilion the river displays an irregular meandering pattern characterized by mid-channel and point bars and a channel bed consisting predominately of sand. Throughout the entire reach the river is partly entrenched and confined to the river valley."*

Data relevant to modeling thermal river ice processes on the Peace River include: (1) channel geometry and resistance along the entire study reach; (2) inflow discharge and water temperature at the upstream boundary; and (3) air temperature throughout the study area. In order to calibrate and validate the model, water temperature and ice front observations are also required, at a minimum.

All of the available data on the variables listed above were obtained directly from Alberta Environment; however, a great deal of it originated from other sources and agencies that work with Alberta Environment on issues relating to the Peace River. These sources include BC Hydro, Trillium Engineering and Hydrographics (TEH), Northwest Hydraulic Consultants, and Glacier Power.

Some of the available historical data, such as regulated discharge and ice front observations, go back to the beginning of the regulated period in 1973 (when the Bennett Dam was commissioned). However, only the most recent twenty years of record were selected for analysis in this study. This period of record essentially represents the current regulated conditions on the Peace River, as controlled by both the Bennett Dam and Peace Canyon Dam (which was commissioned in the early 1980s).

3.2. ICE-RELATED FLOOD HISTORY AT THE TOWN OF PEACE RIVER

The Town of Peace River is both the largest community along the Peace River in Alberta and the location of several ice-related flooding problems dating back to the 1970s (Table 3.1). The events that have occurred at the Town have resulted in the construction of an extensive dyke system along the banks of the river. Although these high earth embankments provide protection from high water levels, groundwater seepage flooding remains a problem throughout the winter whenever water levels increase to basement level.

In 1975, an Alberta-British Columbia Joint Task Force was created, with representatives from BC Hydro, Alberta Environment, and B.C. Environment, to coordinate observation and measurement programs (TEH, 1997). Their mandate was, and remains today, to control high water levels through responsible hydropower operations. In 1994, the Joint Task Force issued guidelines for winter flow release patterns from the Bennett Dam (TEH, 1997).

A common motivation for both observing and modeling the ice cover on a river such as the Peace River is to assess and mitigate flood risk. Due to the complex and constantly changing behaviour of river ice, this can be extremely difficult in contrast to summer open water flood level forecasting. Open water floods tend to develop over long distances and travel along the river in a predictable manner. In contrast, river ice related flooding tends to occur due to highly unpredictable circumstances over relatively localised areas. In addition, there are many variables involved; some, such as the discharge, may be controlled by humans while others, such as the weather, are not.

In the case of thermal modeling of river ice on the Peace River, the desire is to locate and track the ice front as it approaches the Town of Peace River. This is because there is often a substantial water level increase associated with ice cover formation at a given location along the river. Since this river is regulated, discharges often need to be reduced during the period of freezeup at the Town of Peace River to prevent ice-related flooding or ice jam formation. There are presently guidelines set for the operation of the Bennett Dam during the progression of the ice front through the Town of Peace River for this very reason, and Alberta Environment and BC

Hydro work closely together during this time window to ensure the Town is adequately protected.

Typical water level increases that coincide with the arrival of the ice front at the Town of Peace River are on the order of two to three metres. Examining the water level record for 2003/04, shown in Figure 3.1, the arrival of the ice front is clearly evident in the three metre water level rise in a period of two to three days. The discharge in the river over this period was relatively constant during this time at about 1800 cubic metres per second.

Comparing photographs of the rail bridge over the Peace River at the Town of Peace River before and after the ice cover forms puts this water level change in perspective. Prior to freezeup, the water level and running ice are well below the top of the bridge piers as shown from a fly-over in photograph (Figure 3.2) taken in December 2004. By early January 2005, after freezeup, most of the bridge piers are under water and ice as shown in Figure 3.3. This is an example of a typical year in which no significant freezeup ice jam formation occurred. If and when an ice jam poises itself near the town, the risk of sudden water level rise and flooding can be high, demonstrating the importance of both studying and modeling river ice processes.

3.3. CHANNEL GEOMETRY

The geometric database of the Peace River used in this thermal river ice process model employed a rectangular channel approximation developed by Hicks

(1996), who combined available cross section data with topographic map data to define the study reach channel widths at 1 kilometre intervals. Hicks (1996) generated an effective bed profile by selecting the bed elevation of an equivalent rectangular section approximating the actual channel geometry; more specifically, the effective bed profile was taken as the mean bed level at each surveyed cross section computed by first determining the hydraulic mean depth (flow area divided by top width) at the 1:2 year flood level and then subtracting this depth from 1:2 year flood stage. Hicks (1996) established the effective bed profile by drawing a best-fit line through the mean bed points established from the surveyed sections.

Between surveyed reaches, the water surface slope, obtained by identifying locations where topographic contours intersected the river channel on 1:250,000 scale National Topographic Series (NTS) maps, was used to estimate the gradient of the effective bed profile. Surveyed water level profiles by the Alberta Research Council and Environment Canada were also used to refine the profile (e.g. to define the Vermilion Chutes downstream of Fort Vermilion). The input channel widths were based on channel top widths measured from the 1:250,000 NTS maps. The resulting geometric database consists of more than 1100 computational nodes spaced at 1 kilometre intervals. Figure 3.4 illustrates the bed profile developed by Hicks (1996).

For thermal ice process modeling, it was deemed appropriate to situate the upstream boundary of the modeled domain at the base of the Peace Canyon Dam, as this is where the thermal boundary condition data (i.e. discharge and water temperature) are available, and the downstream boundary at Fort Vermilion, as this is known as the location where bridging is initiated on the Peace River in most years. In

reality, the geometric database used in this study only extends as far upstream as Hudson Hope, which is a short distance downstream of the Peace Canyon Dam (approximately five kilometres). Therefore, over the reach between the Peace Canyon Dam tailrace and Hudson Hope some water cooling is neglected in the simulations presented in this study. The significance of this will be addressed in Section 4.5.2.

With the reach downstream of Fort Vermilion removed from the geometric database developed by Hicks (1996), the remaining geometry consisted of 802 nodes, at one kilometre spacing, within the reach of interest. No further changes were made to the remaining geometry: bed slopes, invert elevations, or top widths. Bed slopes in the modeled domain range from 0.00055 in the upper reach within British Columbia and decrease progressively to 0.00009 in the reach from about 145 kilometres north of the Town of Peace River to the downstream boundary at Fort Vermilion. Table 3.2 summarises the slope segments of the Peace River study reach.

Hick's (1996) smoothed channel widths have been used in the present geometric database. Despite the smoothing, the width of the channel varies considerably over the length of the study reach, as illustrated by the channel width profile in Figure 3.5. On average, the river width in the geometric database is 560 metres, with maximum and minimum widths of 1000 metres and 250 metres, respectively.

3.4. CHANNEL RESISTANCE

A detailed hydraulic calibration of the *River1D* hydraulic model to observed water levels was not considered necessary for this analysis as the objectives were thermal river ice model development and successful simulation of water temperature and ice front conditions under historical and climate change conditions. Calibrated water levels are not significant to the overall performance of the thermal simulation in this context. In addition, the rectangular channel approximation used in the model limits the accuracy of site-specific water level results, which although not ideal, is not particularly significant to the current study objectives.

Several previous open water flood studies provide resistance values for this reach of the Peace River. Hicks (1996) based channel resistance values on Water Survey of Canada (WSC) gauge data, as analysed by Kellerhals *et al.* (1972); however, for this study, more recent calibration advice from Alberta Environment was adopted with permission. The result is an updated set of Manning's n values for the study reach, summarised in Table 3.3.

3.5. STREAMFLOW REGULATION

With the completion of the Bennett Dam in 1972, winter flows on the Peace River have greatly increased. In a comprehensive study of regulated ice conditions on the Peace River, TEH (1997) provided a comparison of pre- and post-regulation winter discharges, based on the means of the 1960 through 1992 period of record. The relative magnitudes of the winter discharges are illustrated by Figure 3.6. Winter

discharges in the post-regulation period, 1972 to 1992, are considerably higher than those observed in the pre-regulation period (Table 3.4).

In addition to the general increase in winter discharge consistent with regulated conditions, fluctuations in winter discharge in response to changes in power demand, and thus flow releases from the dam, are common. These discharge variations are commonly referred to as hydropeaking. A typical discharge profile from the Peace Canyon Dam, just below the Bennett Dam, is shown in Figure 3.7 to illustrate this feature of the Peace River's winter flow regime.

The complete historical discharge record for the Peace Canyon Dam was supplied by Alberta Environment for this study. This data serves as one component of the upstream boundary condition and is necessary to complete a given model run. Fortunately, this data set is extremely comprehensive and complete. Mean daily discharges are available from August 1 to May 31 for the years 1967/68 through 2003/04. Additional discharge data is available from WSC monitoring records. A summary of this data coverage is provided in Table 3.5. Tributary flow data is also available from the WSC. The relevant gauging sites and their mean January flows, for the period of record from 1994 to 2003, are outlined in Table 3.6.

Earlier thermal modeling efforts on the Peace River by others have neglected the contribution of tributary streamflow. This is mainly because regulation results in relatively high winter flows on the Peace River, in comparison to the very low tributary inflows that occur naturally at this time of year. As the data in Table 3.6 indicates, these tributary contributions amount to only 109 cubic metres per second or

7.3% of the mean January regulated Peace Canyon discharge of 1497 cubic metres per second. Consequently, it was considered reasonable to neglect these lateral inflows in the present study also.

3.6. WATER TEMPERATURE

BC Hydro has made efforts to measure and record the water temperature at the tailrace of the Peace Canyon dam since 1977. This data is extremely important as it provides data to define the thermal boundary condition at the upstream end of the study reach. Unfortunately, there are many gaps in the historical record, as indicated in Table 3.7.

To overcome this limitation in the input data required for the model, an average water temperature profile was established for the Peace Canyon Dam discharge (Figure 3.8) and used in place of any measured data that was too incomplete to be used as model input. This typical water temperature profile from October 1 to May 1 was computed from a selection of ten years over the period of record for which a complete dataset was available over the winter period. The years used in the calculation were: 1980/81; 1982/83; 1990/91; 1991/92; 1994/95; and 2000/01 through 2004/05.

Fortunately, the discharge variation at the reservoir is relatively consistent from year-to-year, so substituting the mean water temperature profile for unavailable data is expected to have a negligible overall impact on the present analysis. However, measured water temperature data is certainly preferable to the substitute profile.

Within the modeled reach itself, there are limited observations of water temperature, both in terms of the number of monitoring sites and the length of record at each. Table 3.7 summarises the data availability for the two sites that do provide data, specifically at the WSC gauge at Alces (164 kilometres downstream of the Bennett Dam) and the Town of Peace River (397 kilometres downstream of the Bennett Dam). The most complete data at these locations is for the 2002/03 and 2003/04 seasons.

3.7. AIR TEMPERATURE

The air temperature record at three major locations along the Peace River study reach is very complete and spans all of the years of interest for historical modeling. These stations are located at: Fort St. John, British Columbia; the Town of Peace River; and High Level, Alberta (see Figure 1.1). While the record at each of the three sites is good, their spatial coverage and proximity to the river are limiting factors. Since air temperature is a highly variable meteorological parameter with respect to location and elevation, three points characterising air temperatures along a river reach over 800 kilometres long is not ideal. Also, the stations themselves are not in the actual river valley and therefore may not be representative of the true conditions over the river. Positive features of the air temperature monitoring sites are their overall distribution, covering approximately equal lengths of the river over the study reach, and the completeness of their records.

Data from the meteorological stations mentioned above were provided by Alberta Environment. More recently, air temperature sensors have been installed at

the WSC gauges at Alces and Dunvegan, but these stations were not used in this study because of their limited period of record. Excluding this data also kept the air temperature input consistent over the twenty-year period simulated. The period of record at each of these locations is summarised in Table 3.8.

3.8. SOLAR RADIATION

Very little solar radiation data is available for the Peace River study area. In recent years, some attempts have been made to monitor solar radiation at the Alces and Town of Peace River WSC gauge sites. However, all of the data recorded at the Town of Peace River is considered suspect due to difficulties with the instrument. The Alces data covers the period from June 22, 2001, through September 8, 2004.

Solar radiation is highly site-specific in nature, because conditions such as cloud cover, elevation, and exposure affect the amount of solar radiation reaching the ground or the river at a given place. In fact, solar radiation is generally much more spatially variable than air temperature, which makes it very difficult to operate a sufficient number of instrument stations to adequately cover any sizeable study area. Considering these issues, no attempt was made to incorporate the solar radiation data available for the Alces site because the dataset is simply too limited to use effectively in the present modeling effort. However, future modeling efforts could employ grid-based data from climate models as they become available.

Fortunately, the lack of solar radiation data is not a serious limitation for general thermal river ice modeling. Due to the low horizon of the sun in northern

regions during the winter period, the relative amount of solar radiation in the complete energy budget at the river surface is negligible compared to the convective heat energy exchange between the river and the air above it. In the spring, during thermal melt, solar radiation can be a more comparable component in the energy budget. As a result, any lag in the recession of the simulated ice cover in the spring is likely attributable to the omission of solar radiation in the heat transfer model. However, due to the large late winter and spring flows on the river resulting from regulation, thermal breakup generally precedes snowmelt in the basin, suggesting that it is early enough that solar heat input is not a major factor. Simulation results presented in Chapter 4 confirm that this does not appear to be a concern for the Peace River study area.

3.9. ICE FRONT LOCATION

Alberta Environment and BC Hydro have been collaboratively monitoring ice front location since the year after the Bennett Dam was completed in 1972. This information is recorded during observation flights along the river, conducted approximately every three to four days over the past twelve years (less frequently, about every nine days, prior to 1992/93). In the winter seasons from 1973/74 through 2003/04, only one year of record is missing: 1980/81. The reason for this gap is unknown. Table 3.9 summarises the date range and number of ice front observations available for each of the years on record.

3.10. SURFACE ICE CONCENTRATION

Quantifying the surface concentration of frazil pans over a long river reach at a given point in time can be extremely difficult. The main reason is that it is impossible to make an instantaneous visual observation of the entire 800 kilometre river reach, except perhaps by satellite remote sensing, which is an area of current research (eg. Weber *et al.*, 2003).

The present method for actually quantifying a surface ice concentration profile for the river is to fly and photograph the length of the river. The photographs can then be digitised and processed by a computer program that distinguishes ice from open water to compute a surface area concentration. Since this is can be a time-consuming and expensive undertaking, limited surface ice concentration data was available for the study area. In January 2004, TEH conducted two observation flights, on January 1 and January 9, to photograph the river during the freezeup and compile ice concentration profiles for those days.

Some subjective ice concentration observations have been made by Alberta Environment observers from December 1998 to May 2002. The data in the reports is referenced by range and townships and would need to be converted to river stationing. Because the data is highly subjective and sparse, it was not considered sufficient for model comparison and validation.

3.11. ICE COVER THICKNESS

Some ice thickness measurements have been made by the WSC, Alberta Environment, and BC Hydro. All available ice thickness information on the Peace River was obtained during the data assembly portion of this study. The cross sectional ice thickness profiles on record are located at the Town of Peace River WSC gauge and, in some cases, at the Shaftesbury Ferry site or near the Peace River Correctional Institute.

Measurements were taken on specific days in 1983 through 1986 and in 2002, as summarised in Table 3.10. The WSC data provides the thickness and area of the slush and solid ice layers, while the Alberta Environment data for February 24, 1983, and March 15, 2002, is given in terms of the elevation of the top of the ice, the bottom of the ice, and the bottom of the deposited slush.

The thickness of a river ice cover is highly variable and site specific. In addition, the occurrence of ice jams and hydraulic thickening, which are dynamic processes not included in the present thermal ice process model, can have a substantial effect on the thickness of the ice cover. Also, due to the fact that the available measurements are all in the vicinity of the Town of Peace River, the data does not provide enough information to attempt an ice thickness calibration or comparison at this time. With improved ice thickness measurement frequency and coverage along the study reach, as well as future development of the model to include the dynamic processes that affect the ice cover thickness, it would be more feasible to perform an analysis of the model that could benefit from this type of data.

3.12. SUMMARY OF APPLICABLE MODELING DATA

The period of record selected for application of the model to the historical record in Chapter 4 is the 1984/85 through 2003/04 winter seasons. This is essentially the period representing the current regulated conditions on the Peace River following the commission of the Peace Canyon Dam. A summary of the quality of the applicable input variables is provided in Table 3.11 and the availability of relevant calibration and validation data for the study period can be found in Table 3.12. The main consideration in regards to the input data is the 10 years for which the "typical" inflow water temperature profile was used as a substitute for incomplete or absent water temperature measurements at the Peace Canyon Dam. On the calibration and validation side, Table 3.12 clearly demonstrates the data limitations and the reason the majority of model validation relies on the ice front observations.

The thermal river ice process modeling data used in this study has been provided on a CD-ROM, which can be found in Appendix D. Also on the CD-ROM are the *River1D* output files generated during the model application discussed in Chapter 4 and Chapter 5.

Table 3.1 **Ice-related flood history at the Town of Peace River (source: Alberta Environment).**

Year	Problem	Contributing Factors	Damages
1973	Breakup ice jam	Believed to have been caused by Smoky River breakup	Unknown
1974	Breakup ice jam	Caused by Smoky River breakup	Unknown
1979	Breakup ice jam	Caused by Smoky River breakup	Minor flooding
1982	Freezeup ice jam	Low freezeup level; Rapid ice cover progression due to extreme cold; Water level fluctuations possibly a factor	Seepage flooding
1992	Freezeup ice jam	Very high freezeup levels; Sudden warming preceded secondary consolidation movement; Increase in discharge a possible factor	Severe flooding; Several million dollars in damages
1997	Breakup ice jam	Caused by Smoky River breakup; Possibly exacerbated by an ice run on the Peace River itself	Severe flooding; Several million dollars in damages
2005	Freezeup ice jam	High freezeup level	Prolonged basement flooding

Table 3.2 **Peace River bed slopes used in the *River1D* model based on the geometry developed by Hicks (1996).**

Reach (km downstream of Bennett Dam)	Bed Slope
28 to 83	0.00055
84 to 124	0.00048
125 to 165	0.00045
166 to 234	0.00036
235 to 542	0.00029
543 to 829	0.00009

Table 3.3 **Channel resistance values used in the present model and by Hicks (1996).**

Reach (km)	Manning's *n* (present model)	Reach (km)	Manning's *n* (Hicks, 1996)
28 to 152	0.025	28 to 75	0.030
153 to 376	0.030	75 to 210	0.045
377 to 560	0.035	210 to 345	0.025
561 to 829	0.025	345 to 829	0.020

Table 3.4 **Percent increases in winter discharges at selected locations along the Peace River.**

Location	Percent Increase in Observed Mean Discharge					
	Nov.	Dec.	Jan.	Feb.	Mar.	Apr.
Hudson Hope	103	326	367	364	377	142
Town of Peace River	65	234	287	308	323	46
Peace Point	40	193	200	250	272	104

Table 3.5 Available streamflow data along the Peace River.

Location	Available Data	Unavailable Data
Peace at Hudson Hope	Complete record from: Nov. 1, 1973 – Dec. 31, 1998	Jan. 1, 1999 – present
Peace above Pine River	Complete record from: May 29, 1979 – Dec. 31, 1985 July 23, 1986 – Dec. 31, 1998	Jan. 1, 1999 – present
Peace near Taylor	Complete record from: Nov. 1, 1973 – Dec. 31, 1998	Jan. 1, 1999 – present
Peace at Alces	Complete record from: Jan. 1, 1992 – Dec. 31, 1998	Jan. 1, 1999 – present
Peace at Dunvegan	Generally open water season data only (May – Oct. / Nov.): Sep. 27, 1974 – Dec. 31, 1998	Jan. 1, 1999 – present
Peace at Town of Peace River	Complete record from: Nov. 1, 1973 – Dec. 31, 1998	Jan. 1, 1999 – present
Peace at Peace Point	Complete record from: Nov. 1, 1973 – Dec. 31, 1998	Jan. 1, 1999 – present

Table 3.6 **Mean January flows of the Peace River tributaries monitored by the WSC.**

Location	Mean January Flow (m^3/s)
Halfway River near Farrell Creek	13.0
Moberly River near Fort St. John	1.61
Pine River at East Pine	32.8
Beaton River near Fort St. John	1.58
Kiskatinaw River near Farmington	0.83
Clear River near Bear Canyon	no winter record
Smoky River near Watino	44.4
Heart River near Nampa	0.19
Notikewin River at Manning	0.32
Boyer River near Fort Vermilion	no winter record
Ponton River above Boyer River	no winter record
Wabasca River at Walden Lake Road	14.5

Table 3.7 Available water temperature monitoring data along the Peace River.

Location	Available Record	Unavailable Data
Peace Canyon Dam	Complete ice season coverage: 1983, 1995, and 2000	1984 – 1988, 1998, and 2002 to present
	90% to 99% ice season coverage: 1977, 1981, 1991, 1992, and 1996	Various gaps in all other years but 1983, 1995, and 2000
Peace River at Alces River	Reasonably good (65% to 97%) coverage: Mar. 20, 2002 – Sept. 8, 2004	Prior to March 2002
Town of Peace River	Limited coverage (21% to 55%) of ice season from: Sep. 13, 2001 – Sept. 8, 2004	Prior to Sep. 2001

Table 3.8 Available air temperature record within the study area.

Station	Available Record	Unavailable Data
Fort St. John	1953 – 2004 (Oct. 1 – May 31)	N/A
Town of Peace River	1958 – 2004 (Oct. 1 – May 31)	N/A
High Level	1970 – 2004 (Oct. 1 – May 31)	N/A
Alces	Jan. 2, 1994 – Sep. 8, 2004	Prior to Jan. 2, 1994
Dunvegan	Nov. 1, 1999 – Sep. 8, 2004	Prior to Nov. 1, 1999

Table 3.9 Summary of Peace River ice front observation flights on record.

Season	First Observation	Last Observation	Number of Observations
2003/04	November 22	May 5	78
2002/03	December 2	May 2	62
2001/02	November 27	April 30	47
2000/01	December 14	April 24	37
1999/00	November 22	April 12	28
1998/99	December 4	April 25	40
1997/98	December 22	April 16	33
1996/97	November 26	April 22	30
1995/96	November 11	April 24	48
1994/95	November 29	April 21	38
1993/94	December 27	April 13	32
1992/93	December 18	April 17	29
1991/92	November 26	March 18	20
1990/91	November 28	April 17	15
1989/90	November 20	April 22	30
1988/89	December 7	April 23	15
1987/88	January 2	March 14	7
1986/87	November 19	April 5	9
1985/86	November 23	April 19	15
1984/85	November 10	May 3	25
1983/84	December 8	April 16	20
1982/83	November 23	March 26	44
1981/02	January 2	May 4	26
1980/81	N/A	N/A	0
1979/80	December 5	February 7	10
1978/79	December 20	May 1	26
1977/78	November 28	April 17	14

Season	First Observation	Last Observation	Number of Observations
1976/77	January 10	March 14	14
1975/76	December 12	April 13	16
1974/75	January 11	April 19	14
1973/74	December 12	April 20	4

Table 3.10 Summary of ice thickness measurements on the Peace River.

Year	Day	Measurement Location
1982/83	January 21	WSC gauge
	February 22	WSC gauge
	February 24	Shaftesbury Ferry crossing and Peace River Correctional Institute
	March 17	WSC gauge
1983/84	January 6	WSC gauge
	January 31	WSC gauge
	February 20	WSC gauge
	March 16	WSC gauge
1984/85	January 10	WSC gauge
	February 6	WSC gauge
	March 12	WSC gauge
1985/86	January 8	WSC gauge
	February 4	WSC gauge
	March 4	WSC gauge
2001/02	March 15	Peace River upstream of Smoky River

Table 3.11 **Summary of applicable model input data on the Peace River for the period of record selected.**

Season	Peace Canyon Dam		Fort St. John Town of Peace River High Level
	Discharge	Water Temperature	Air Temperature
2003/04	G	G	G
2002/03	G	G	G
2001/02	G	G	G
2000/01	G	G	G
1999/00	G	P; S	G
1998/99	G	P; S	G
1997/98	G	P; S	G
1996/97	G	P; S	G
1995/96	G	G	G
1994/95	G	G	G
1993/94	G	G	G
1992/93	G	G	G
1991/92	G	G	G
1990/91	G	G	G
1989/90	G	P; S	G
1988/89	G	P; S	G
1987/88	G	P; S	G
1986/87	G	P; S	G
1985/86	G	P; S	G
1984/85	G	P; S	G

Note: **G = good data; P = poor or no data; S = substituted "typical" water temperature profile**

Table 3.12 Summary of applicable model calibration and validation data on the Peace River for the period of record selected.

Season	Water Temperature		Number of Ice Front Observations	Other
	Alces	TPR		
2003/04	Oct. – May	Oct. – May	78	C – Jan. 1 and 9
2002/03	Oct. – May	Oct. – Feb.	62	
2001/02	Mar. – May	Oct. – Nov.	47	T – Smoky River 3/15
2000/01	N	N	37	
1999/00	N	N	28	
1998/99	N	N	40	
1997/98	N	N	33	
1996/97	N	N	30	
1995/96	N	N	48	
1994/95	N	N	38	
1993/94	N	N	32	
1992/93	N	N	29	
1991/92	N	N	20	
1990/91	N	N	15	
1989/90	N	N	30	
1988/89	N	N	15	
1987/88	N	N	7	
1986/87	N	N	9	
1985/86	N	N	15	T – WSC gauge (1/8, 2/4, 3/4)
1984/85	N	N	25	T – WSC gauge (1/10, 2/6, 3/12)

Note: TPR = Town of Peace River; N = no data; C = surface ice concentration; T = ice thickness (dates noted by month/day)

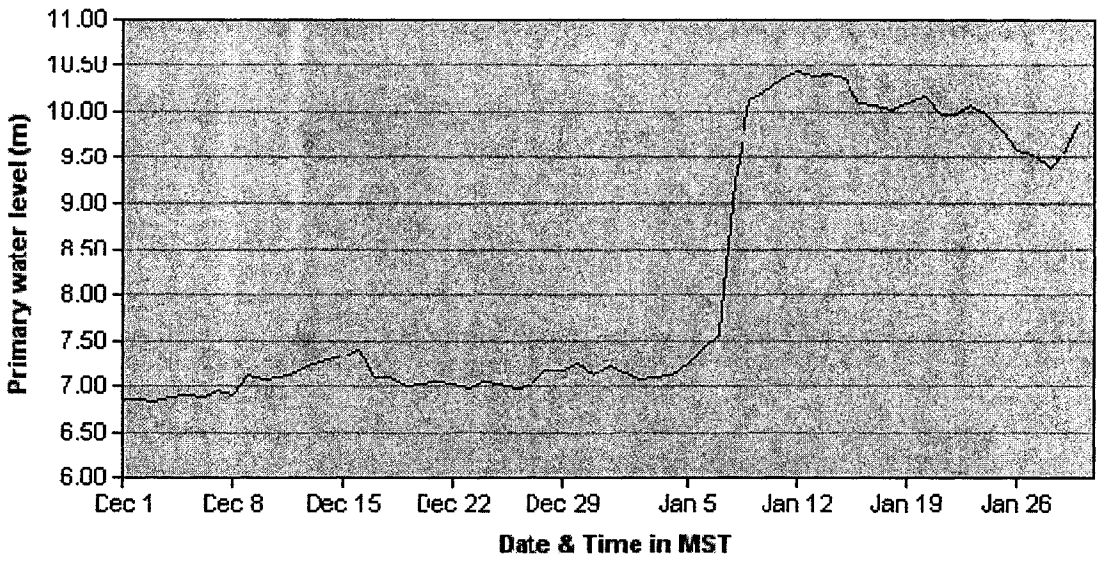

Figure 3.1 **Water level progression at the Town of Peace River through the arrival of the ice front during the 2003/04 winter season.**

(Source: Environment Canada Real-Time Hydrometric Data website - http://scitech.pyr.ec.gc.ca/waterweb/main.asp)

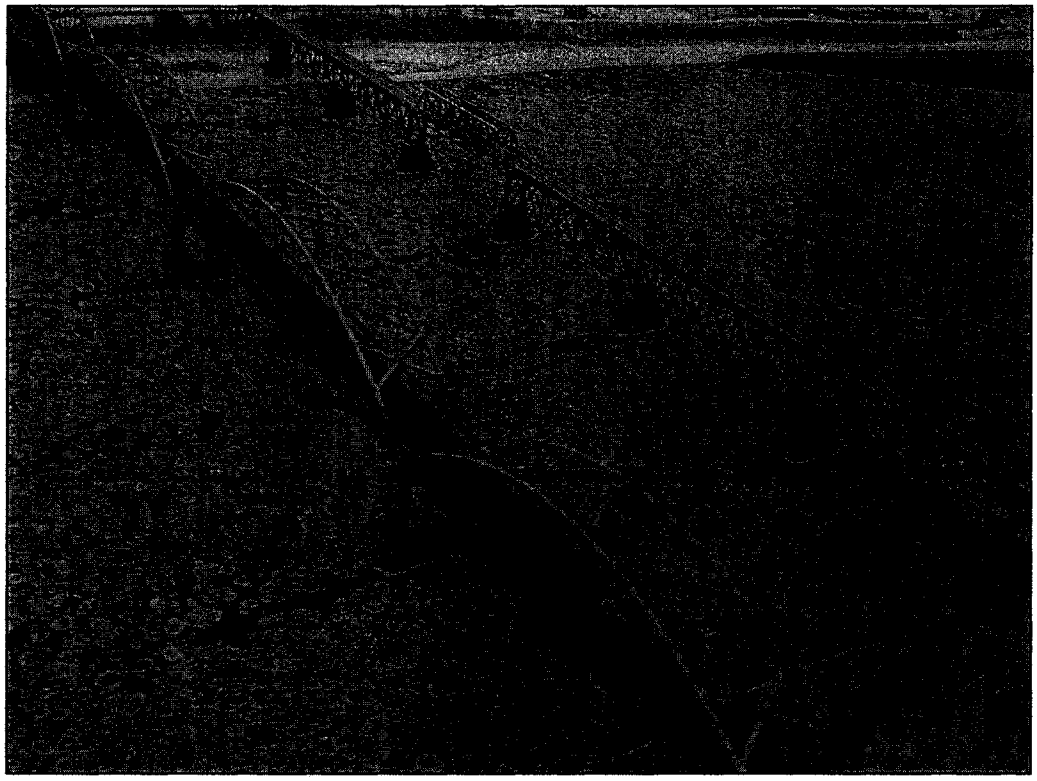

Figure 3.2 **Rail bridge over the Peace River at the Town of Peace River prior to freezeup (December 2004).**

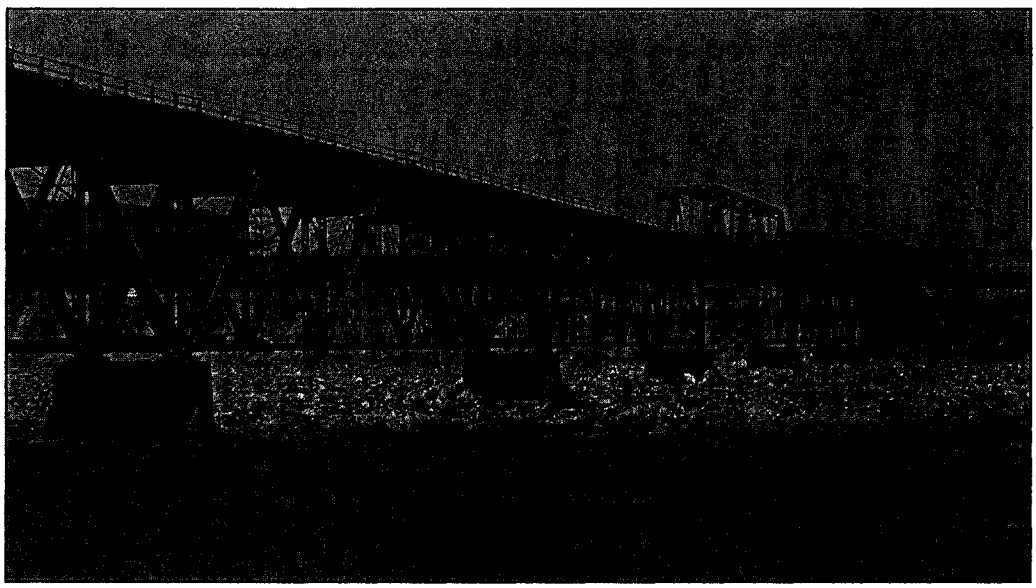

Figure 3.3 **Rail bridge over the Peace River at the Town of Peace River after freezeup (early January 2005).**

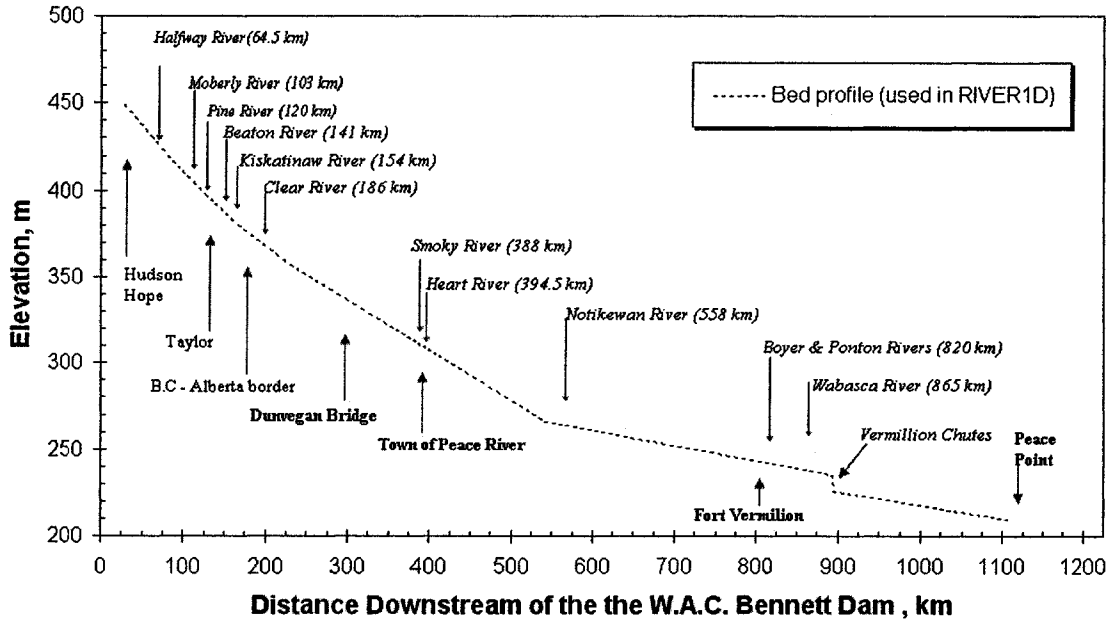

Figure 3.4 Peace River bed profile developed by Hicks (1996).

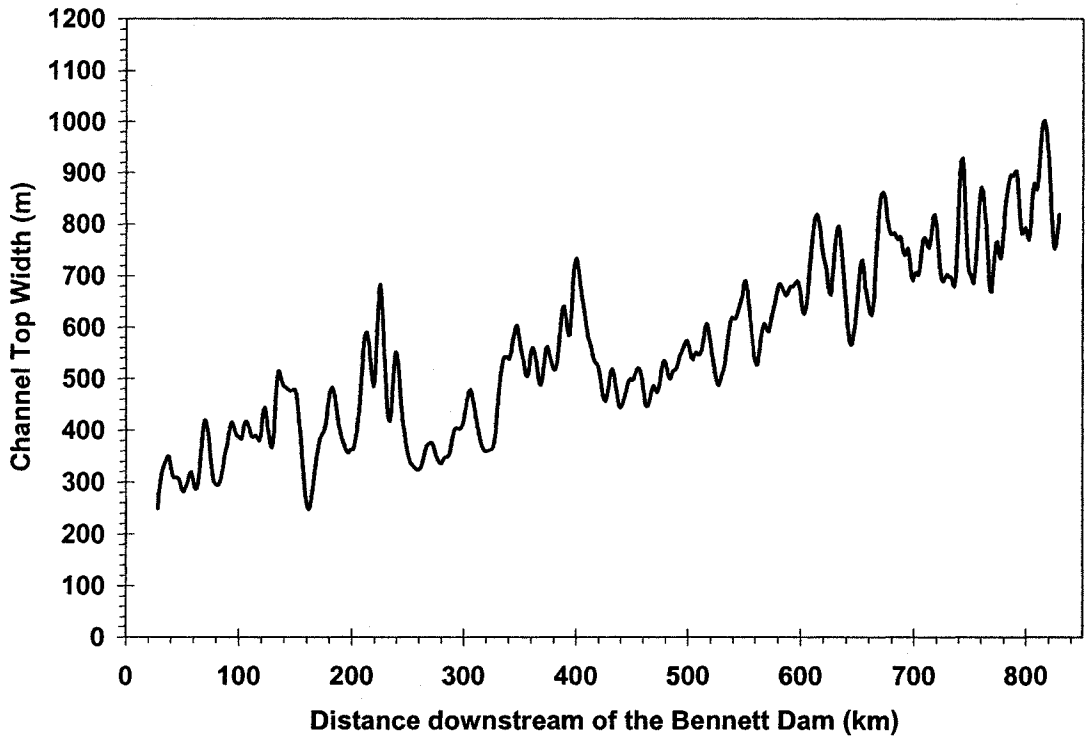

Figure 3.5 **Channel top width profile used in the *River1D* model based on the geometry developed by Hicks (1996).**

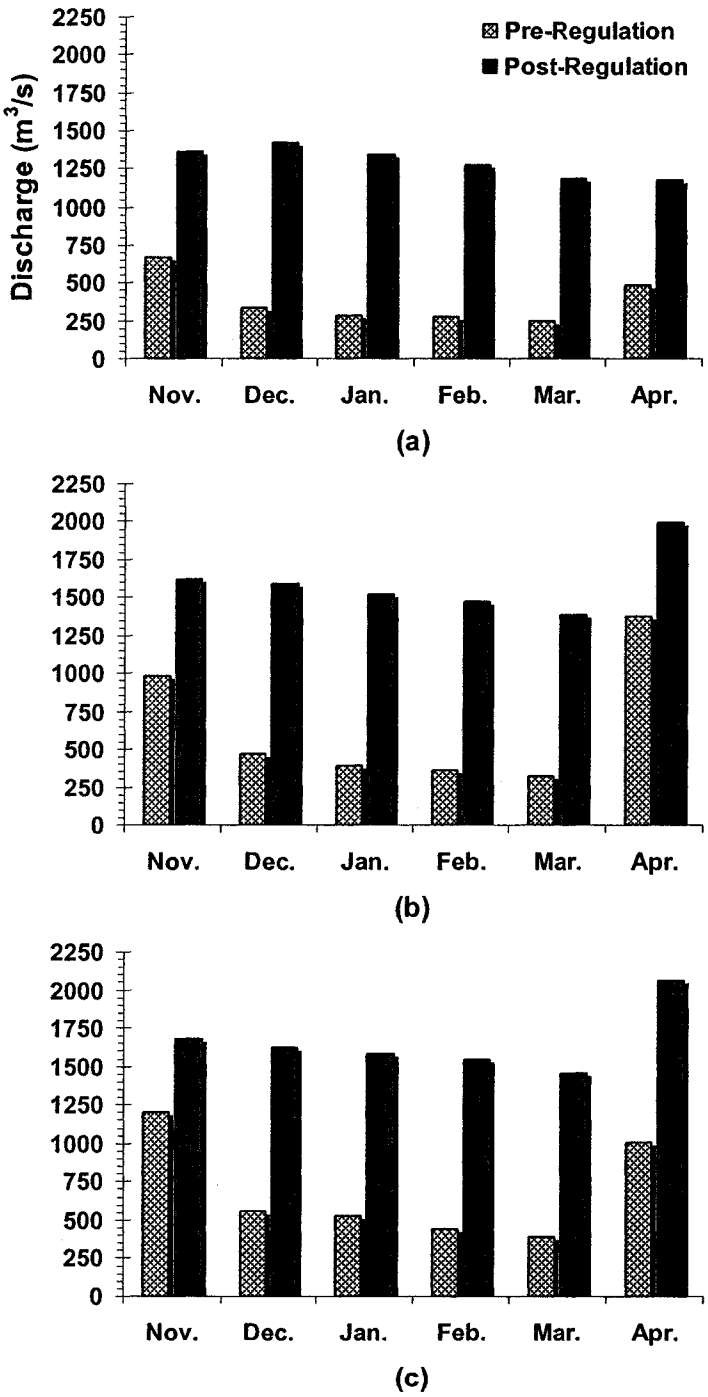

Figure 3.6 **Comparison of pre- and post-regulation winter discharges at: (a) Hudson Hope; (b) Town of Peace River; and (c) Peace Point.**

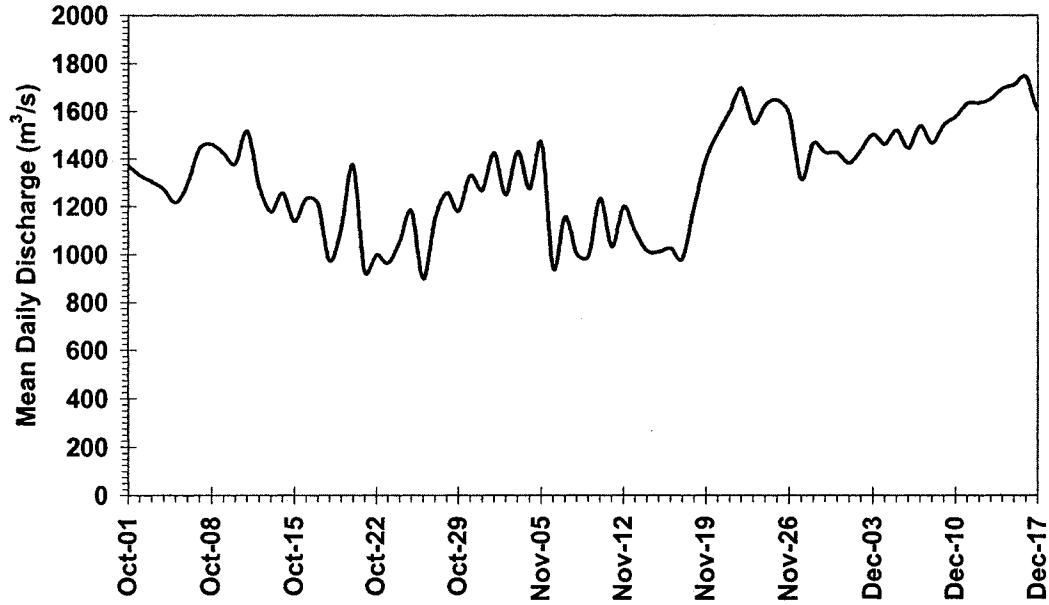

Figure 3.7 **Typical discharge variation at the headwaters the Peace River due to regulation and hydropeaking (source: 2003 data provided by Alberta Environment).**

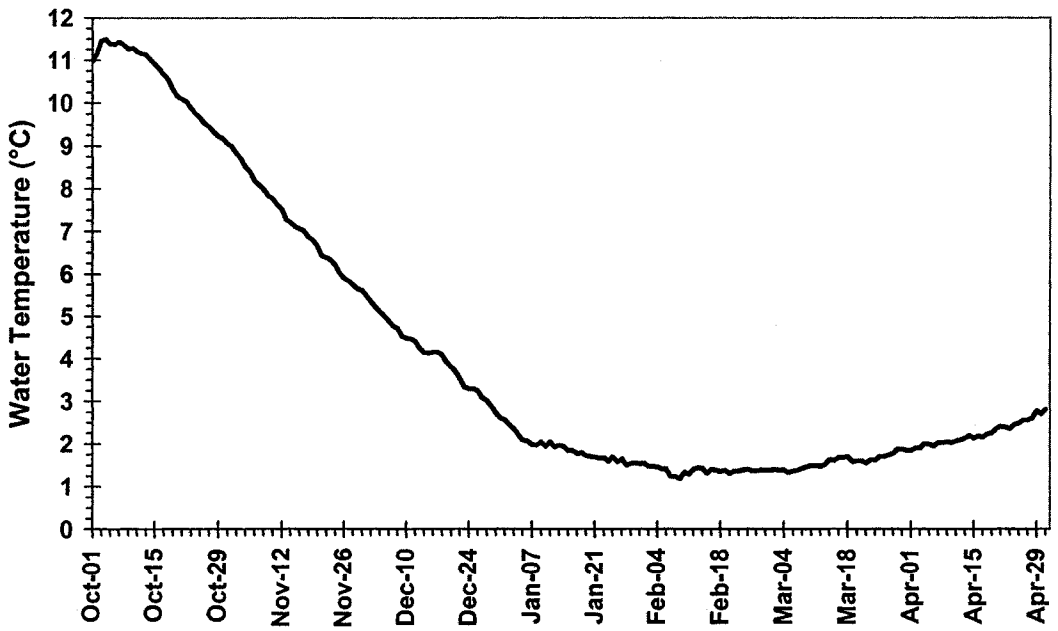

Figure 3.8 **Typical water temperature variation at the headwaters the Peace River due to the reservoir behind the Bennett Dam.**

CHAPTER 4 MODEL APPLICATION USING THE HISTORICAL RECORD

4.1. INTRODUCTION

Thermal river ice process model calibration is a multi-step process that involves the adjustment of several parameters that are characteristic of the study area being modeled. Since water temperature dominates ice formation and deterioration processes on a river, simulation results for this variable should be calibrated prior to and independent of ice conditions.

Calibration of the remaining solution variables, all dealing with ice conditions, depends on the amount and quality of observations available for comparison. In addition, the limitations of the present model (Section 2.6) must be taken into account. For this study, it was determined that calibration to observed ice front profiles (i.e. ice front location as a function of time) would be the most reasonable measure of the model's performance at this time considering the data availability and model limitation issues just mentioned.

As a result, this chapter describes the methodology of calibration and validation of the *River1D* thermal model for simulated water temperatures and ice front profiles. Reasonable calibration of ice concentration and thickness requires more data than is currently available, as well as further development of the present model to include dynamic processes.

4.2. MODEL RUN PARAMETERS

Unless otherwise noted, each simulation presented in this chapter and in Chapter 5 was run with the parameters outlined below. The general solution parameters discussed here are: the modeled domain; discretization; boundary conditions; time step; Courant number; upwinding; and numerical implicitness.

As mentioned previously, the modeled reach of the Peace River extended from an upstream boundary at Hudson Hope (28 kilometres downstream of the Bennett Dam) to Fort Vermilion (829 kilometres downstream of the Bennett Dam). This 801 kilometre river reach was composed of 802 computational nodes, spaced equally at 1 kilometre, that were derived by Hicks (1996) from topographic maps.

Several boundary conditions are required to run the thermal river ice process model. In terms of the hydraulic component, a discharge hydrograph based on the mean daily flow release data from the Peace Canyon Dam was used at the upstream boundary; at the downstream boundary, a constant water depth of 2.5 metres was used. For the thermal component, only upstream boundary conditions are required, as the model uses the applicable "natural" boundary conditions for water temperature and ice at the downstream boundary. Due to the effects of regulation, the water temperature at Hudson Hope is always above 0°C, which makes it possible to set all four upstream ice boundary conditions (suspended frazil concentration, surface ice concentration, and frazil and solid ice thicknesses) equal to zero. Therefore, the only thermal boundary condition required is the inflowing water temperature time series,

which was based on the mean daily water temperature data measured at the Peace Canyon Dam.

All simulations were run with a time step of twelve minutes (or 720 seconds) for the hydraulic, water temperature, and ice computations. This selection was made to keep the value of the Courant number below one, as this improves the accuracy of the simulation. For average discharge conditions of about 1400 m^3/s, the domain discretization and time step result in an average Courant number of 0.75.

An upwinding coefficient can also be specified under the finite element method used. This parameter can improve the solution of convection dominated problems such as the hydraulic and thermal river ice processes being modeled in this study. The default value of ω = 0.25 was applied to all model components. In addition, θ = 0.5 was used for all computations. This numerical implicitness value represents trapezoidal time integration of the finite element method (Equation [2.43]), which has been shown by Hicks and Steffler (1992) to be second order accurate for a range of transient conditions.

The water temperature and ice mass conservation computations have been limited to a maximum of eight iterations each per time step in the model. Generally, each full winter simulation of the study reach of the Peace River takes approximately 18 to 20 hours to execute on a 2.8 Gigahertz desktop computer with 512 Megabytes of random access memory. Prior to simulated ice formation on the river, time step computations progress relatively quickly. However, particularly once the simulated ice front has formed, time step computations slow substantially as a greater number of

iterations are required to resolve the discontinuity between moving and stationary ice, thus increasing computing time.

4.3. CALIBRATION METHODOLOGY

Calibration and validation runs were developed for the most recent winter seasons: 2003/04 and 2002/03. The data collection program undertaken by BC Hydro and Alberta Environment in these most recent years has yielded the most comprehensive data sets in the historical record for the Peace River, particularly in terms of the availability of calibration and validation data for water temperature. As mentioned in Section 4.1, the present calibration scheme (discussed below) focuses on the performance of both the water temperature and ice front simulations.

Water temperature is calibrated by adjusting the linear heat transfer coefficient and constant, h_{wa} and k_{wa}, respectively. Previous and present studies on the Peace River (e.g. Andres, 1993) indicate that the constant k_{wa} can be neglected or set equal to zero and typical values for the coefficient h_{wa} range from 10 to 20 $W/m^2/°C$.

Several physical parameters affect the ice front profile simulation result; typical values for each of these were used in the calibration and validation runs (Table 4.1). Frazil floe porosity and initial pan thickness are properties that have been observed and measured in the field in recent years, so the values adopted were considered adequate for this analysis without further adjustment or calibration. Aside from h_{wa}, only the juxtaposition parameter, P_{jux}, was adjusted to calibrate the simulated ice front profile to the observed data.

4.4. CALIBRATION RESULTS

4.4.1. Water Temperature

Water temperature observations on the Peace River are currently limited to two locations: the Water Survey of Canada gauges at Alces River (164 km downstream of the Bennett Dam) and the Town of Peace River (396 km downstream of the Bennett Dam). Unfortunately, the length of record is limited only to the last two ice seasons, 2002/03 and 2003/04. The 2002/03 season was selected for calibration and the 2003/04 for validation of the water temperature model.

Based on the range for the heat exchange coefficient suggested by Andres (1993), water temperature calibration runs were performed for h_{wa} values of 10, 15, and 20 $W/m^2/°C$. A key objective of this type of study is to see if one value of h_{wa} would be appropriate for all years and the whole river. However, the lack of water temperature calibration and validation data downstream of the Town of Peace River makes it difficult to assess whether one value is appropriate along the entire river reach.

Figure 4.1 shows the simulation results at the Alces gauge site for the early winter period for these calibration runs. All three calibration runs agree with the measured data reasonably well, particularly from December onward. Recalling that water temperature cooling to zero degrees Celsius governs the formation of river ice, it is important to evaluate the simulation results in terms of the time this condition is reached at a given location along the river, compared to the observations. The

location (or locations) along the river where the water temperature drops to the freezing point is referred to as the "zero degree isotherm". In particular, achieving the best possible match for the arrival of the zero degree isotherm at the Town of Peace River, approximately mid-way along the study reach, was considered an important criterion in the calibration process.

Considering this criterion, using $h_{wa} = 20\ W/m^2/°C$ does not seem to be the best selection since a zero degree isotherm is predicted on December 29, much earlier than the observed date of January 20. Figure 4.2 shows the water temperature profile over the course of the entire winter season of 2002/03, including spring thaw. A value of $h_{wa} = 15\ W/m^2/°C$ appears to be very representative of the late winter and early spring conditions as well, based on the results shown.

Examining the simulation results shown in Figure 4.1 for the Alces site more closely, the model appears to over-predict water temperatures in the early freezeup period and under-predict them from January 1 onward. This is likely due to the questionable quality of the water temperature measurements at the Peace Canyon Dam, used for the inflow thermal boundary condition, and may also be due to the fact that these measurements are not made precisely at the upstream boundary of the model. In fact there is a small distance on the order of about five kilometres between the Peace Canyon Dam and the model boundary at Hudson Hope. This would tend to explain the warmer simulated water temperatures in the early freezeup period (i.e. November), as some additional cooling is not accounted for between the dam and the model boundary. The remaining discrepancies between the simulations and the

observations may be attributable to the limited air temperature input data coverage (discussed in Section 3.7).

As Figure 4.3 shows, comparing the simulated water temperature profiles at the Town of Peace River to the observations, it appears that $h_{wa} = 20\ W/m^2/°C$ results in premature water cooling around November 12 and an early arrival of the zero degree isotherm on December 18, compared to its observed arrival on December 21. The simulation run with $h_{wa} = 15\ W/m^2/°C$, however, matches the observed date the water temperature reached zero degrees at the Town of Peace River extremely well, both on December 21 and again, following a brief period of warm weather, on January 10. Unfortunately, as shown in Figure 4.4, late winter and early spring water temperature data is not available for comparison due to failure of the instrument on January 29 as a result of ice cover consolidation at the Town of Peace River.

Again, looking more closely at the overall quality of the simulation results in Figure 4.3, it should be noted that at the Town of Peace River, the simulated water temperature profiles display both positive and negative peaks that are not seen in the measured data. This behaviour is possibly a result of the boundary condition issue described above. In this case, it is more probably due to the air temperature representation of the reach upstream of this location, since one would expect that the upstream boundary condition disparity would become less important at locations farther downstream and the effect of spatial variability of air temperature would dominate the error.

Based on the three simulated profile's ability to accurately model the arrival of the zero degree isotherm at the Town of Peace River, h_{wa} = 15 $W/m^2/°C$ was selected as an appropriate calibration of the model's heat transfer component for the purposes of this study. Comparatively, h_{wa} = 10 $W/m^2/°C$ resulted in much slower water cooling than the observations indicated, while h_{wa} = 20 $W/m^2/°C$ caused premature arrival of the zero degree isotherm at both Alces and the Town of Peace River.

4.4.2. Ice Front Location

Using the calibrated water to air heat exchange coefficient from Section 4.4.1 above, the ice front profile for the same season, 2002/03, was calibrated by adjusting the juxtaposition parameter, P_{jux}. The juxtaposition parameter controls the rate of ice cover advance during freezeup and provides an approximate means to empirically account for the effects of the crushing and under-turning of pans as they arrive at the ice front, as well as the occurrence of secondary consolidation movements.

The calibration objective was to match the date the ice cover reached the Town of Peace River (at freezeup and breakup) as closely as possible, as opposed to obtaining overall agreement between the observations and the simulation result. Since the Town of Peace River is the subject of most of the post-regulation ice-related flood history along the Peace River and is mid-way along the study reach, achieving model accuracy at this location was considered a priority.

During the initial calibration process, it was found that, over a range of reasonable P_{jux} values (i.e. one to three), the simulated ice front progressed more rapidly than observed in the river reach downstream of the Town of Peace River. Rather than using unreasonably large values of P_{jux} to reduce the rate of ice cover advance, the heat exchange coefficient for the northern reach of the river (upstream of the Town of Peace River) was reduced from 15 $W/m^2/°C$, which was calibrated for the southern river reach up to the Town of Peace River, to 10 $W/m^2/°C$ for all simulation runs. This change does not affect the simulated water temperatures at Alces or the Town of Peace River, shown previously.

A series of juxtaposition parameter values were selected for the calibration runs, beginning with P_{jux} = 1.5. The initial simulation run with this juxtaposition parameter value indicates a much earlier arrival of the ice front at the Town of Peace River, labeled as "TPR" on the ice front profile plot shown in Figure 4.5. Progressively larger values for the juxtaposition parameter in half-increments were run until the simulated ice front arrived the Town of Peace River later than the observations indicated, as shown by the ice front profile corresponding to P_{jux} = 3.0 in Figure 4.5.

Based on the simulated profiles' agreement with the observations in the one- to two-week period leading up to the arrival of the ice front at the Town, the best value for P_{jux} was found to be 2.5. This value was adopted and used in all subsequent simulation runs.

4.5. MODEL VALIDATION

4.5.1. Water Temperature

A validation run for the water temperature simulation was done for the only other year where adequate water temperature measurements were available, the 2003/04 winter season. The result of this simulation at the Alces gauge, shown in Figure 4.6, demonstrates good agreement with the observed arrival of the zero degree isotherm at this location, but the simulated water temperatures appear to be warmer than the measured ones, more so than for the calibration year.

Figure 4.7 illustrates much better overall agreement at the Town of Peace River gauge. While the simulation displays some notable peaks that are inconsistent with the observations, the arrival of the zero degree isotherm remains in good agreement with the observations on at least two out of three instances during this freezeup season.

4.5.2. Ice Front Location

The historical monitoring program on the Peace River provides an extensive record of the seasonal progression and recession of the ice front. As discussed earlier, the progression of the ice front with time was documented in a series of reconnaissance flights conducted throughout the winter. As described in Section 3.9, this information dates back to 1973/74; therefore some model validation data for this variable is available for the full record.

For the present analysis of the model, the twenty most recent years of historical data (1984/85 through 2003/04) were used to validate the model. In terms of input data, daily mean inflow discharge and air temperature values were available for this 20-year period; however, the historical record was not complete for inflow water temperature. In these cases, the "typical" water temperature profile discussed in Section 3.6 was used in place of any incomplete or unavailable inflow water temperature boundary conditions (see Table 3.11).

It is important to note that the distance of about five kilometres between the upstream boundary of the modeled domain at Hudson Hope and the Peace Canyon Dam (where the boundary condition data comes from) has no significant effect on the simulated ice front profiles. This was confirmed by artificially extending the modeled domain five kilometres upstream and re-running a very cold year (1995/96), which is one that would be expected to be most affected by this excluded reach of the river. The result of this simulation is shown in Figure 4.8. The only deviation in the simulated profiles occurs during the spring breakup period, where the profile for the modeled river reach extended up to the Peace Canyon Dam is less representative of the observed data during breakup.

The initial validation run, for the 2003/04 season, is shown in Figure 4.9. The simulated ice front profile agrees well with the observations made during the early freezeup period. However, into the month of January, the simulated ice front advances much more quickly than the observations indicate. Initially it was thought that this was because consolidation events in January shortened the length of the ice cover beyond what the juxtaposition parameter could account for. However, in

reviewing the ice front calibration runs shown in Figure 4.5, it is seen that the maximum extent of the ice cover remains relatively consistent regardless of the juxtaposition parameter used. This would seem to indicate that the exclusion of ice cover consolidation in the present model is not directly responsible for the greater maximum extent of ice cover simulated both in 2002/03 and 2003/04.

A second consideration was that the simulated water temperatures were too cool in the reach upstream of the Town of Peace River, resulting in ice production where there should not have been any. While this may be partly responsible for the extent of the ice front profile, as shown in the water temperature calibration and validation, the location of the zero degree isotherm appears to agree reasonably well with the observations. However, more water temperature measurements both along the river and over more years are required to make a conclusive determination.

Based on a qualitative assessment of the model's ability to simulate the ice front progression and recession on the Peace River, it seems clear that the model is performing very well, considering the data limitations and the level of physics incorporated into the model. An overview of the remaining eighteen years simulated is provided in Figure 4.10, Figure 4.11, and Figure 4.12 (full-size plots for each of these years can be found in Appendix A). A summary of the simulation quality for each of the historical seasons modeled can be found in Table 4.2.

As the table indicates, the majority of the simulations produced good overall agreement with the observed data, and the over-extension of the simulated ice cover described earlier in regards to the 2002/03 and 2003/04 seasons is much less of an

issue in the other years modeled. Based on this assessment, the calibration using a value of P_{jux} = 2.5, h_{wa} = 15 $W/m^2/°C$ in the river reach up to the Town of Peace River, and h_{wa} = 10 $W/m^2/°C$ downstream of the Town of Peace River is considered valid for reasonably simulating the Peace River ice cover in most years. For this reason, it is also considered reasonable to use the present model to evaluate the potential effects of climate change on the ice regime of the Peace River. Overcoming the various data limitations discussed earlier, permitting a more intensive calibration of the model, would improve the model's overall performance and consistency. However, this is not possible at this time and does not prohibit the objectives of this study from being met.

4.6. SENSITIVITY ANALYSIS

The sensitivities of the five ice-related parameters, whose values were adopted based on previous and current work of fellow researchers (see Table 4.1), to the simulated ice front profile were tested. This was done by establishing a reasonable range of values for each physical parameter and re-running the simulation for a selected season (1995/96) using two additional values for each parameter. The 1995/96 season was selected because the simulated ice front profile agreed very well with the observations for that year, thus any differences due to the parameter sensitivity would be most apparent. A list of the parameters along with their calibrated values from Section 4.4.2, the ranges established, and the values tested are provided in Table 4.3.

Figure 4.13 illustrates the sensitivity of the simulated ice front profile to the frazil floe porosity value chosen. Based on the differences between the three simulated profiles, it appears that the chosen floe porosity within the generally accepted range of values has a moderate effect on the simulated ice front profile. Since more porous frazil slush rising to the surface would tend to take up more space than the same amount of less porous frazil slush, higher porosity values tend to increase the rate of ice front advance, as evident in the Figure. In the vertical direction, the ice cover would also be expected to develop much thicker for the same reasons. This could explain why the simulation (Figure 4.13) suggests slower thermal melt of the spring ice cover that was formed from more porous frazil slush, because thicker ice would take longer to melt.

Considering the initial thickness of frazil pans at the surface, Figure 4.14 shows that this parameter has a significant effect on the simulated ice front profile. In particular, values smaller than 0.3 metres seem to make the simulated ice front unstable such that it changes locations very rapidly. Using the same argument as for floe porosity, in terms of the amount of space a given amount of ice occupies, smaller initial floe thicknesses would tend to cover the width of the river more quickly with ice and generally take up more surface space. This is verified by the more rapid rate of freezeup advance on the left-hand side of these curves as initial floe thickness is decreased. It is also possible that thinner initial ice thickness results in thinner simulated ice covers overall, which would explain how the ice cover could retreat so quickly due to warm conditions around February 18 and March 19. Similarly, thicker initial floes seem to damp the fluctuation of the ice front location during brief warm

weather spells, which can be seen very clearly in the Figure between December 22 and January 5.

The remaining three parameters appear to have a negligible impact on the simulated ice front profile. The rate of frazil rise, at least within the order of magnitude suggested by others using comparable models, does not affect ice front profile through the entire freezeup period (Figure 4.15). Even less important to the ice front profile advance and retreat is the roughness of the ice cover (Figure 4.16). All three simulations produced virtually identical results. It would be expected that this parameter would be more significant to simulated water levels because it is a factor that directly impacts the hydraulic computations but does not appear in any of the thermal model equations. Thus any modeling effort focusing on water level issues would have to look carefully at calibration of this parameter. Finally, as Figure 4.17 shows, any value for the ice-water heat exchange parameter within the range suggested in the literature will produce very similar results. Increasing values for this parameter will increase the rate of ice cover melt but will have no effect on the advance of the ice cover.

4.7. SUMMARY OF RESULTS

The application of the present model to the historical record of the Peace River using calibrated values of the heat transfer coefficient equal to 15 $W/m^2/°C$ and a juxtaposition parameter equal to 2.5 produces good overall results for both water temperature and ice front location, where data is available for comparison. In some cases, the simulated water temperatures reach extremes that are not observed in the

data and the simulated ice front progresses farther upstream than observed. Both of these issues are likely attributable to the limitations of the air and water temperature input data. However, some of the river ice processes neglected in the present model may also be a factor in the quality and consistency of the ice front simulations.

Evaluating the ice front simulation results more quantitatively, the comparison between observed and simulated date of freezeup at the Town of Peace River, mid-way along the study reach, can be considered. Table 4.4 outlines this information. While some of the errors in individual years are large, the average modeled freezeup date (January 6) over the twenty years simulated is within two-and-a-half days of the observed mean freezeup date (January 8) for the same period.

Similarly, comparing the observed and simulated dates of breakup at the same location, on average the model again performs well. As Table 4.5 indicates, the mean simulated date of breakup at the Town of Peace River (April 6) is 1.2 days earlier than the observed date, April 8, over the period of record simulated.

In terms of ice cover duration at the Town of Peace River, the simulated values compared to the observed are shown in Table 4.6. The mean error of 1.5 days (longer) duration of simulated ice cover at this location is considered to be very good in light of the data limitations and river ice processes that are excluded from the present model.

Finally, looking at the maximum extent of the ice cover simulated and observed, the model is performing reasonably well. As Table 4.7 indicates, the model

is simulating an average ice cover length that is 57 kilometres longer than that observed over the period of record simulated. In terms of the length of the modeled river reach, this error represents about 7%.

In summary, having applied the model to the past twenty years of historical record on the Peace River, the overall ability of the *River1D* thermal river ice process model to simulate water temperatures and, in particular, ice front location, is validated by the comparison of freezeup and breakup dates at the Town of Peace River. The consistency of the results from year-to-year could be improved with more comprehensive air and water temperature monitoring along the study reach. Nevertheless, it does seem reasonable to conclude that the present model could be applied to climate change situations, from which an investigation into the effects of climate change on the dates of freezeup and breakup and the duration of the ice cover at the Town of Peace River could be based. Chapter 5 will look at this very issue in detail.

Table 4.1 Summary of ice modeling parameters for which typical values for were adopted.

Ice Modeling Parameter	Adopted Value	Basis
Frazil floe porosity, e_f	0.5	Field measurements by Alberta Environment and BC Hydro
Initial frazil pan thickness, t'_f	0.30 m	
Frazil rise parameter, η	0.0001 *m/s*	Advice from Alberta Environment
Manning's n for ice cover	0.020	Nezhikhovskiy (1964)
Ice-water heat exchange coefficient, α_{iw}	1187 $W{\cdot}s^{0.8}/m^{2.6}/°C$	Ashton (1973)

Table 4.2 **Summary of simulated ice front profile agreement with observations for historical seasons modeled.**

Season	Overall Simulation Performance
2003/04	Fair
2002/03	Fair
2001/02	Good
2000/01	Good
1999/00	Good
1998/99	Good
1997/98	Good
1996/97	Very Good
1995/96	Very Good
1994/95	Good
1993/94	Good
1992/93	Good
1991/92	Good
1990/91	Good
1989/90	Good
1988/89	Very Good
1987/88	Good
1986/87	Good
1985/86	Fair
1984/85	Good

Table 4.3 Ice parameters adjusted for the sensitivity analysis.

Ice Parameter	Adopted Value	Reasonable Range	Additional Values Tested
Frazil floe porosity, e_f	0.5	0.5 to 0.9	0.7; 0.9
Initial frazil pan thickness, t'_f	0.3	0.1 to 0.5	0.1; 0.5
Frazil rise parameter, η	0.0001	0.0001 to 0.0003	0.0002; 0.0003
Manning's n for ice cover	0.020	0.020 to 0.035	0.027; 0.035
Ice-water heat exchange coefficient, α_{iw}	1187	1000 to 1300	1000; 1300

Table 4.4 Simulated and observed dates of freezeup at the Town of Peace River based on the historical record.

Season	Observed freezeup date	Simulated freezeup date	Error (days)
2003/04	January 11	January 4	-6
2002/03	January 27	January 25	-2
2001/02	January 19	December 30	-20
2000/01	February 11	January 24	-17
1999/00	January 16	January 12	-5
1998/99	January 6	January 1	-5
1997/98	January 13	January 17	4
1996/97	December 21	December 20	-1
1995/96	December 10	December 9	-1
1994/95	January 6	January 7	1
1993/94	January 13	January 14	1
1992/93	December 31	January 4	5
1991/92	February 14	January 27	-18
1990/91	December 18	December 22	4
1989/90	January 10	December 21	-20
1988/89	December 30	January 6	6
1987/88	January 31	January 18	-13
1986/87	January 21	January 7	-15
1985/86	December 4	January 23	51
1984/85	December 22	December 23	1
Mean	**January 8**	**January 6**	**-2.5***

***Note:** **The mean error shown is the average of the error column.**

Table 4.5 Simulated and observed dates of breakup at the Town of Peace River based on the historical record.

Season	Observed freezeup date	Simulated freezeup date	Error (days)
2003/04	April 4	April 7	3
2002/03	April 14	April 17	3
2001/02	April 22	April 22	0
2000/01	March 18	April 7	20
1999/00	March 31	March 28	-3
1998/99	April 3	April 4	1
1997/98	March 30	April 3	4
1996/97	May 4	April 20	-14
1995/96	April 21	April 17	-3
1994/95	April 21	April 19	-2
1993/94	April 13	April 1	-11
1992/93	March 29	March 25	-4
1991/92	February 29	March 14	14
1990/91	April 18	April 9	-9
1989/90	April 10	April 8	-2
1988/89	April 24	April 19	-4
1987/88	March 12	March 9	-3
1986/87	April 6	April 5	-1
1985/86	April 24	April 19	-5
1984/85	April 12	April 4	-8
Mean	**April 8**	**April 6**	**-1.2***

***Note:** **The mean error shown is the average of the error column.**

Table 4.6 **Simulated and observed duration of ice cover at the Town of Peace River based on the historical record.**

Season	Observed Ice Cover Duration (days)	Simulated Ice Cover Duration (days)	Error (days)
2003/04	85	94	9
2002/03	78	83	5
2001/02	93	113	20
2000/01	36	73	37
1999/00	75	77	2
1998/99	87	93	6
1997/98	76	76	0
1996/97	134	120	-14
1995/96	132	130	-2
1994/95	105	102	-2
1993/94	89	78	-11
1992/93	88	80	-8
1991/92	15	47	32
1990/91	121	108	-13
1989/90	89	107	18
1988/89	114	104	-10
1987/88	41	51	10
1986/87	74	88	14
1985/86	141	86	-55
1984/85	111	102	-9
Mean	**89**	**91**	**1.5***

***Note:** **The mean error shown is the average of the error column.**

Table 4.7 **Simulated and observed maximum extent of ice cover, as minimum distance (in kilometres) downstream of the Bennett Dam, based on the historical record.**

Season	Observed Maximum Extent (km)	Simulated Maximum Extent (km)	Error (km)
2003/04	217	116	101
2002/03	228	106	122
2001/02	207	156	51
2000/01	298	183	115
1999/00	219	166	53
1998/99	217	154	63
1997/98	280	200	80
1996/97	125	130	-5
1995/96	101	111	-10
1994/95	196	141	55
1993/94	160	127	33
1992/93	190	181	9
1991/92	325	230	95
1990/91	138	118	20
1989/90	163	118	45
1988/89	161	125	36
1987/88	269	157	112
1986/87	282	178	103
1985/86	165	124	41
1984/85	121	99	22
Mean	**203**	**146**	**57***

* **Note:** **The mean error shown is the average of the error column.**

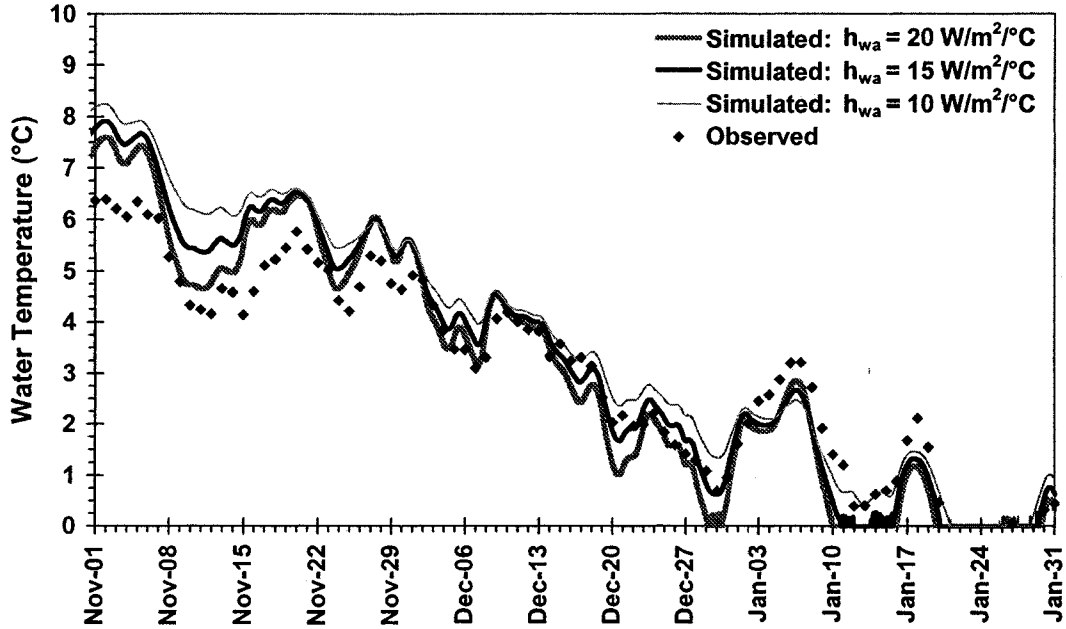

Figure 4.1 **Peace River water temperature calibration to the Alces gauge (2002/03).**

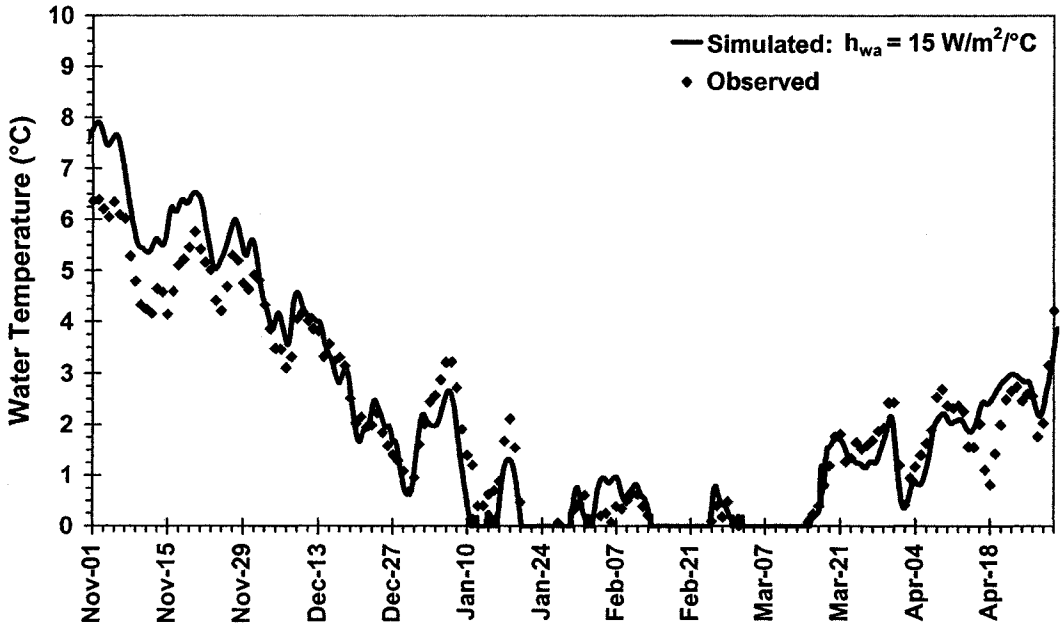

Figure 4.2 **Calibrated water temperature profile at the Alces gauge for the entire 2002/03 winter season.**

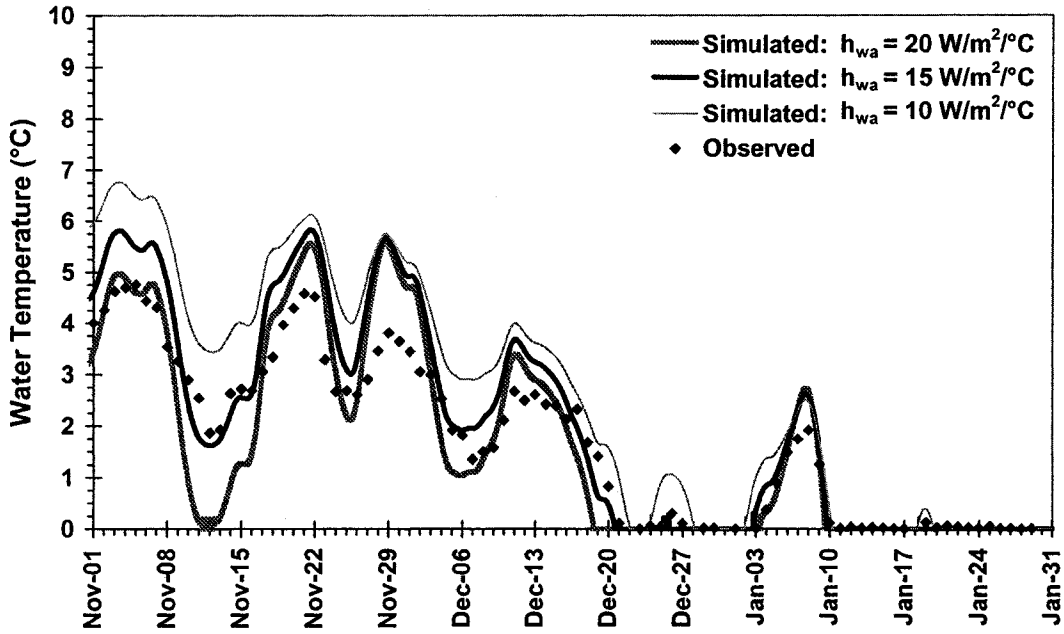

Figure 4.3 **Peace River water temperature calibration to the Town of Peace River gauge (2002/03).**

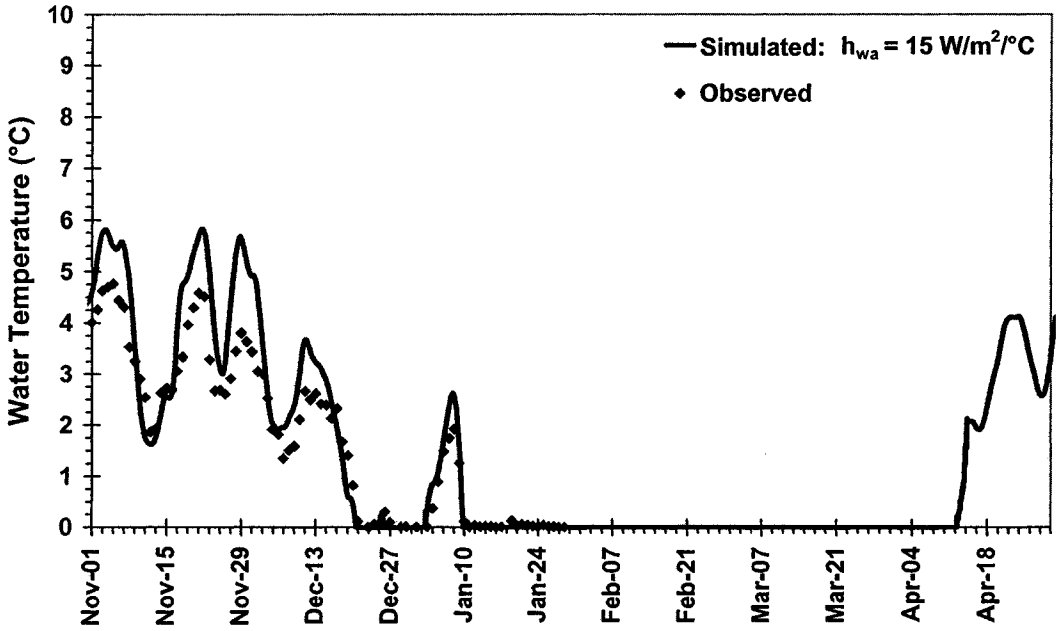

Figure 4.4 **Calibrated water temperature profile at the Town of Peace River gauge for the entire 2002/03 winter season.**

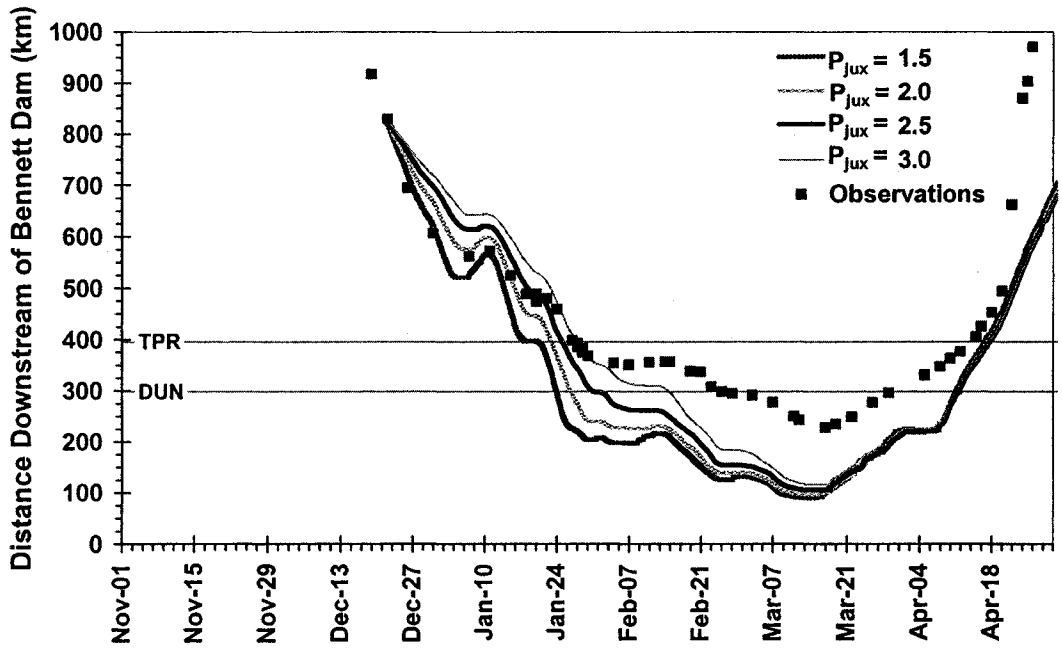

Figure 4.5 **Ice front profile calibration to 2002/03 ice season observations. (TPR: Town of Peace River, 396 km; DUN: Dunvegan, 298 km)**

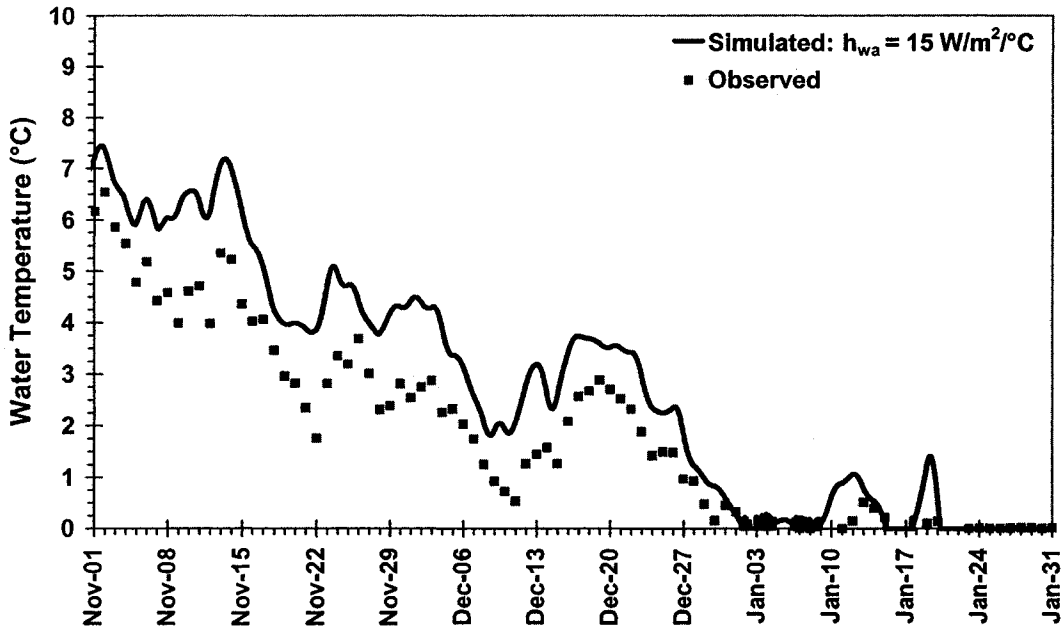

Figure 4.6 **Water temperature validation at Alces using $h_{wa} = 15\ W/m^2/°C$ and 2003/04 freezeup data.**

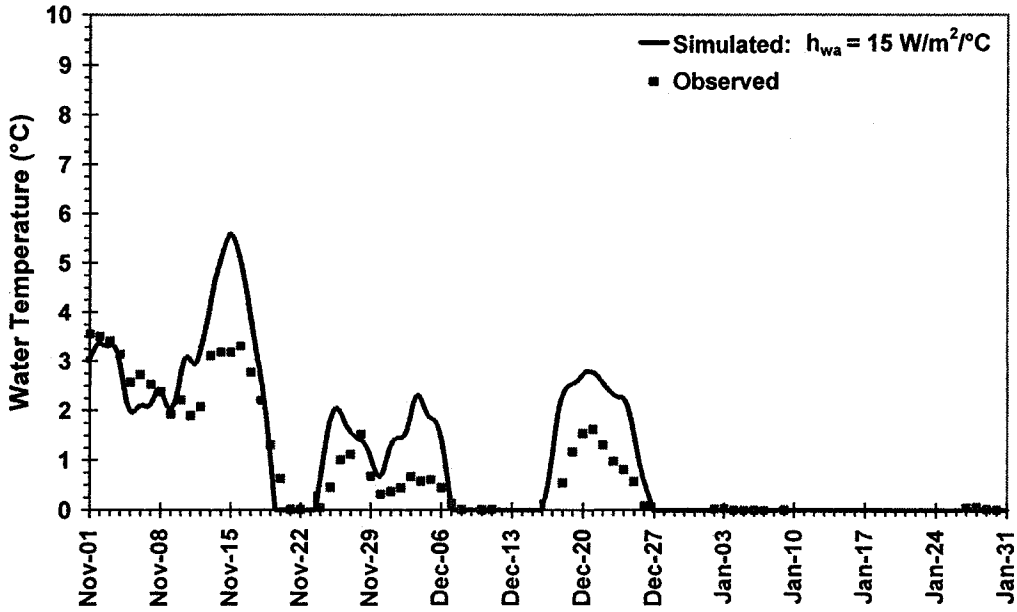

Figure 4.7 **Water temperature validation at the Town of Peace River using $h_{wa} = 15\ W/m^2/°C$ and 2003/04 freezeup data.**

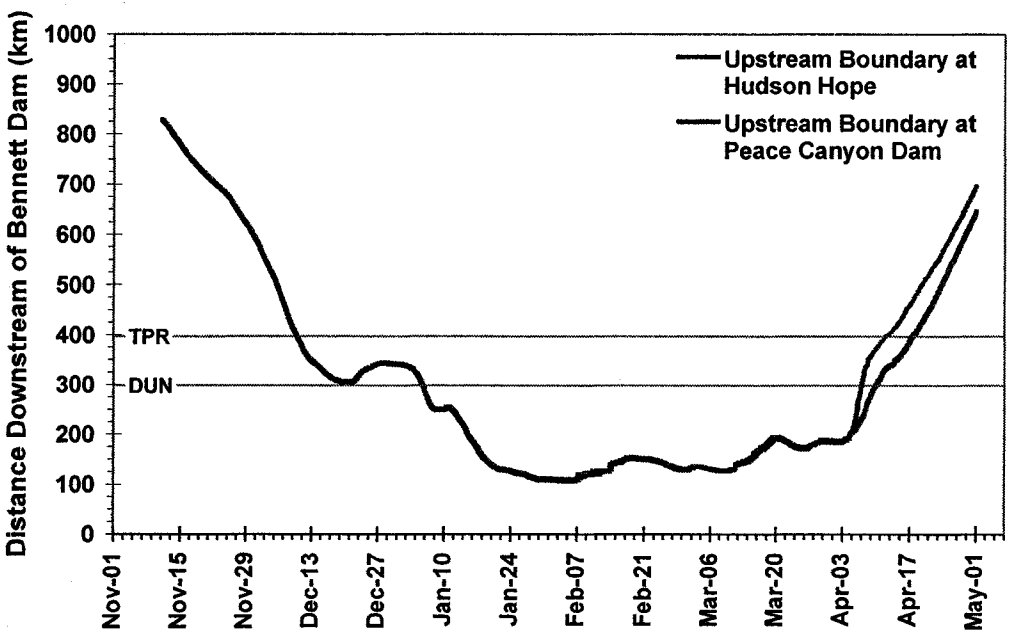

Figure 4.8 **Effect of locating the upstream modeled boundary at Hudson Hope versus at the Peace Canyon Dam on the simulated ice front profile using 1995/96 ice season data.**

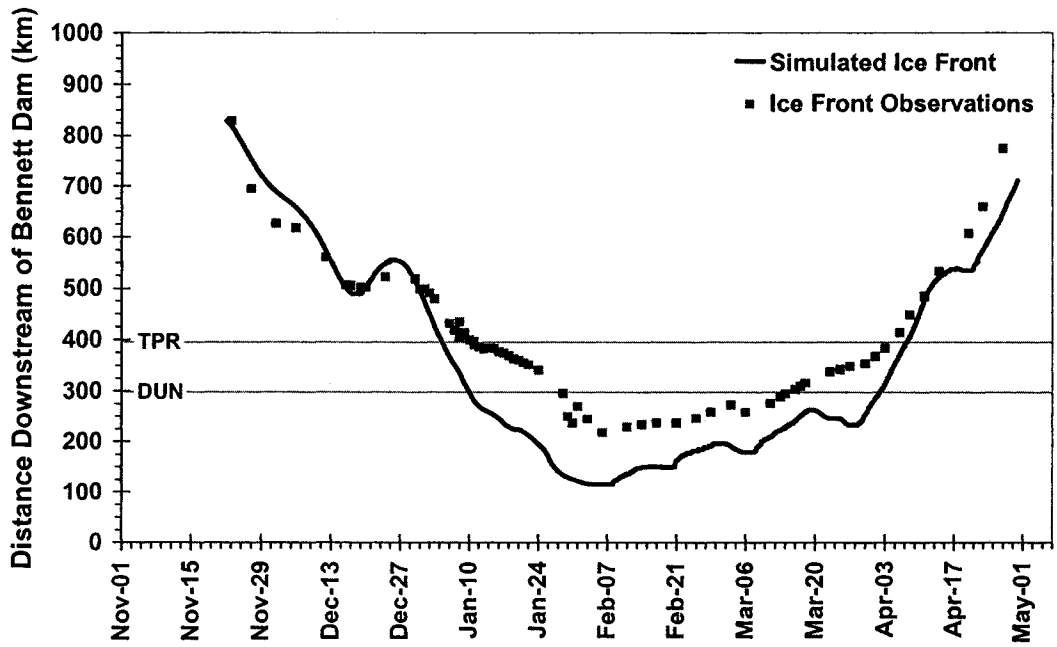

Figure 4.9 **Ice front profile validation using P_{jux} = 2.5 and 2003/04 ice season data.**

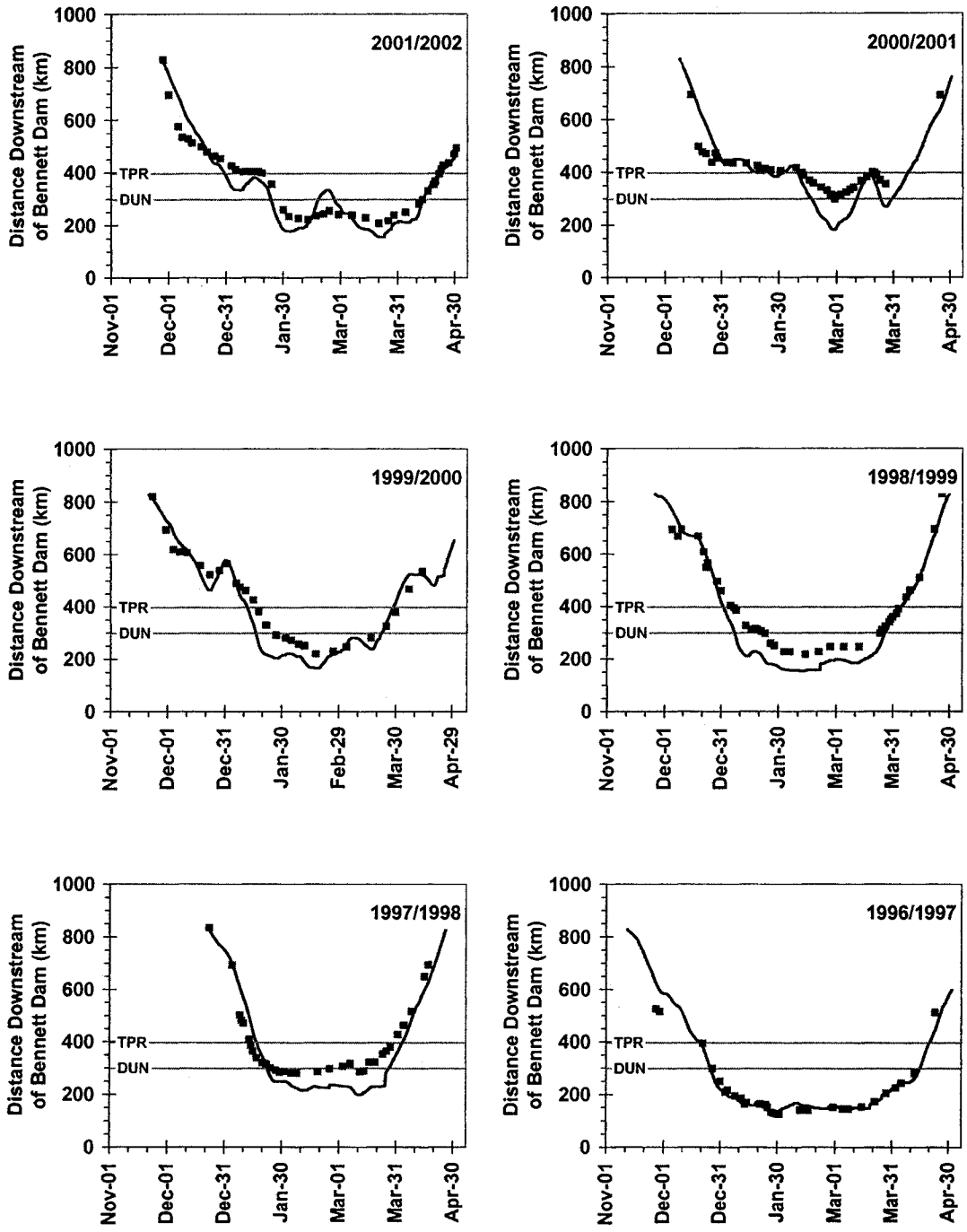

Figure 4.10 Peace River simulated ice front profile validation for historical ice seasons 2001/02 through 1996/97.

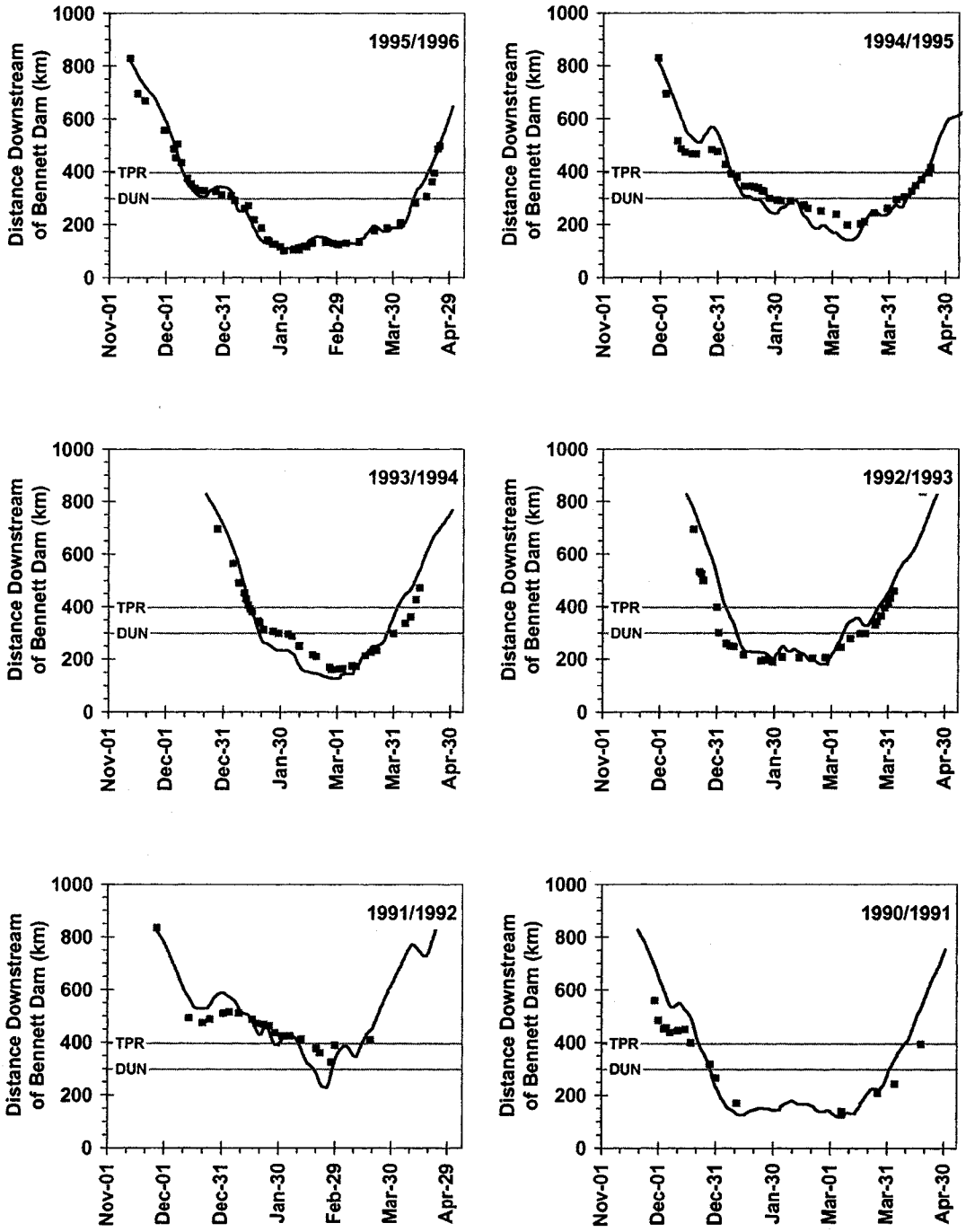

Figure 4.11 Peace River simulated ice front profile validation for historical ice seasons 1995/96 through 1990/91.

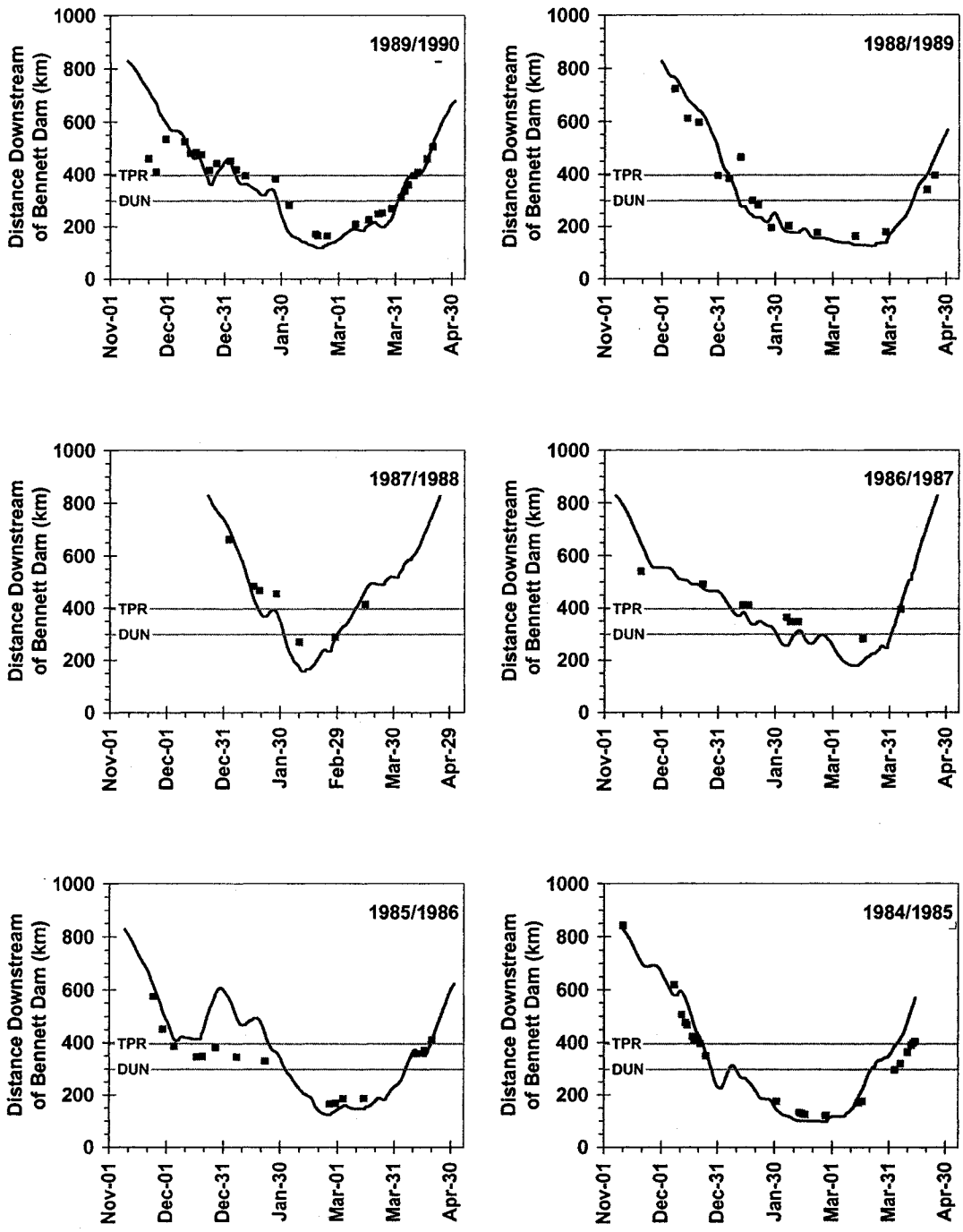

Figure 4.12 Peace River simulated ice front profile validation for historical ice seasons 1989/90 through 1984/85.

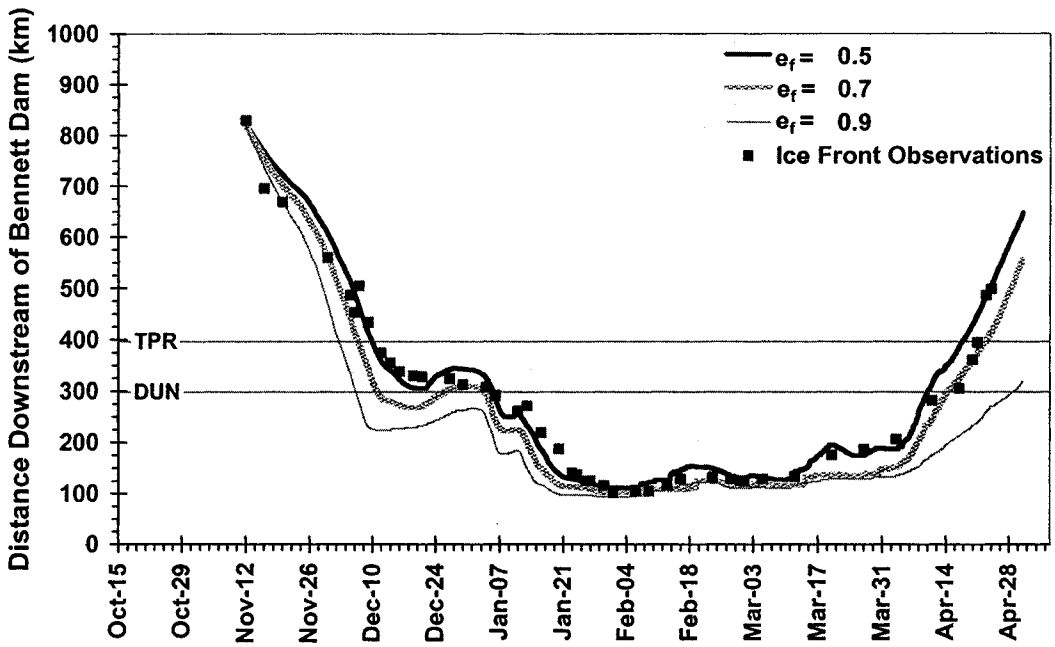

Figure 4.13 Sensitivity of simulated ice front profile to frazil floe porosity, e_f.

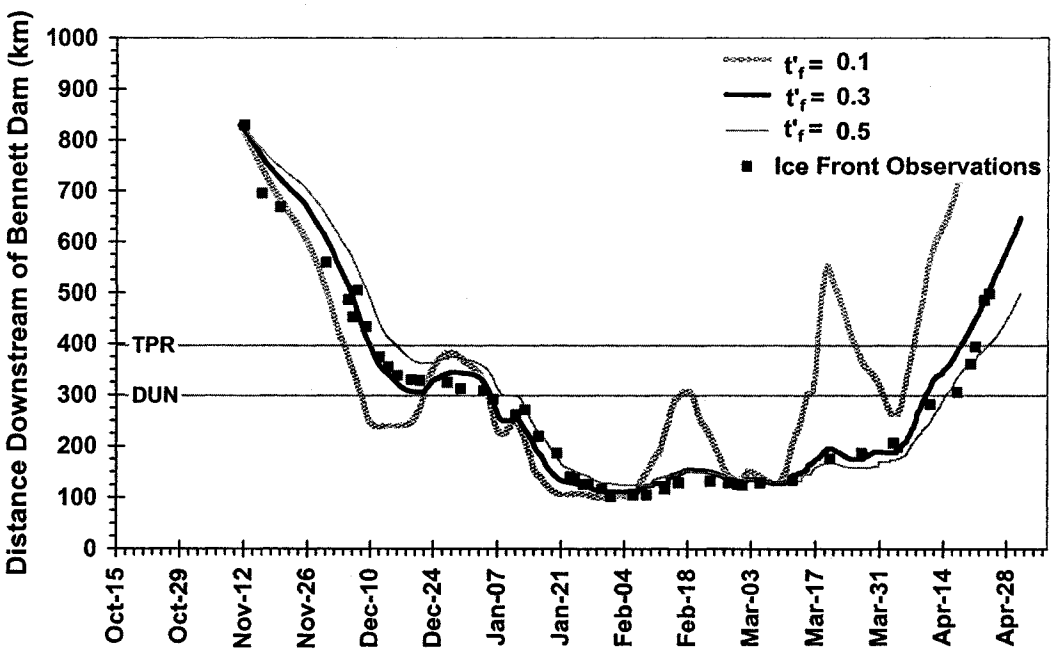

Figure 4.14 Sensitivity of simulated ice front profile to initial frazil pan thickness, t'_f.

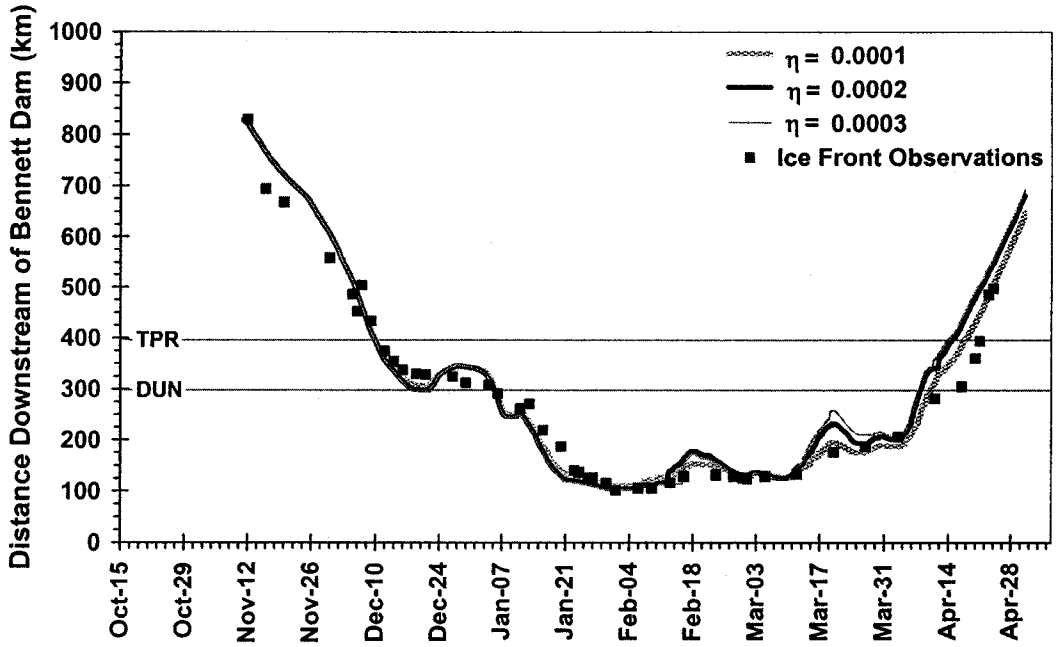

Figure 4.15 Sensitivity of simulated ice front profile to frazil rise parameter, η.

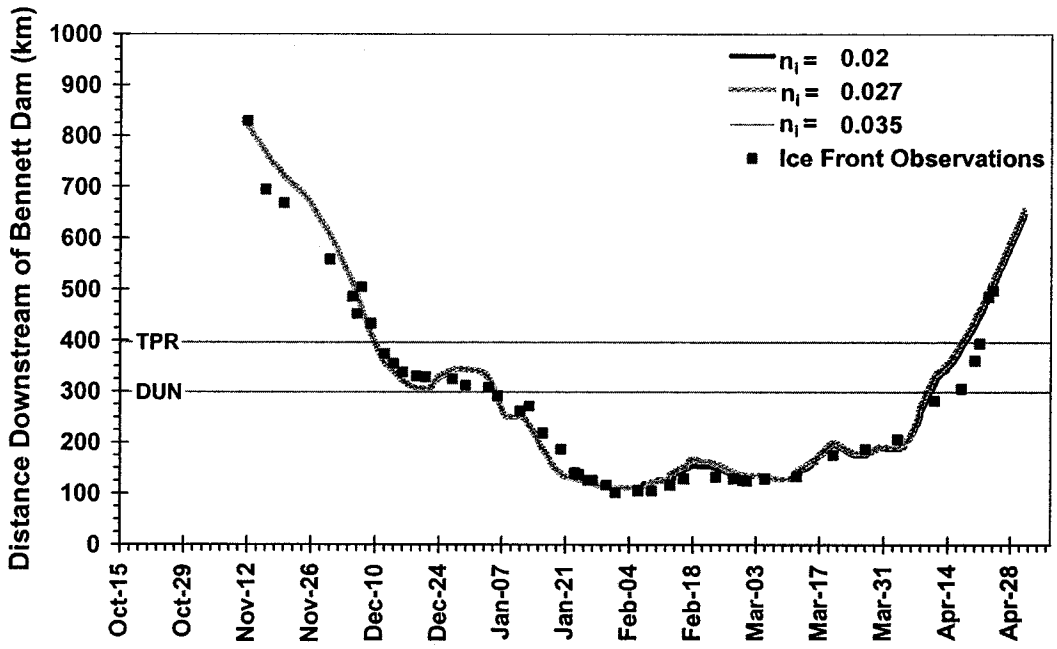

Figure 4.16 Sensitivity of simulated ice front profile to Manning's ice cover roughness, n_i.

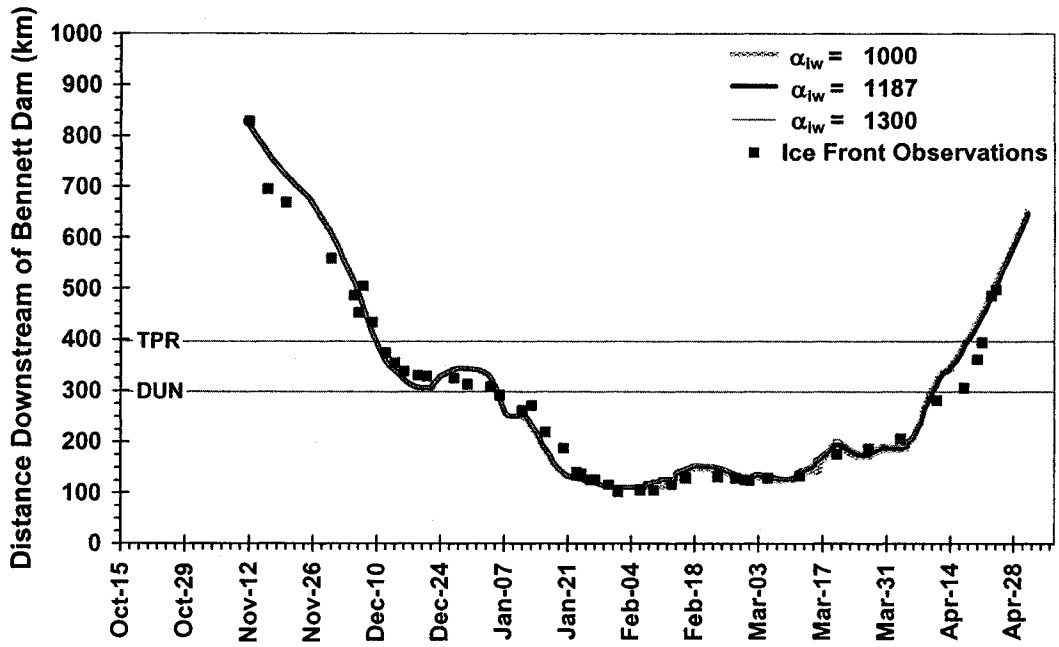

Figure 4.17 Sensitivity of simulated ice front profile to ice-water heat exchange parameter, α_{iw}.

CHAPTER 5 MODEL APPLICATION TO A CLIMATE CHANGE SCENARIO

5.1. INTRODUCTION

The CGCM2 climate model was selected to assess the impact of climate change on the historical winter seasons modeled. This model is one of a series of climate simulation models developed by the Canadian Centre for Climate Modelling and Analysis (CCCma). CGCM2 is a second generation coupled global climate model and is based on the first generation model (CGCM1). Some improvements have been made to the CGCM2 model: according to the CCCma (2005), these changes include an improved ocean mixing parameterization and the inclusion of sea-ice dynamics.

Two standard future climate scenarios (from the Intergovernmental Panel on Climate Change (IPCC) Special Report on Emissions Scenarios (SRES)) have been run with the CGCM2 model and were made available for use in this study by MAGS: the "A2" and "B2" scenarios. The "A2" scenario, compared to the "B2" scenario, is based upon projections of larger population growth and higher cumulative carbon dioxide (CO_2) emissions over the period 1990 to 2100. The "A2" scenario was selected for investigation in this study on its basis of greater severity. Appendix C provides a detailed description of the premise behind the "A2" scenario.

Three future benchmark years are established in each of the two scenarios: 2010, 2050, and 2080. The mid-range projection to 2050 was selected for this climate

change analysis since 2010 is considered too near and 2080 too far into the future for this initial winter regime comparison.

5.2. EFFECTS OF THE SELECTED CLIMATE CHANGE SCEANARIO ON MODEL INPUT

The climate change data obtained from MAGS provided grid-based future projections for two climate variables, air temperature and precipitation. Töyrä and Pietroniro (2003) provide a detailed description of the grid generation and resolution of this data. In this study, only the effects of future air temperatures on the river ice regime of the Peace River have been considered. Although precipitation has some bearing on river ice processes, there is insufficient historical precipitation data from which to base future projections.

Air temperature is the primary driving force for river ice formation and deterioration considered in this study. However, climate warming can also have secondary impacts on reservoir outflow water temperatures and dates of bridging. Warmer air temperatures, elevated water temperatures entering the Peace River, and delayed initiation (bridging) of the ice cover each tend to reduce the extent and duration of ice cover along the Peace River.

5.2.1. Air Temperature

For the scenario considered, the projected effect of climate change on warmer air temperatures is particularly significant in the northern regions of Canada, such as

the Peace River study area. To capture this effect, the meteorological stations at Fort St. John, the Town of Peace River, and High Level were located on the grid developed by Töyrä and Pietroniro (2003) by latitude and longitude so that the appropriate spatial air temperature increases from the CGCM2 model would be applied. The air temperature increase for the grid cell belonging to each station was used directly; no interpolation between grid centres was applied.

Table 5.1 presents the mean monthly air temperature increases at the three stations used to model the historical winter seasons on the Peace River. Figure 5.1 illustrates the difference between the historical and future "A2" climate mean monthly air temperatures for the months of October through May. Immediately apparent is the relative magnitude of the December, January, February, and March temperature increases, relative to the October and November ones. In light of this, one would expect that early winter freezeup processes would be less affected by this climate change scenario than those occurring in the December through March winter period.

For this climate change analysis, the mean monthly air temperature increases indicated in Table 5.1 were simply added to the mean daily air temperature record for corresponding months of each of the historical seasons modeled. In other words, the degree of warming predicted by the CGCM2 model was applied in a stepwise fashion, with no transitioning of the air temperature increases from one month to the next. The adjusted air temperatures are thus a future climate comparison to each of the past winter seasons, but should not be considered a prediction of future conditions in a particular year, such as 2050.

5.2.2. Inflow Water Temperature

It is possible that climate warming could elevate the reservoir water temperature in the Bennett and/or Peace Canyon Dam reservoirs, shifting the mean discharge water temperature profile (Figure 3.8) upward. However, assessing the impact of climate change on large reservoirs is a complex task that is beyond the scope of this river ice engineering study.

Although this matter has not been addressed in detail, its importance has been evaluated, in a general sense, with a supplementary sensitivity analysis. The 1995/96 simulation was repeated with the inflow water temperature time series at the upstream boundary increased uniformly by 0.5°C and 1.0°C, values considered within the realm of possibility based on intuitive judgment.

Figure 5.2 shows the results of the reservoir water temperature sensitivity analysis. As anticipated, the increasing water temperatures at the headwaters of the Peace River result in an upward shift of the ice front profile. However, this change has little effect on the early winter freezeup conditions. The effect of warmer water temperatures is much more pronounced in the late winter and during spring melt.

5.2.3. Date of Bridging

The conditions that will initiate a stationary ice cover are not fully explained by the research available to-date. The attempts that have been made to understand bridging involve empirical correlations to accumulated degree-days of freezing

(ADD_F) at or near the typical bridging location. The relationship between accumulated degree days of freezing at High Level and the observed date of bridging is shown in Figure 5.3. Although the coefficient of determination is reasonable at 0.74, it is not considered sufficient to reliably predict the bridging date because this relationship does not alone provide a deterministic criterion for bridging, which is the primary need in this case.

Due to this difficulty, it is commonplace for river ice modelers to simply rely on observed date of bridging as an input boundary condition. This has severely limited the ability of present models to predict future conditions, such as those resulting from climate change. In order to conduct better analyses, an acceptable bridging criterion needs to be established.

Due to the lack of research available to address this need, the initial efforts to run climate change scenarios for this study simply assumed no change in date of bridging. This assumption is certainly conservative, as later bridging would intuitively be expected to further shorten the duration and maximum extent of ice cover along the Peace River, in addition to the reduction in ice production due to a warmer climate. Therefore, as part of this study, a new bridging criterion was developed. This method looks at the relationship between the accumulated degree days of freezing at High Level after the zero degree isotherm reached the bridging location at Fort Vermilion and the concentration of ice required to initiate bridging. The former is an independent variable that can be calculated based on the air temperature and simulation results for water temperature; it is a measure of the border ice growth (i.e. channel constricting) potential at the bridging site.

To investigate this criterion, a sample of seven years with a range of observed bridging dates from as early as November 11 to as late as December 22 were selected from the historical series. The accumulated degree days of freezing at High Level after the arrival of the zero degree isotherm at Fort Vermilion at each of the reported bridging dates was computed and plotted against the simulated ice concentration at the observed date of bridging. The result is shown in Figure 5.4. This method provides a reasonably reliable, deterministic bridging criterion for the Peace River, based on information that can be easily assembled. One factor remains excluded from the proposed bridging criterion: discharge. Higher discharges would tend to impede bridging while lower discharges would encourage bridging at lower concentrations. This factor could be investigated to further refine the relationship, once more data becomes available.

It is important to consider this methodology in terms of its ability to predict bridging in terms of days, rather than in terms of the ice concentration versus accumulated degree days of freezing at High Level after the zero degree isotherm reached the bridging location at Fort Vermilion. To accomplish this, the proposed criterion was applied to the seven sample years from which it was developed, and a date of bridging was calculated for each. These dates were compared to the observed dates in the historical record, as shown in Figure 5.5. The indication is that this method returns a date of bridging accurate to two days or better in all but one of the test cases, where low discharge and cold early November weather is suspected to have resulted in a very early freezeup.

5.3. SIMULATED ICE FRONT PROFILES UNDER CLIMATE CHANGE CONDITIONS

As mentioned previously, the initial climate change comparison simulations were based on unchanged bridging dates, which was the only assumption available at the time. This complete set of climate change simulations can be found in Appendix B.

Six representative years were selected for climate change re-analysis using the method developed to compute and adjust the date of bridging (Section 5.2.3). The most recent three years with relatively good input data and observations were chosen along with the two years for which the historical simulations agreed with the ice front observations extremely well and one more average year. Applying this method results in the adjusted bridging dates summarised in Table 5.2.

This sample was deemed sufficient to form a general conclusion as to the significance of the change in date of bridging and its impact on the Peace River ice cover formation. The results for the six years selected are presented in this section together with their corresponding profiles from the initial climate change analysis.

The 2003/04 climate change comparison for the original analysis that did not considered delayed bridging is shown as a dashed line in Figure 5.6. The upward shift of the future climate ice front profile above the historical profile is clearly significant, meaning less ice cover on the river throughout the winter. Also shown in Figure 5.6 is the future climate simulation (solid line) with the bridging date delayed by 39 days, as predicted by the bridging criterion. Surprisingly, the two climate change profiles are

quite similar, with the exception of the left half of the ice front profile, which represents advance of the ice cover in the upstream direction during freezeup. The delay in date of bridging does not seem to have a dramatic effect on the maximum extent or the thermal recession of the ice cover. The influence of the delayed initiation of ice cover seems to extend no farther than delaying the dates of freezeup along the river.

The same characteristics are evident for the 2002/03 simulations as shown in Figure 5.7. In this case, delaying the date of bridging by 30 days drastically changes the advancing portion of the ice front profile, but the timing and location of the maximum ice cover extent remain unaffected. Again, the recession of the ice cover looks the same in both cases.

For 2001/02, the calculated 36-day delay in bridging date under climate change conditions combines with a mid-winter warm weather period in the middle of February to drastically change the two future climate freezeup profiles shown in Figure 5.8. As with the other cases, the remainder of these two climate change profiles looks nearly identical, from about March 10 onward.

The initial formation of the ice cover in 1996/97 was earlier than average, but a comparable delay of 39 days in the date of bridging under future climate conditions is predicted by the bridging criterion, despite the less significant magnitude of November air temperature warming. This results in drastically different freezeup profiles under historical and future climate conditions, as shown in Figure 5.9. Again,

the late-winter and spring profile of the ice front looks quite similar regardless of the bridging date used.

In contrast to 1996/97, the very early freezeup that occurred in 1995/96 results in a less significant delay of only 13 days in date of bridging in response to the un-seasonably cold early November air temperatures across the entire study area. Both climate change profiles for this year (Figure 5.10) suggest much less notable shifts in the overall ice front profile over the historical one. This is most likely due to the much more prolonged cold weather that was experienced in this year. In fact, the total degree days of freezing (from October 1 through May 31) at High Level was 3020°C·days in 1995/96, compared to the average of 2356°C·days over the period of record dating back to 1970/71. Similarly, at the Town of Peace River, located more centrally within the study area, the 1995/96 total degree days of freezing was 2235°C·days, where the mean over the period of record dating back to 1970/71 is 1545°C·days.

Finally, the 1994/95 simulations shown in Figure 5.11 are consistent with all of the previous cases shown, except perhaps 1995/96 for the reasons described above. In this year, the date of bridging was delayed by 35 days under future climate conditions, which changes the freezeup ice front profile substantially. This set of simulations reinforces the conclusion suggesting that a delayed date of bridging under future climate conditions has no significant effect on the peak extent of the ice cover and the timing of ice cover retreat in the spring, compared to the effects attributable to air temperature warming. Rather, its only cumulative effect is on the arrival of the ice front during freezeup.

5.4. SUMMARY OF RESULTS

As mentioned in Section 5.2.1, this climate change analysis does not predict ice conditions in any particular future year. The use of the CGCM2 "A2" scenario for the year 2050 simply provides appropriate magnitudes of air temperature increase, month-by-month, at various locations within the study basin. Individual simulation results should be interpreted as what a particular past river ice condition might look like if it were to occur around the mid-twenty-first century, under warmer climate conditions.

This particular climate change analysis does demonstrate that future climate warming that may occur within the next 45 to 50 years will have a substantial impact on the ice regime of the Peace River. Further, it suggests strongly that the ice cover will tend to form much later, spring breakup will occur earlier, and the ice cover will generally not progress as far upstream as it once did.

Table 5.3 summarises the effect of the selected climate change scenario on the date of freezeup at the Town of Peace River. Based on this analysis, freezeup would occur about 30 to 40 days later in most circumstances. Warm weather spells in the mid-winter have the potential to increase this delay even more.

The timing of breakup appears to be less affected by climate warming, although it is consistently simulated earlier. Table 5.4 summarises the breakup results for the Town of Peace River. At typical range of 10 to 25 days earlier breakup seems to be indicated.

The freezeup and breakup changes together correspond to an overall reduction in the duration of ice cover at the Town of Peace River of approximately 40 to 50 days, as indicated in Table 5.5 and plotted graphically in Figure 5.12. Comparing this reduction to the mean historical duration of ice cover at that location (89 days), this amounts to a substantial change (45 to 55% reduction).

The simulated maximum extent of the river ice cover is also reduced as a result of the warmer future climate air temperatures. Figure 5.13 illustrates the less conclusive relationship (compared to ice cover duration) between the historical and future climate maximum extent of ice cover. As Table 5.6 summarises, it could be expected that the ice cover extent would decrease on the order of 75 to 100 kilometres under the scenario applied. For colder than normal winters, this change is likely to be less dramatic, as indicated for the 1995/96 season. This change in the ice regime essentially means that the ice cover on the Peace River will probably no longer reach the Alberta-British Columbia border under future climate conditions, except in the occasional, abnormally cold winter.

Table 5.1 **Applied mean monthly air temperature changes (°C) for the year 2050 relative to the period 1961 to 1990.**

Month	Fort St. John	Town of Peace River	High Level
October	0.9847	0.9118	0.9118
November	0.442	0.3008	0.3008
December	4.2276	3.8196	3.8196
January	4.5516	5.6675	5.6675
February	3.8059	3.9024	3.9024
March	4.1415	4.0523	4.0523
April	2.0063	1.6975	1.6975
May	3.6521	3.9656	3.9656

Table 5.2 **Comparison of historical dates of bridging at Fort Vermilion and predicted future bridging dates under climate change conditions.**

Year	Historical Date of Bridging (Observed)	Future Climate Date of Bridging (Predicted by model)	Change (days)
2003/04	November 22	December 31	39
2002/03	December 21	January 20	30
2001/02	November 27	January 2	36
1996/97	November 12	December 21	39
1995/96	November 11	November 23	13
1994/95	November 29	January 2	35

Table 5.3 **Change in simulated date of freezeup at the Town of Peace River under future climate conditions (considering the effect of climate change on date of bridging).**

Season	Simulated Historical Freezeup Date	Simulated Future Climate Freezeup Date	Change (days)
2003/04	January 4	January 27	23
2002/03	January 25	February 23	29
2001/02	December 30	March 8	68
1996/97	December 20	January 13	23
1995/96	December 9	January 8	29
1994/95	January 7	February 18	42

Table 5.4 **Change in simulated date of breakup at the Town of Peace River under future climate conditions (considering the effect of climate change on date of bridging).**

Season	Simulated Historical Breakup Date	Simulated Future Climate Breakup Date	Change (days)
2003/04	April 7	March 12	-26
2002/03	April 17	March 30	-19
2001/02	April 22	April 13	-9
1996/97	April 20	March 29	-22
1995/96	April 17	April 8	-9
1994/95	April 19	March 30	-20

Table 5.5 **Change in simulated duration of ice cover at the Town of Peace River under future climate conditions (considering the effect of climate change on date of bridging).**

Season	Simulated Historical Duration of Ice Cover	Simulated Future Climate Duration of Ice Cover	Change (days)
2003/04	94	46	-48
2002/03	83	35	-48
2001/02	113	36	-77
1996/97	120	75	-45
1995/96	130	91	-39
1994/95	102	40	-63

Table 5.6 **Change in minimum ice cover distance downstream of the Bennett Dam under future climate conditions (considering the effect of climate change on date of bridging).**

Season	Simulated Historical Minimum Distance	Simulated Future Climate Minimum Distance	Change (km)
2003/04	116	215	-99
2002/03	106	178	-72
2001/02	156	231	-75
1996/97	130	214	-85
1995/96	111	131	-20
1994/95	141	227	-86

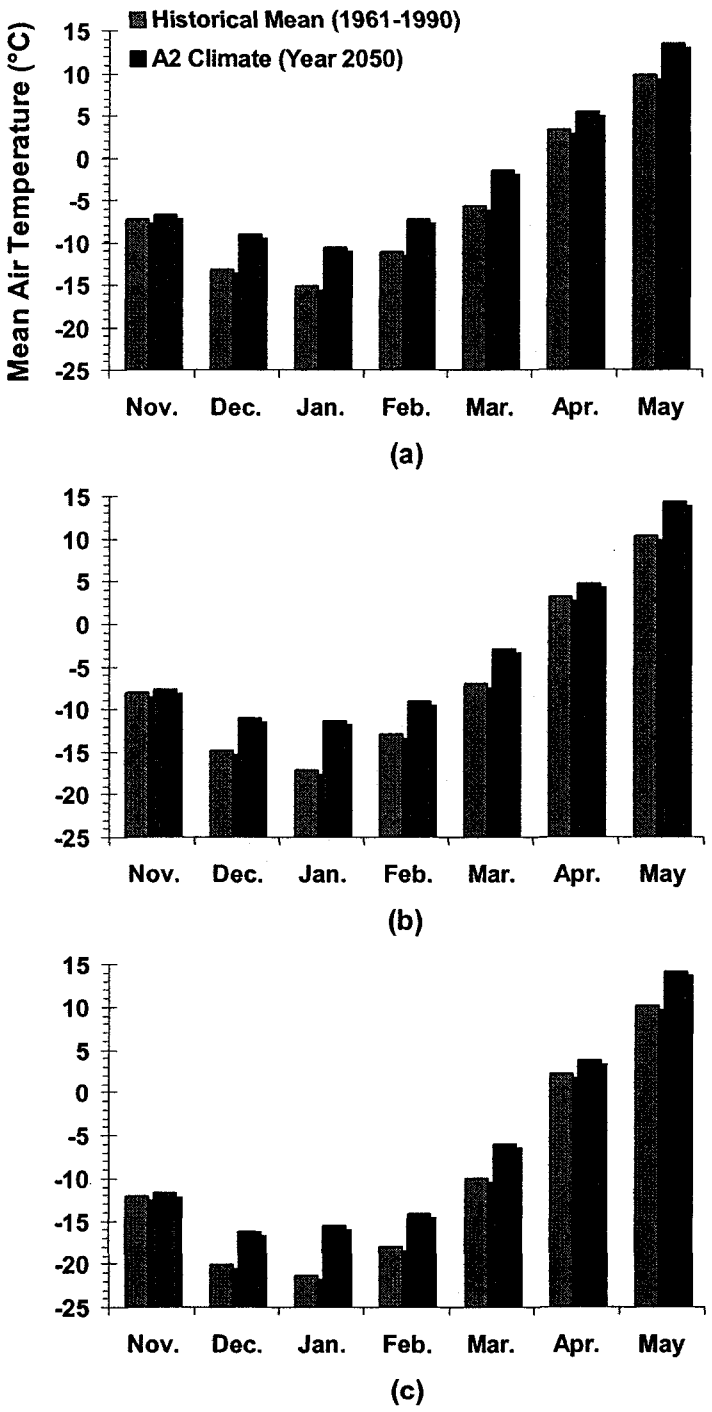

Figure 5.1 **Comparison of historical and future climate mean monthly air temperatures at: (a) Fort St. John; (b) Town of Peace River; and (c) High Level.**

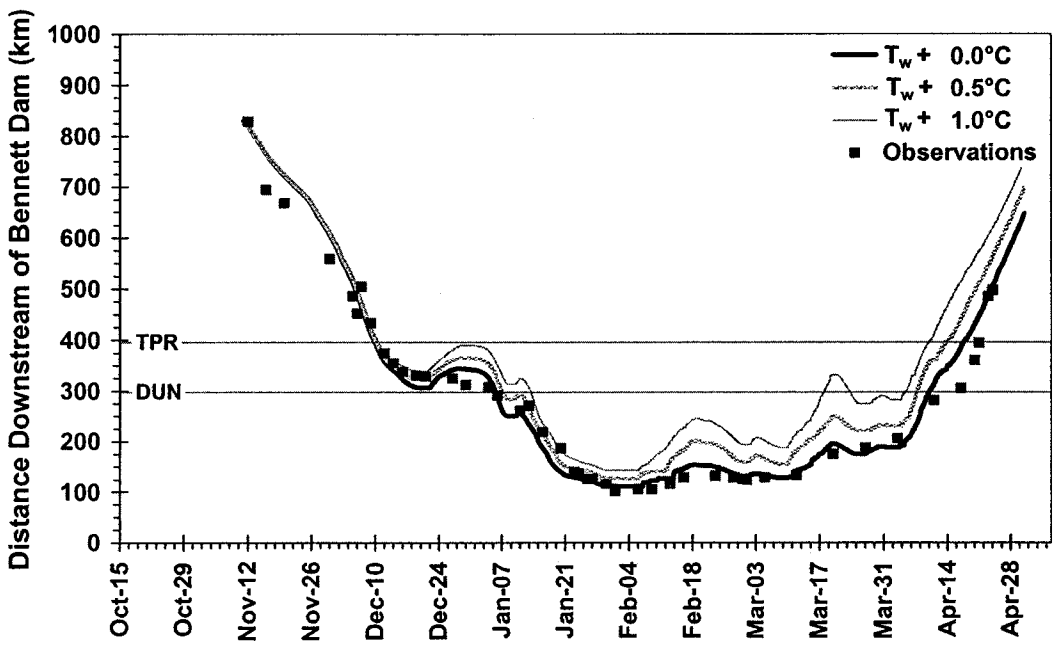

Figure 5.2 **Effect of reservoir warming on the simulated ice front profile using 1995/96 ice season data.**

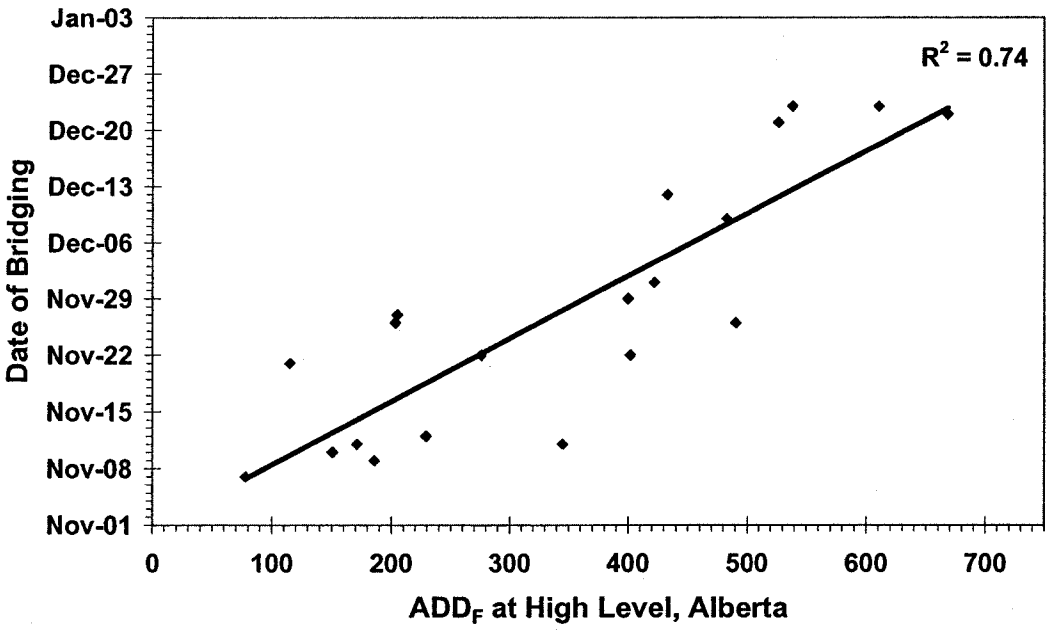

Figure 5.3 **Correlation between accumulated degree days of freezing at High Level and observed date of bridging.**

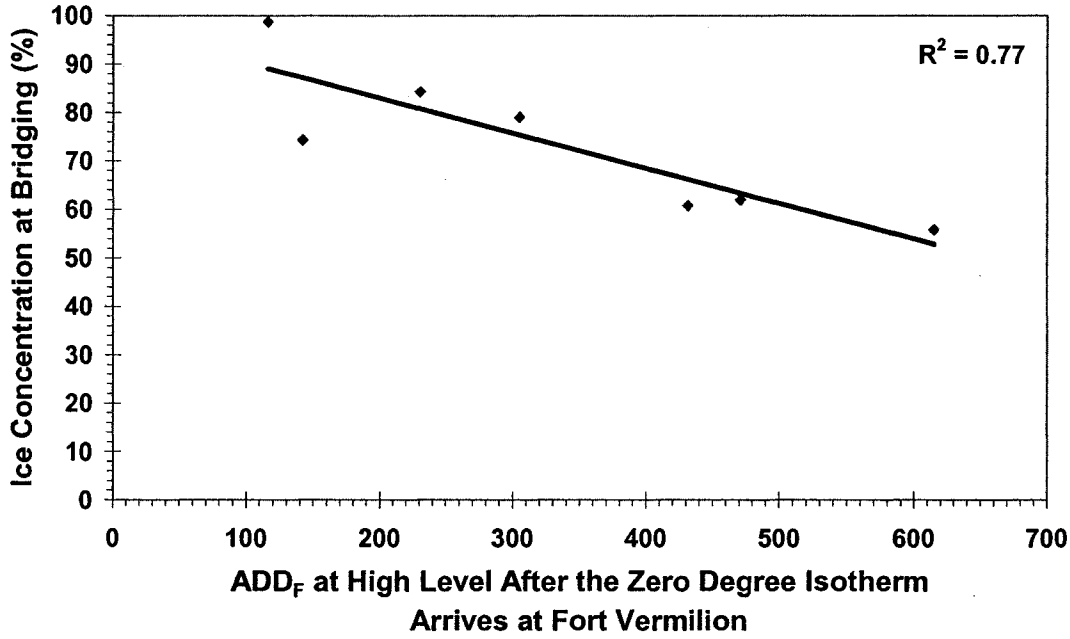

Figure 5.4 **Correlation between accumulated degree days of freezing at High Level after the zero degree isotherm arrives at Fort Vermilion and surface concentration of ice at the observed date of bridging.**

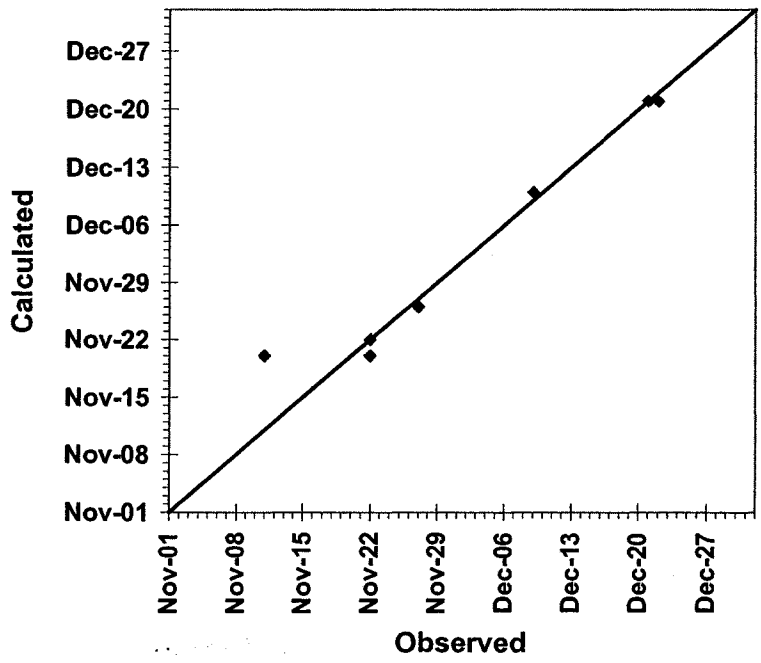

Figure 5.5 **Comparison of observed dates of bridging on the Peace River to those calculated using the bridging criterion developed.**

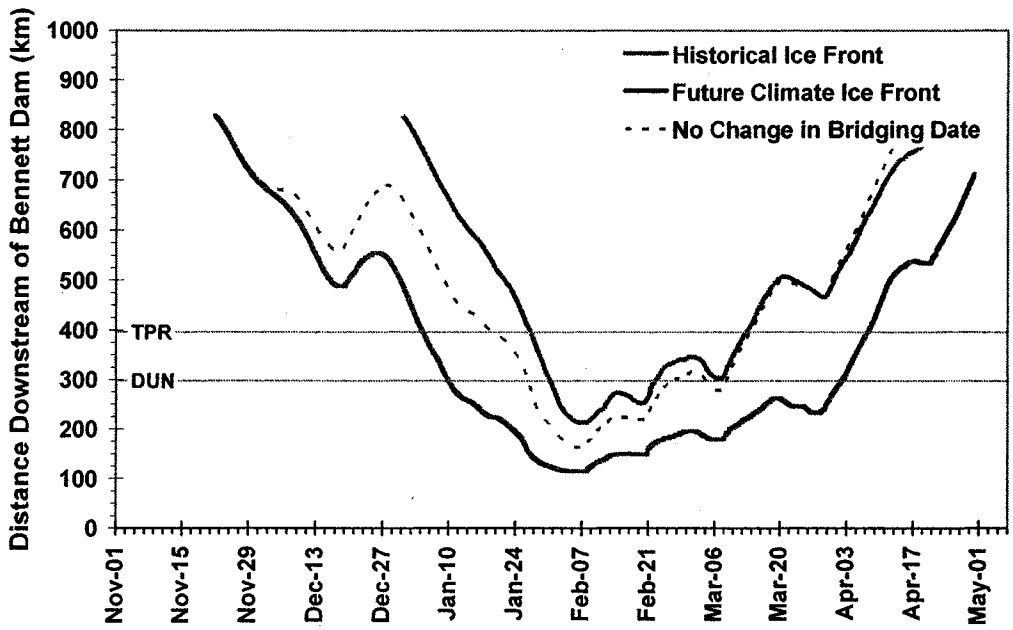

Figure 5.6 **Simulated historical and future climate ice front profiles based on 2003/04 ice season data.**

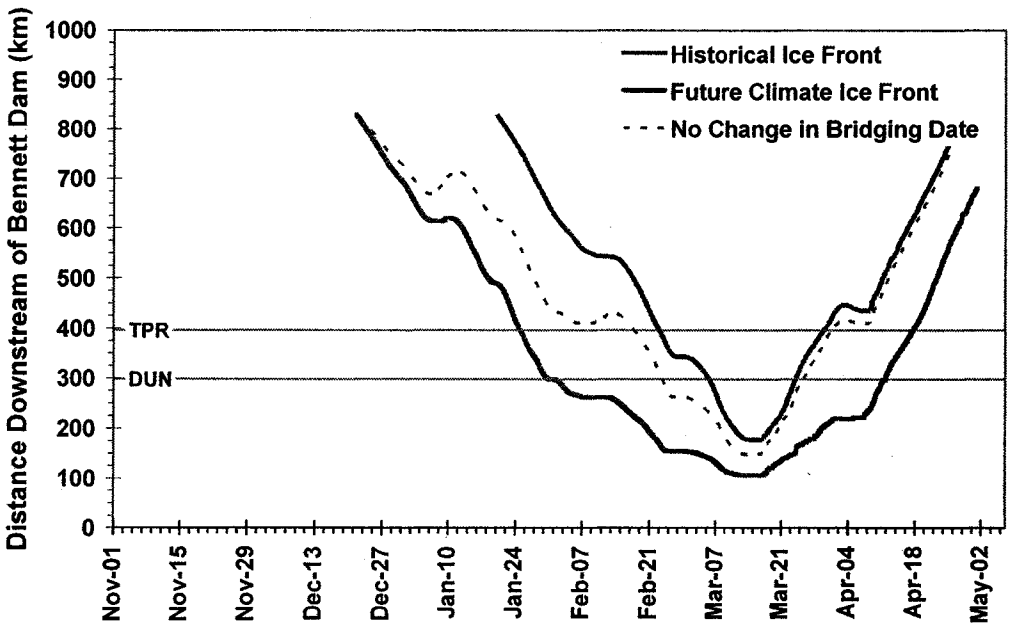

Figure 5.7 **Simulated historical and future climate ice front profiles based on 2002/03 ice season data.**

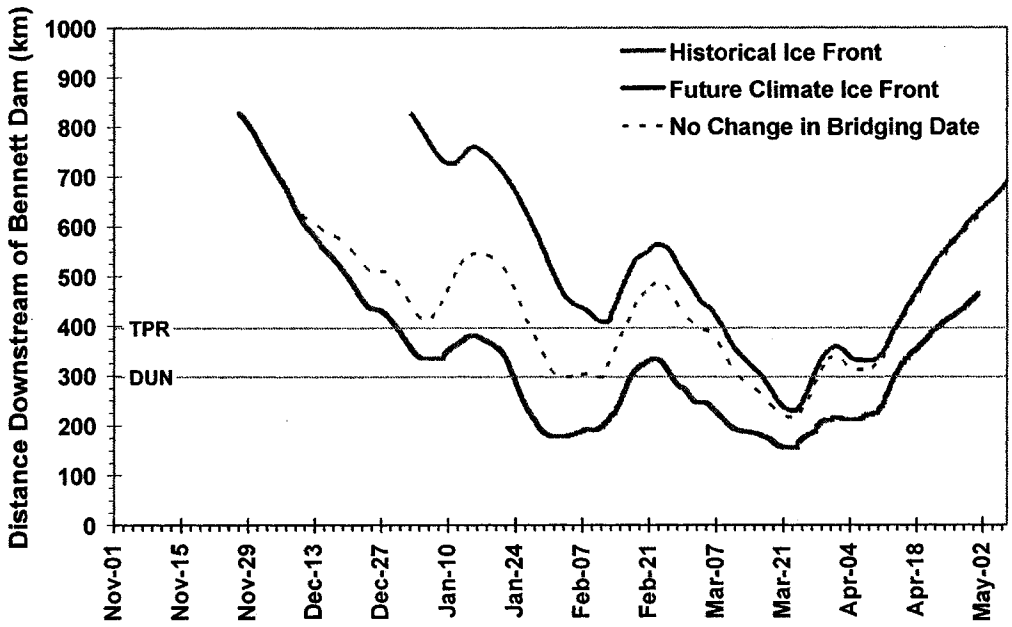

Figure 5.8 **Simulated historical and future climate ice front profiles based on 2001/02 ice season data.**

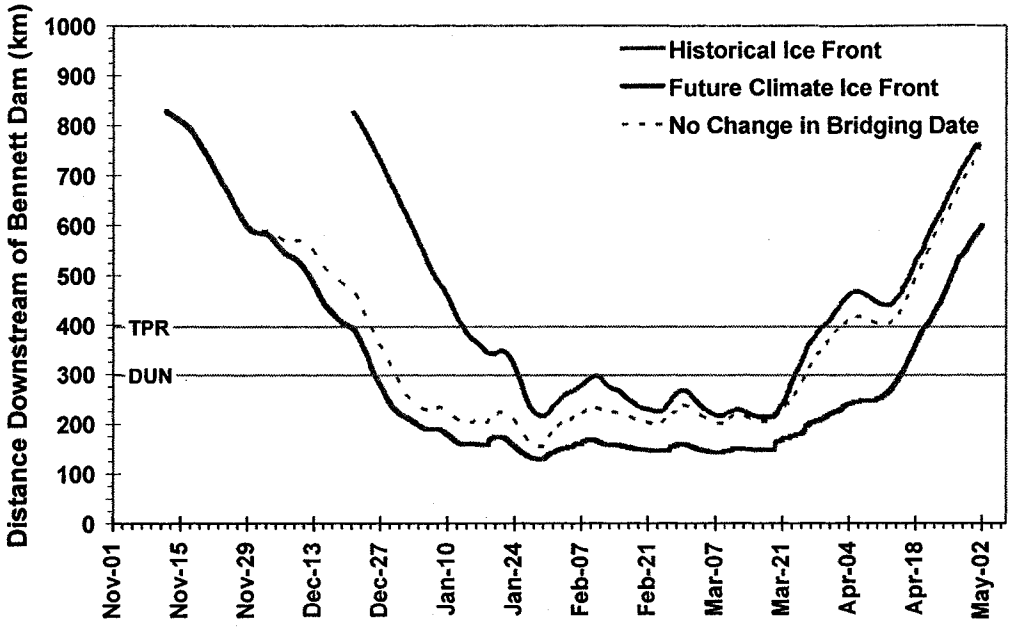

Figure 5.9 **Simulated historical and future climate ice front profiles based on 1996/97 ice season data.**

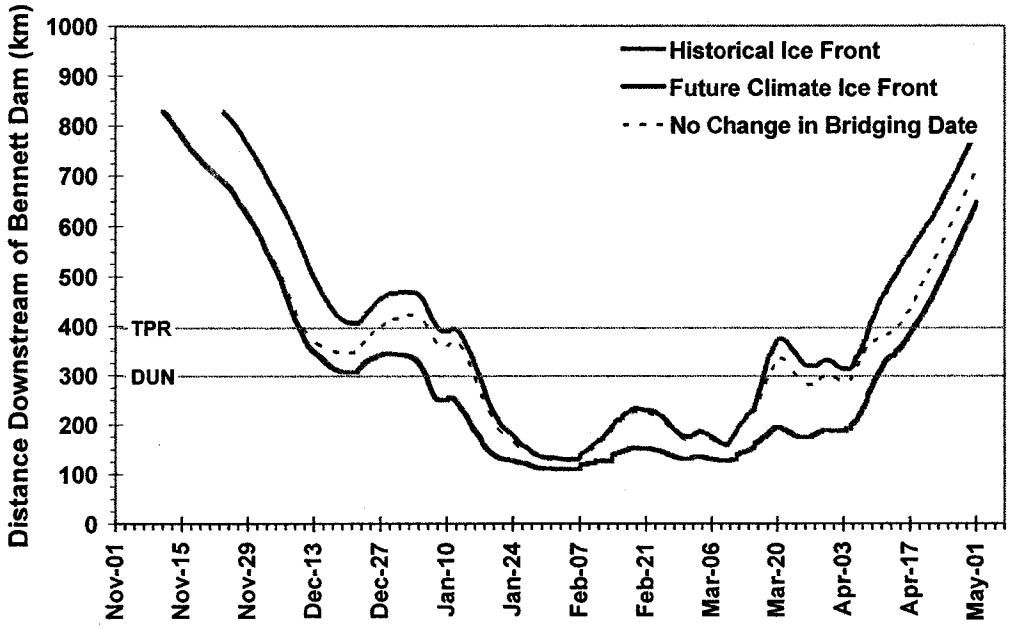

Figure 5.10 **Simulated historical and future climate ice front profiles based on 1995/96 ice season data.**

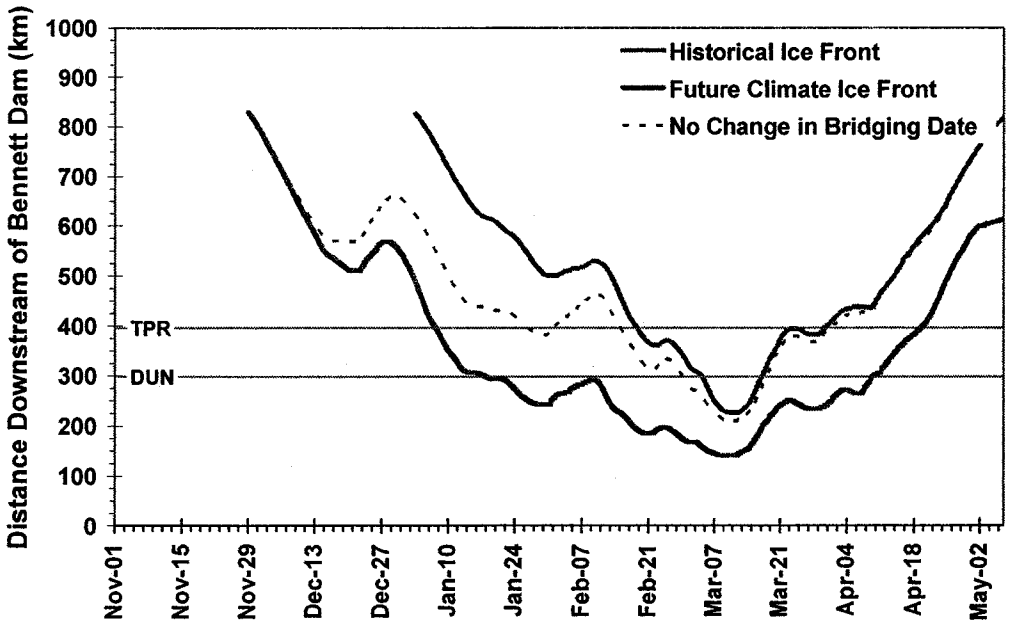

Figure 5.11 **Simulated historical and future climate ice front profiles based on 1994/95 ice season data.**

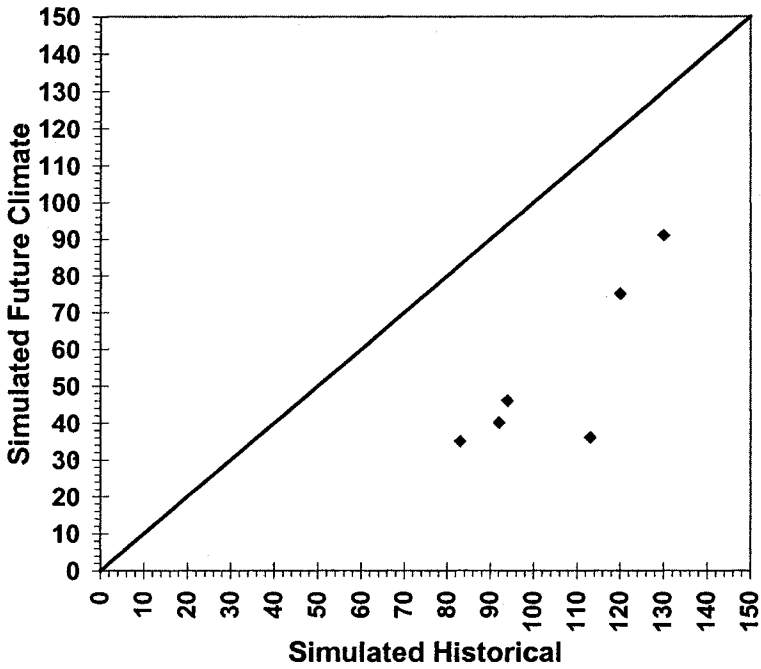

Figure 5.12 **Comparison of simulated historical and future climate duration of ice cover (in days) at the Town of Peace River.**

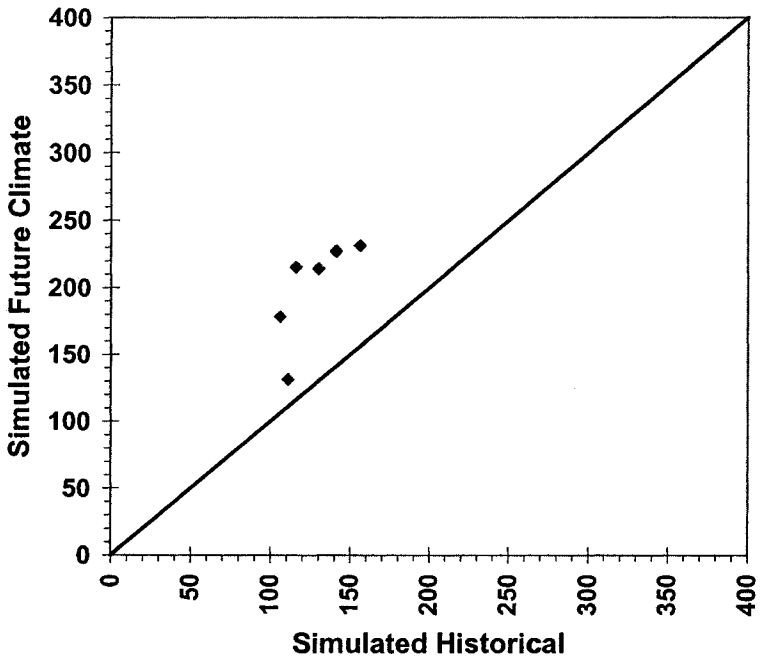

Figure 5.13 **Comparison of simulated historical and future climate peak extent of ice cover (in kilometres downstream of the Bennett Dam).**

CHAPTER 6 CONCLUSIONS AND RECOMMENDATIONS

6.1. CONCLUSIONS

A thermal river ice process and hydrodynamic model considering water temperature, river ice generation, ice cover formation, and thermal melt has been developed, integrated into the *River1D* hydraulic model, and applied to the Peace River in British Columbia and Alberta. The present model is able to simulate the observed historical ice conditions on the Peace River reasonably well, given the uncertainties and regional scale of the input data available. For the twenty years of historical ice conditions simulated, the mean modeled date of freezeup at the Town of Peace River, in the middle of the study area, was two-and-a-half days earlier than the observed.

The validated model was then extended to simulate climate change conditions by repeating the historical simulations with new input air temperatures that were adjusted according to the monthly mean changes predicted by the CGCM2 climate model's "A2" climate change projection for the year 2050. Initially an assumption that climate change would not delay the date of bridging was applied, as no means of predicting the date of bridging or evaluating the impact of climate change on this input parameter was available.

Near the end of this study, a bridging criterion was developed and tested. This method correlates the accumulated degree days of freezing at High Level after the zero degree isotherm arrives at Fort Vermilion to the concentration of ice required to

initiate bridging. For a sample of seven years, with a wide range of bridging dates, the model was able to predict the bridging date with an accuracy of two days or better in all but one instance.

Five representative simulations were repeated for climate change conditions using the new criterion to adjust the date of bridging. Based on the analysis, the date of bridging was typically delayed by 30 to 40 days under future climate conditions. With the adjusted date of bridging, the climate change profiles were found to be remarkably similar to those without any adjustment for date of bridging, with the exception of the freezeup progression of the ice cover. The maximum extent of the ice cover and the recession of the ice cover were very similar under warmer climate conditions regardless of the bridging date applied.

Further analysis of the climate change simulations indicates that the occurrence of freezeup at the Town of Peace River would be 30 to 40 days later under the future climate scenario applied. Interestingly, colder than normal years, such as 1995/96, appear to be less impacted by the climate change conditions than other years. The total duration of ice cover at the Town of Peace River is dramatically changed by the future climate scenario. A reduction on the order of 40 to 50 days is indicated, which amounts to a 45 to 55 percent reduction based on the historical mean for the period of record.

This analysis suggested that the maximum extent of ice cover would also be reduced as a result of warmer air temperatures, and it indicates that ice will cover 75 to 100 kilometres less of the river under the scenario considered. In other words, the

ice cover on the Peace River could potentially stop progressing as far as the Alberta-British Columbia border by the mid-twenty-first century, except in abnormally cold winters such as occurred in 1995/96.

The magnitudes of these changes in the winter regime of the Peace River are extremely significant to the movement of people, goods, and animals across the river in the winter months. Northern communities that rely on summer ferry crossings and winter ice bridges as a means to remain connected with supply and service centres, and are already isolated for weeks during freezeup, have the potential to be unable to cross the river for months.

Given the limitations of the input and validation data, the fact that the model only considers thermal ice processes at this time, and the uncertainties associated with the meteorological climate change analysis itself (as well as its applicability for this particular period of record), the quantitative future climate results presented cannot be considered firm predictions. However, their magnitudes do definitely suggest that there will be a significant, measurable impact on the future ice regime of the Peace River under the type of climate warming projected in the climate scenario considered. Therefore, it is important to start developing adaptive strategies as well as improved models and data archives, in order to gain a more reliable quantitative assessment of these impacts.

6.2. RECOMMENDATIONS

Many opportunities exist to further develop the *River1D* thermal river ice process model created for and applied in this study. In particular, the ongoing work of concurrent studies involving ice jam formation and release processes should eventually be integrated with this thermal ice process model. In addition, further analysis and experimentation with the proposed method for calculating the date of bridging on the Peace River should be done as this is a very promising development in the field of river ice engineering that demands more attention.

Continued and improved data collection on the Peace River is incredibly important to further validating and improving the present model. In particular, one or more water temperature monitoring sites downstream of the Town of Peace River would be extremely beneficial to validation of the model in the northern reach of the study area. The exploration of the potential uses of remote sensing and GIS to observe, quantify, and archive river ice characteristics has begun and should continue. Remote sensing could possibly assist in locating the ice front and zero degree isotherm through ongoing research and development of radar backscatter analysis techniques.

Finally, with the clear indication that climate change over the next half-century will have a substantial effect on the winter regime of the Peace River, development consideration and environmental impact assessment of river works, in particular hydropower projects, along the Peace River must be not be based on the historical ice regime alone. It will be extremely important to evaluate such projects

under the future winter climate conditions they may be exposed to in the relatively near future, so that regulators can fully assess both their positive and negative impacts.

CHAPTER 7 REFERENCES

Andres, D.D. (1993). "Effects of Climate Change on the Freezeup Regime of the Peace River: Phase I Ice Production Algorithm Development and Calibration". Report No. SWE 93/01, Environmental Research & Engineering Department, Alberta Research Council, Edmonton, Alberta, 52 pp.

Ashton, G.D. (1973). "Heat Transfer to River Ice covers". Proc. 30th Eastern Snow Conference, Amherst, Massachusetts, 125-135.

Ashton, G.D. (1986). "River and Lake Ice Engineering". Water Resources Publications, Littleton, Colorado, 485 pp.

Blackburn, J. and Hicks, F. (2002). "Combined Flood Routing and Flood Level Forecasting". Canadian Journal of Civil Engineering, Vol. 29, No. 1, 64-75.

Beltaos, S. and Prowse, T.D. (2001). "Climate Impacts on Extreme Ice-jam Events in Canadian Rivers". Journal of Hydrologic Sciences, Vol. 46, No. 1, 157-181.

CCCma (Canadian Centre for Climate Modelling and Analysis). (2005). "The Second Generation Coupled Global Climate Model (CGCM2)". Online Resource, http://www.cccma.bc.ec.gc.ca/models/cgcm2.shtml.

Chemical Rubber Company. (2004). "CRC Handbook of Chemistry and Physics, 84th Edition". Online Resource, http://www.library.ualberta.ca/databases/databaseinfo/index.cfm?ID=3193.

Gerard, R., Hicks, F.E., MacAlpine, T., and Chen X. (1992). "Severe Winter Ferry Operation: The Mackenzie River at Ft. Providence, NWT". Proc. of the 11th International Assoc. for Hydraulic Research Ice Symposium, Banff, Alberta, June 1992, 503- 514.

Hicks, F.E. (1996). "Hydraulic Flood Routing with Minimal Channel Data: Peace River, Canada". Canadian Journal of Civil Eng., Vol. 23, No. 2, 524-535.

Hicks, F.E. and Steffler, P.M. (1990). "Finite Element Modeling of Open Channel Flow". Water Resources Engineering Report No. 90-6, Department of Civil Engineering, University of Alberta, Edmonton, Alberta, 356 pp.

Hicks, F.E. and Steffler, P.M. (1992). "A Characteristic-Dissipative-Galerkin Scheme for Open Channel Flow". ASCE Journal of Hydraulic Eng., Vol. 118, No. 2, 337-352.

Intergovernmental Panel on Climate Change. (2005). "Presentations and Graphics". Online Resource: http://www.ipcc.ch/present/graphics.htm.

Kellerhals, R., Neill, C.R., and Bray, D.I. (1972). "Hydraulic and Geomorphic Characteristics of Rivers in Alberta." River Engineering and Surface Hydrology Report 72-1, Alberta Research Council, Edmonton, Alberta.

Kuryk, D. and Domaratzki, M. (1999). "Construction and Maintenance of Winter Roads in Manitoba". Proc. of the 10th Workshop on the Hydraulics of Ice-covered Rivers, Winnipeg, 265-275.

Lal, A.M.W., and Shen, H.T. (1989). "A Mathematical Model for River Ice Processes (RICE)". Report No. 89-4, Department of Civil and Environmental Engineering, Clarkson University, Potsdam, New York, 164 pp.

Michel, B. (1971). "Winter Regime of Rivers and Lakes". Cold Regions Science and Engineering Monograph III-B1a, Cold Regions Research and Engineering Laboratory, U.S. Army, Hanover, New Hampshire, 131 pp.

Nezhikhovskiy, R.A. (1964). "Coefficients of Roughness of Bottom Surface on Slush-Ice Cover". Soviet Hydrology, Washington, American Geophysical Union, 127-150.

Peters, D.L. and Prowse, T.D. (2001). "Regulation Effects on the Lower Peace River, Canada". Journal of Hydrologic Processes, Vol. 15, 3181-3194.

Press, W.H., Flannery, B.P., Teukolsky, S.A., and Vetterling, W.T. (1988). "Numerical Recipes in C – The Art of Scientific Computing". Cambridge University Press, New York, New York, 735 pp.

Prowse, T.D. and Culp, J.M. (2003). "Ice Breakup: A Neglected Factor in River Ecology". Canadian Journal of Civil Eng., Vol. 30, 1-17.

Shen, H.T., Wang, S., and Lal, A.M.W. (1995). "Numerical Simulation of River Ice Processes". Journal Cold Regions Eng., Vol. 9, No. 3, 107-118.

Töyrä, J. and Pietroniro, A. (2003). "Generating Vector Polygon Global Climate Model (GCM) Grids for Canada". National Water Resources Institute, Saskatoon, Saskatchewan, 7 pp.

Trillium Engineering and Hydrographics Inc. (1997). "Ice Formation and Breakup at the Town of Peace River: A Study of Regulated Conditions, 1969-94". A Report Prepared for the Town of Peace River, BC Hydro, and Alberta Environment, Edmonton, Alberta, 123 pp.

Weber, B., Nixon, D., and Hurley, J. (2003). "Semi-Automated Classification of River Ice Types on the Peace River Using RADARSAT-1 Synthetic Aperture Radar (SAR) Imagery". Canadian Journal of Civil Eng., Vol. 30, 11-27.

– APPENDIX A –

Simulated Historical Ice Front Profiles (1984/85 through 2003/04)

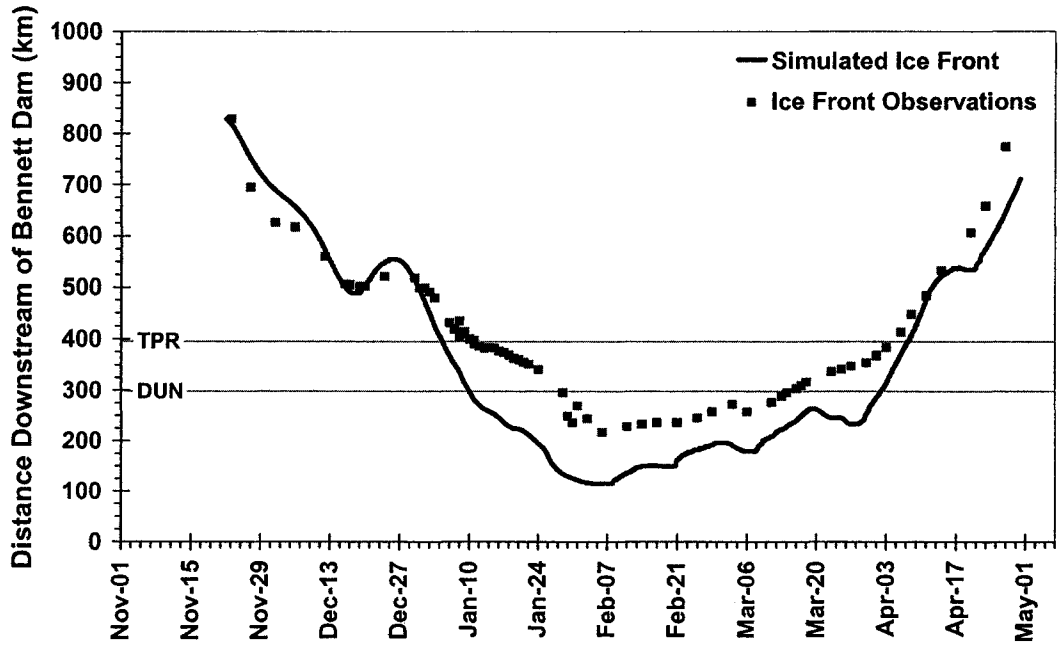

Figure A.1 **Ice front profile validation using $P_{jux} = 2.5$ and 2003/04 ice season data.**

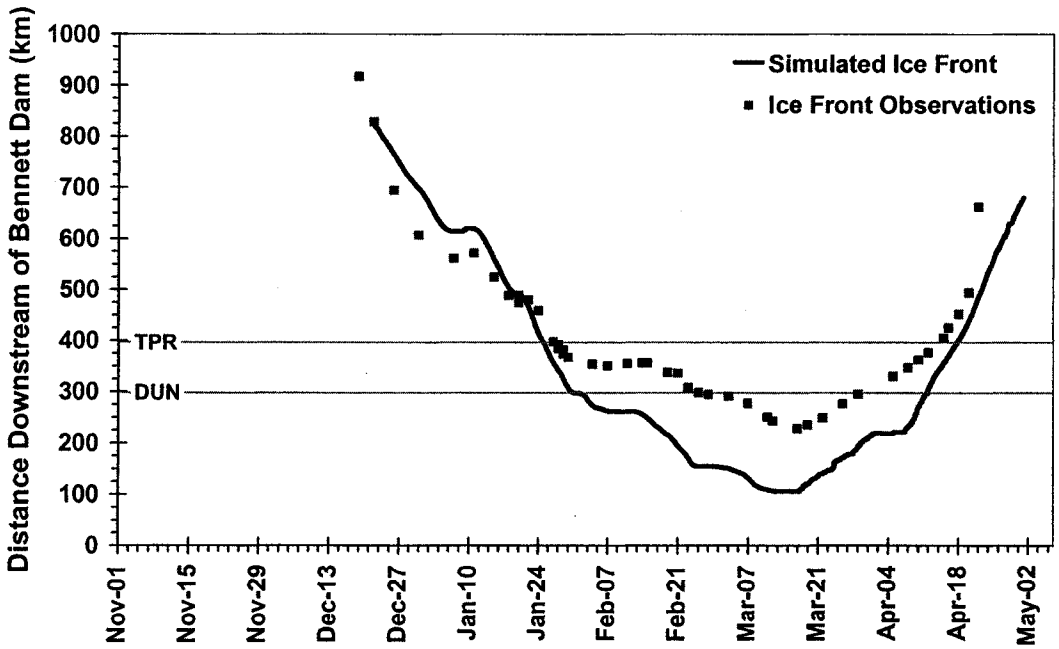

Figure A.2 **Ice front profile (calibration year) showing $P_{jux} = 2.5$ simulation using 2002/03 ice season data.**

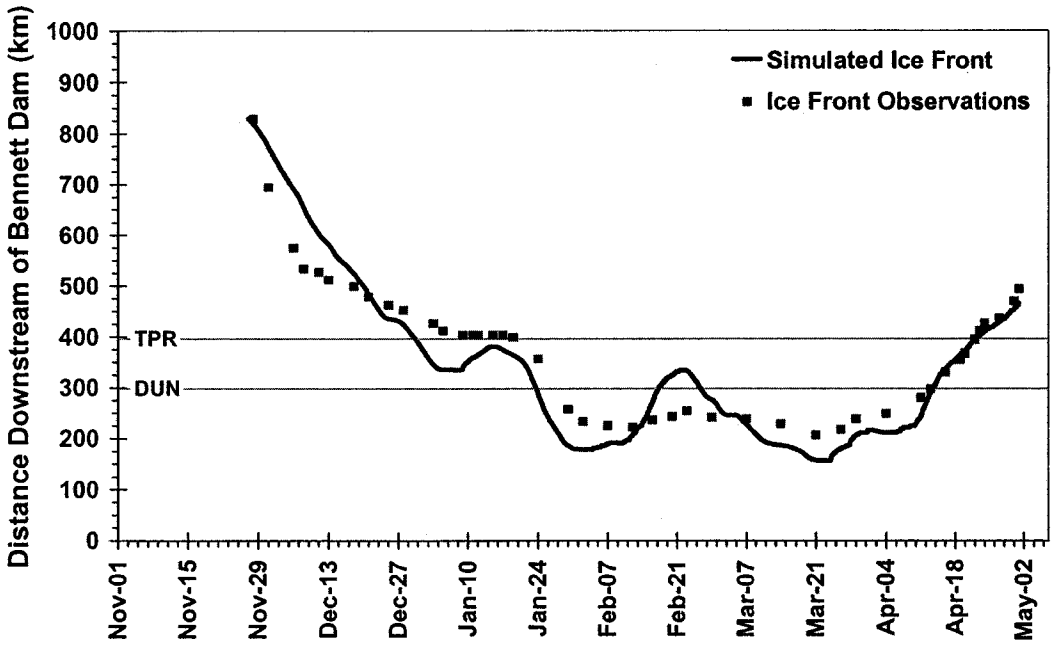

Figure A.3 **Ice front profile validation using P_{jux} = 2.5 and 2001/02 ice season data.**

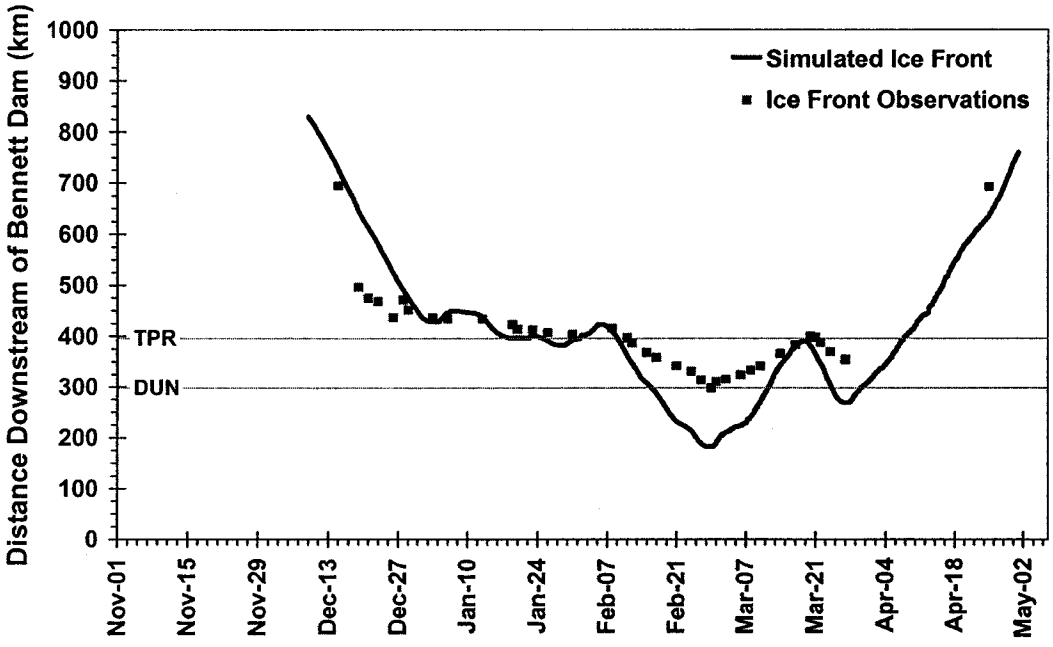

Figure A.4 **Ice front profile validation using P_{jux} = 2.5 and 2000/01 ice season data.**

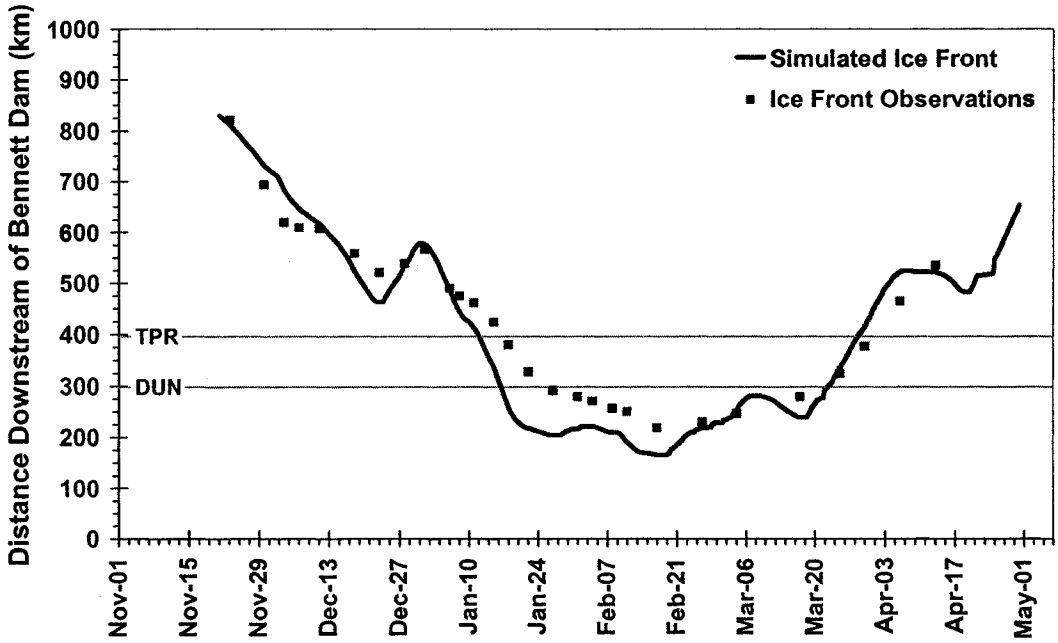

Figure A.5 **Ice front profile validation using P_{jux} = 2.5 and 1999/00 ice season data.**

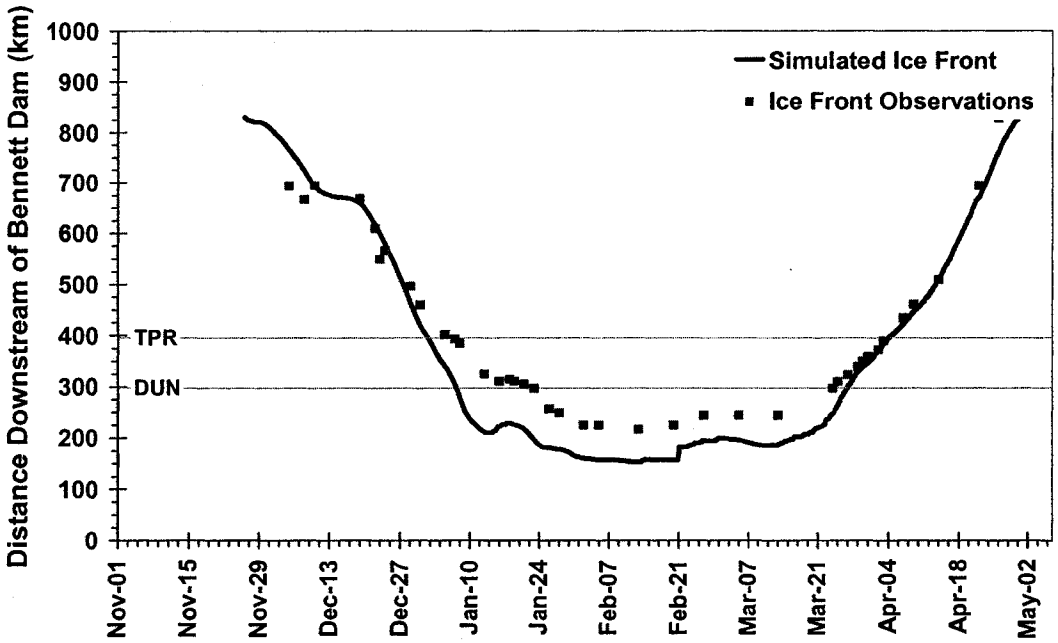

Figure A.6 **Ice front profile validation using P_{jux} = 2.5 and 1998/99 ice season data.**

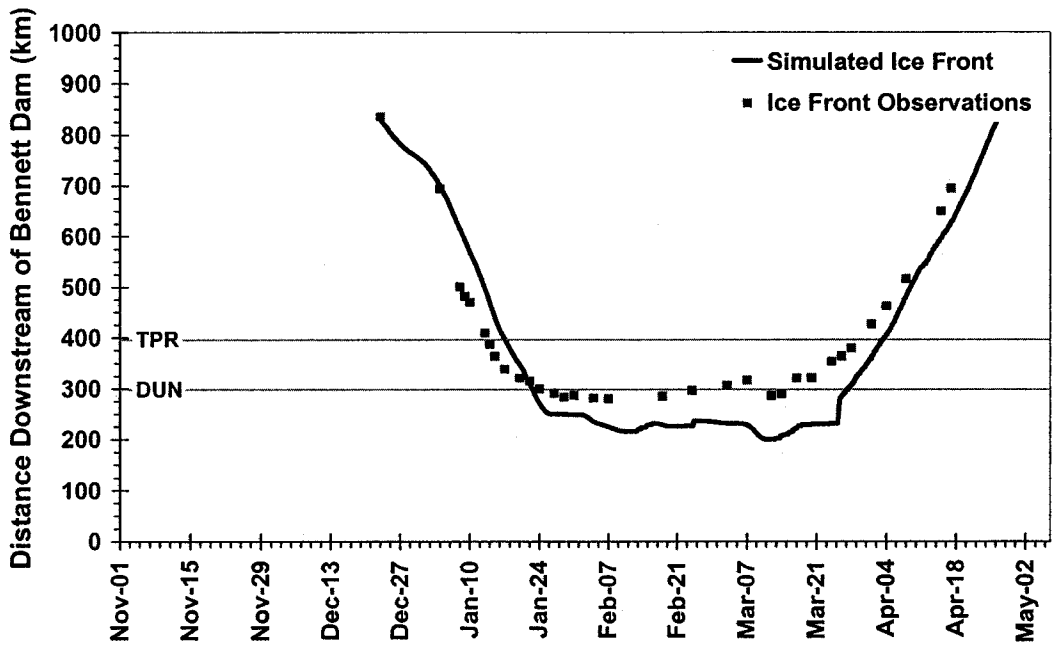

Figure A.7 **Ice front profile validation using $P_{jux} = 2.5$ and 1997/98 ice season data.**

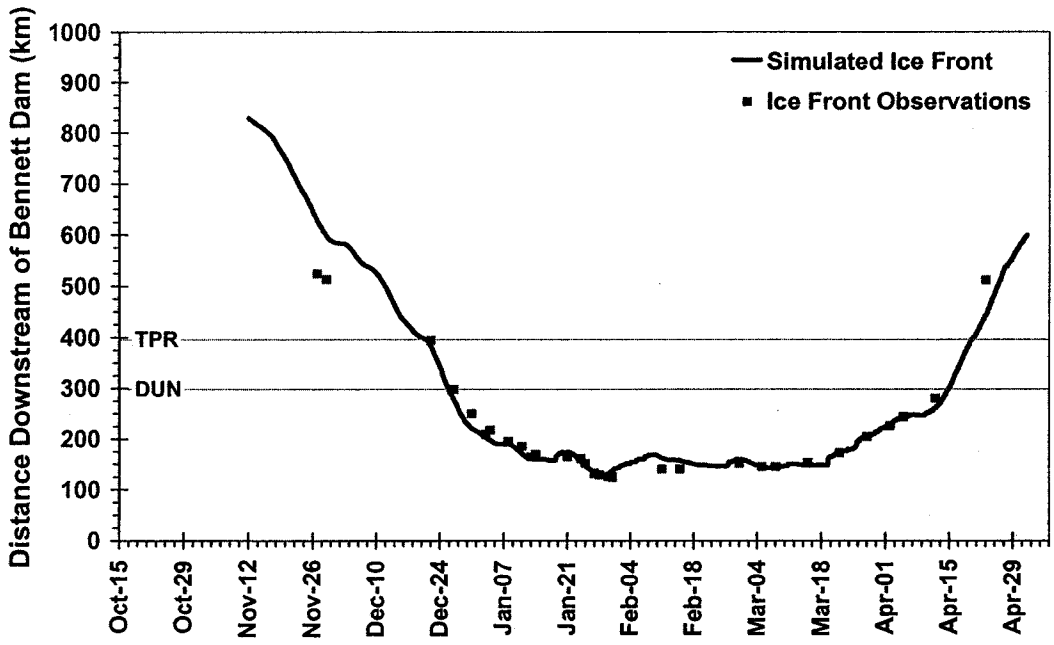

Figure A.8 **Ice front profile validation using $P_{jux} = 2.5$ and 1996/97 ice season data.**

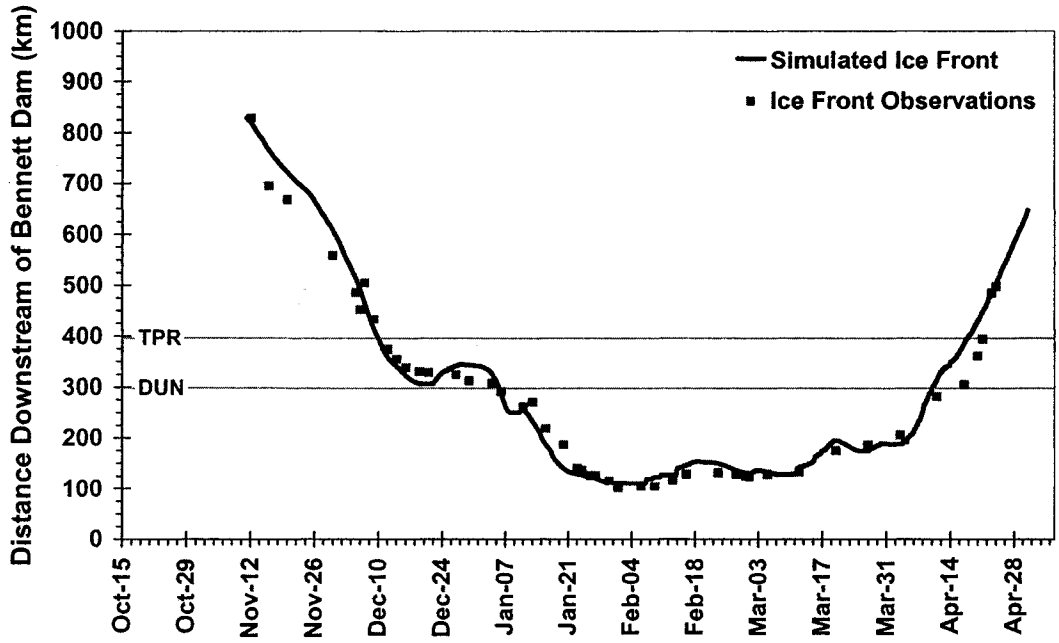

Figure A.9 Ice front profile validation using $P_{jux} = 2.5$ and 1995/96 ice season data.

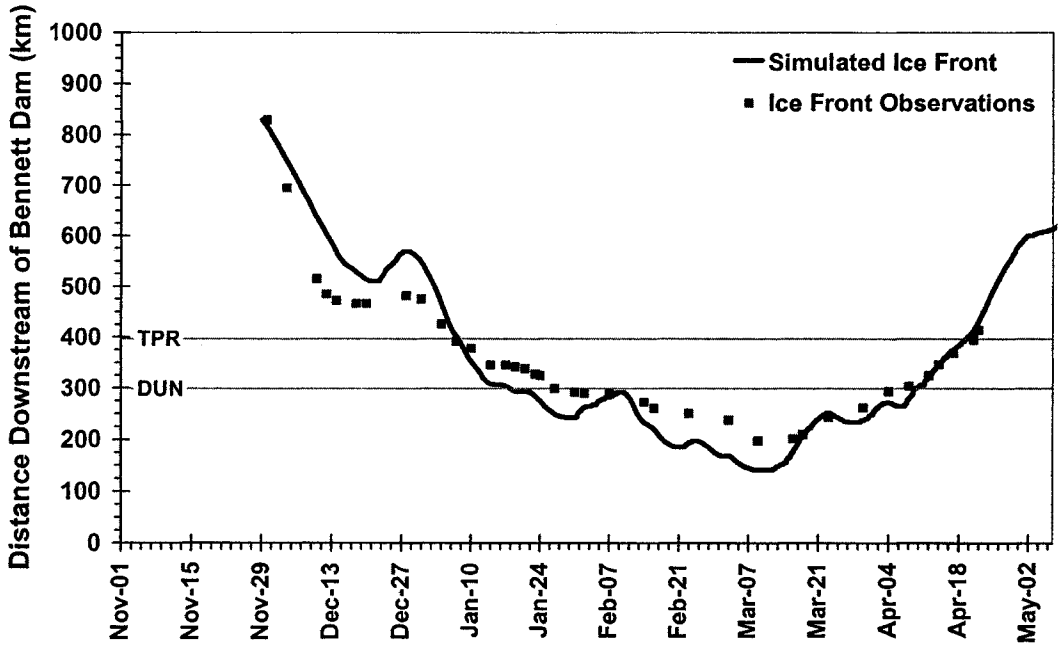

Figure A.10 Ice front profile validation using $P_{jux} = 2.5$ and 1994/95 ice season data.

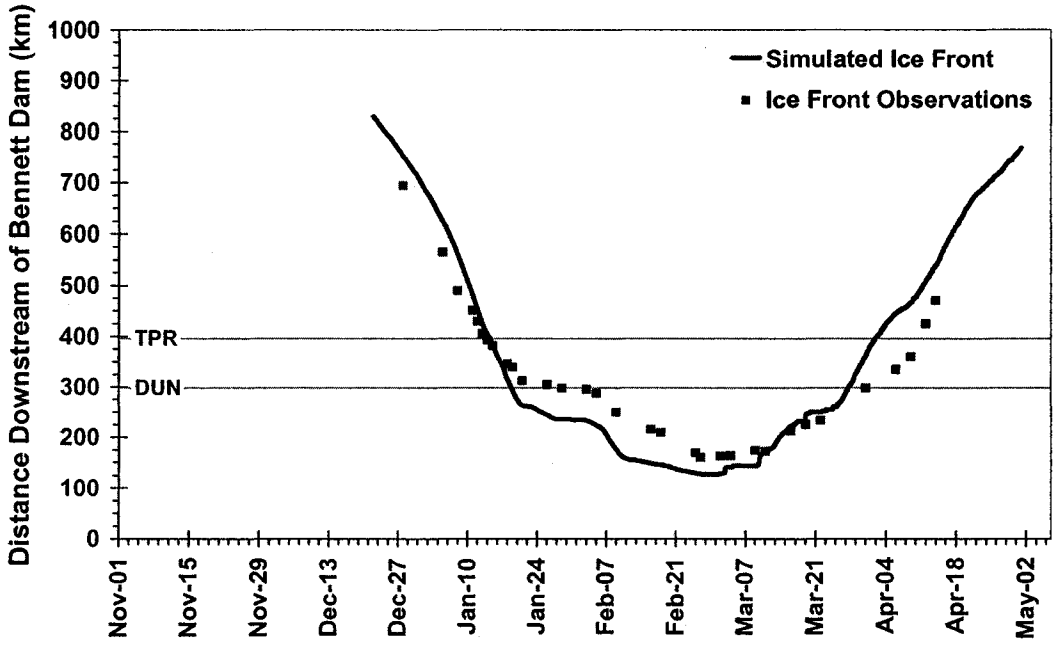

Figure A.11 Ice front profile validation using $P_{jux} = 2.5$ and 1993/94 ice season data.

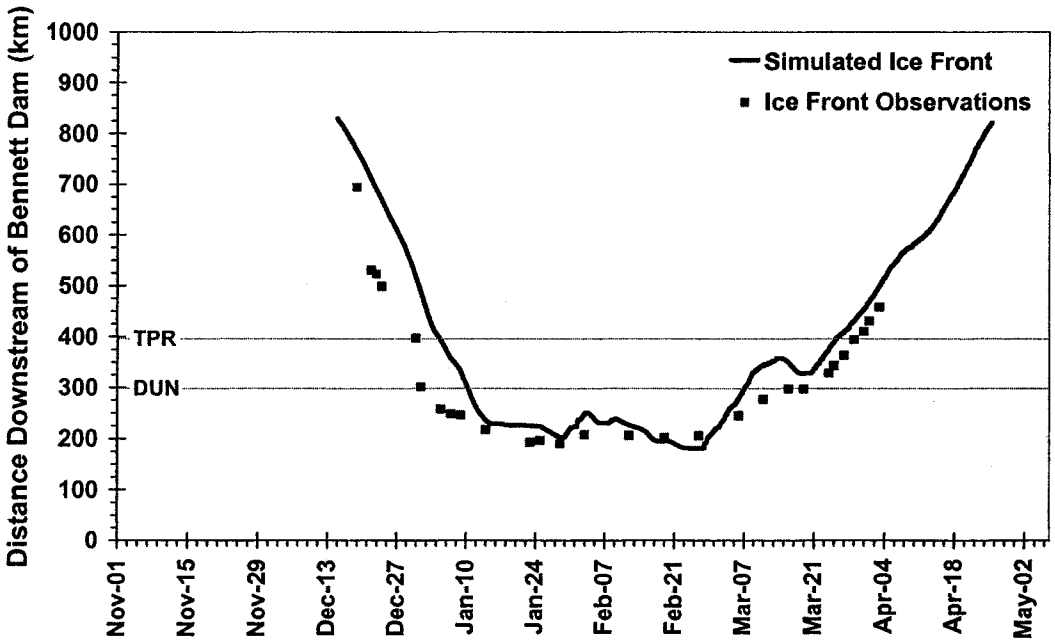

Figure A.12 Ice front profile validation using $P_{jux} = 2.5$ and 1992/93 ice season data.

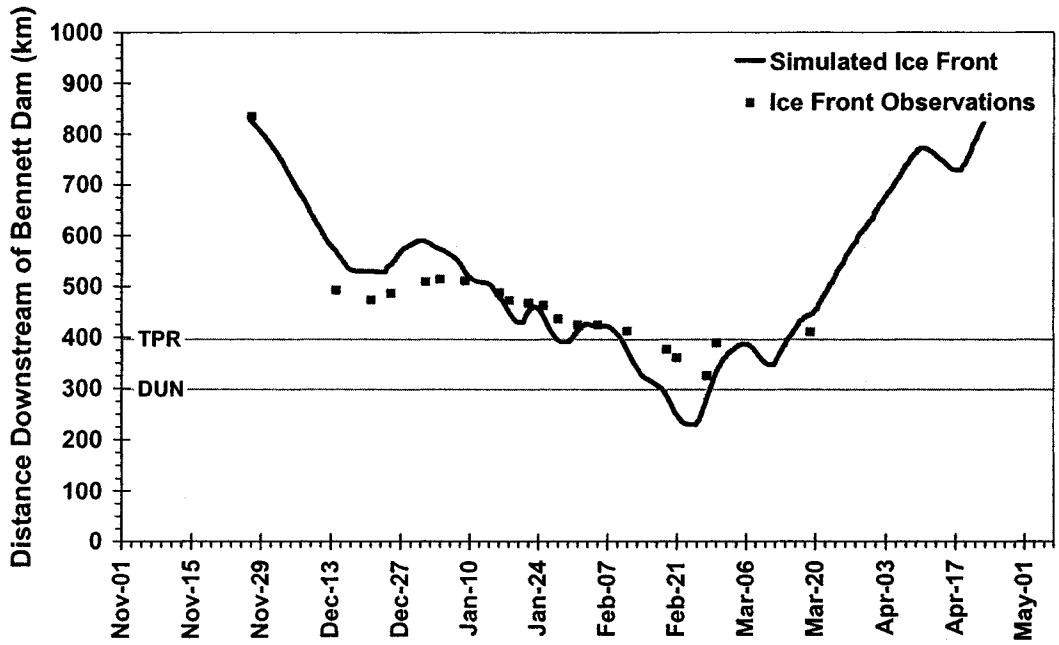

Figure A.13 Ice front profile validation using $P_{jux} = 2.5$ and 1991/92 ice season data.

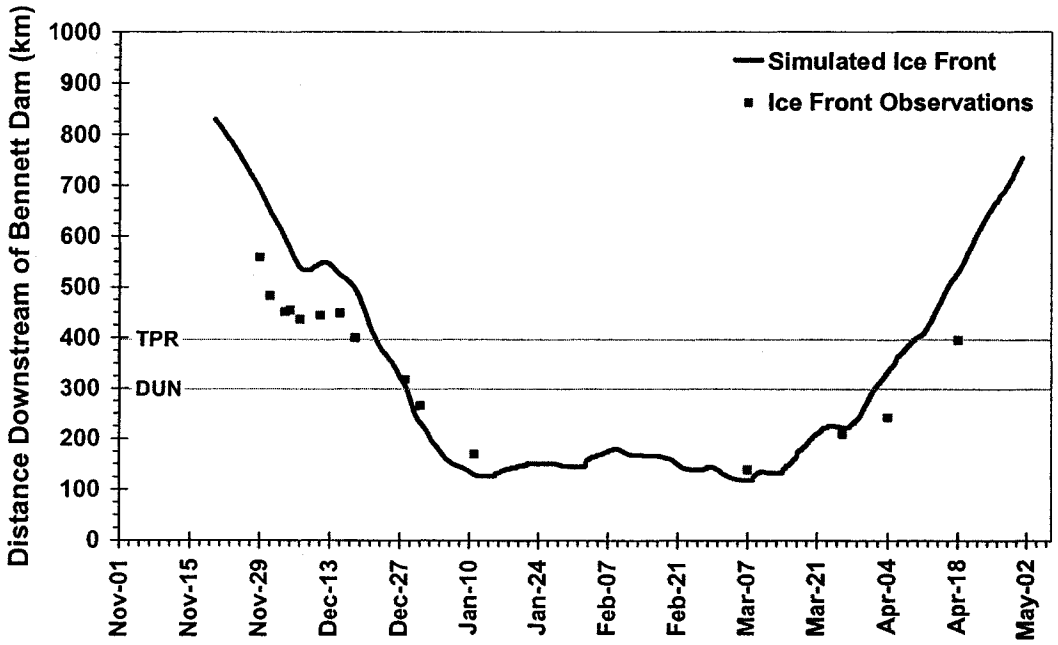

Figure A.14 Ice front profile validation using $P_{jux} = 2.5$ and 1990/91 ice season data.

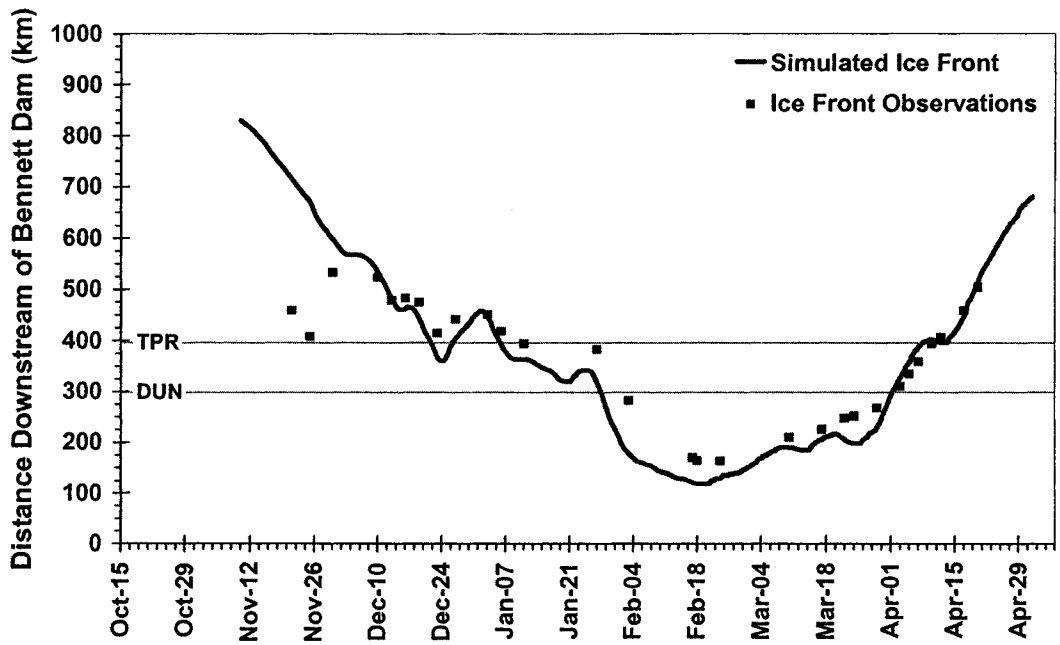

Figure A.15 Ice front profile validation using P_{jux} = 2.5 and 1989/90 ice season data.

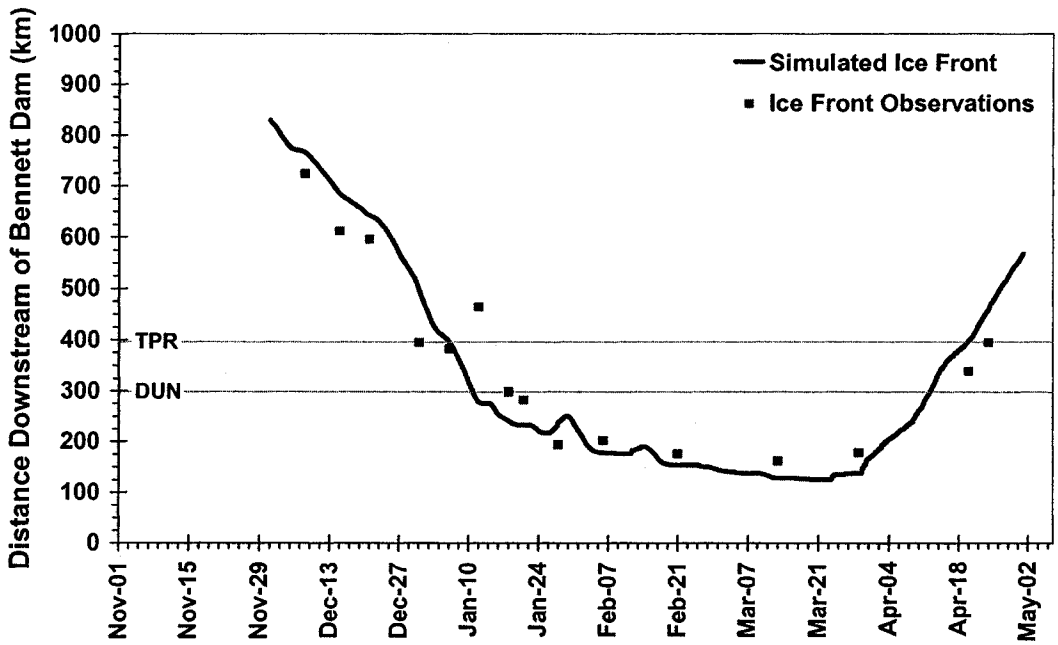

Figure A.16 Ice front profile validation using P_{jux} = 2.5 and 1988/89 ice season data.

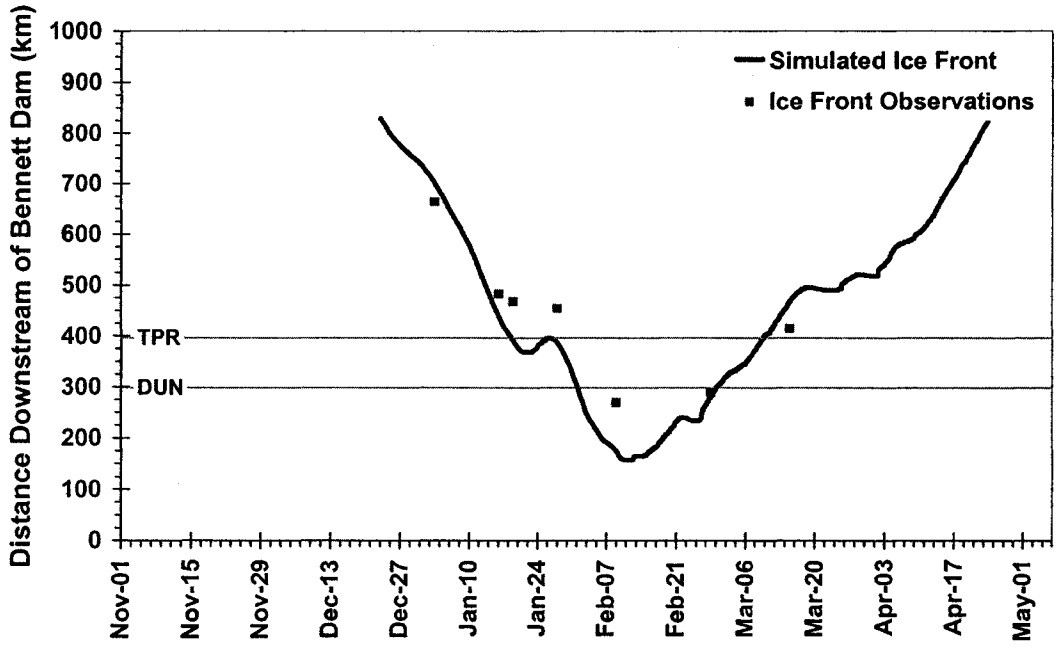

Figure A.17 Ice front profile validation using $P_{jux} = 2.5$ and 1987/88 ice season data.

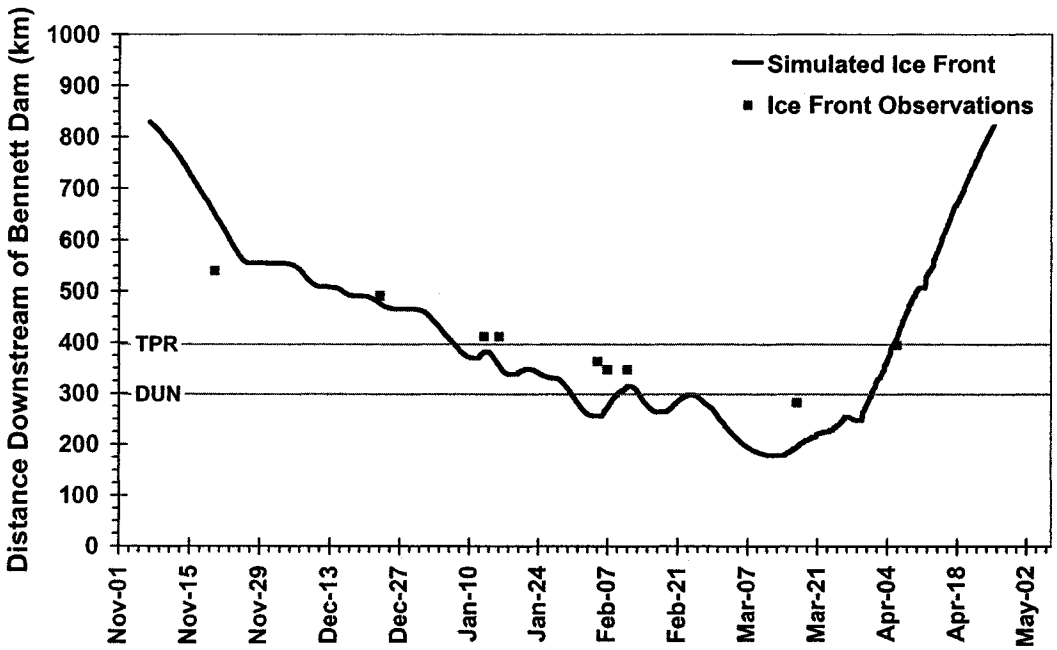

Figure A.18 Ice front profile validation using $P_{jux} = 2.5$ and 1986/87 ice season data.

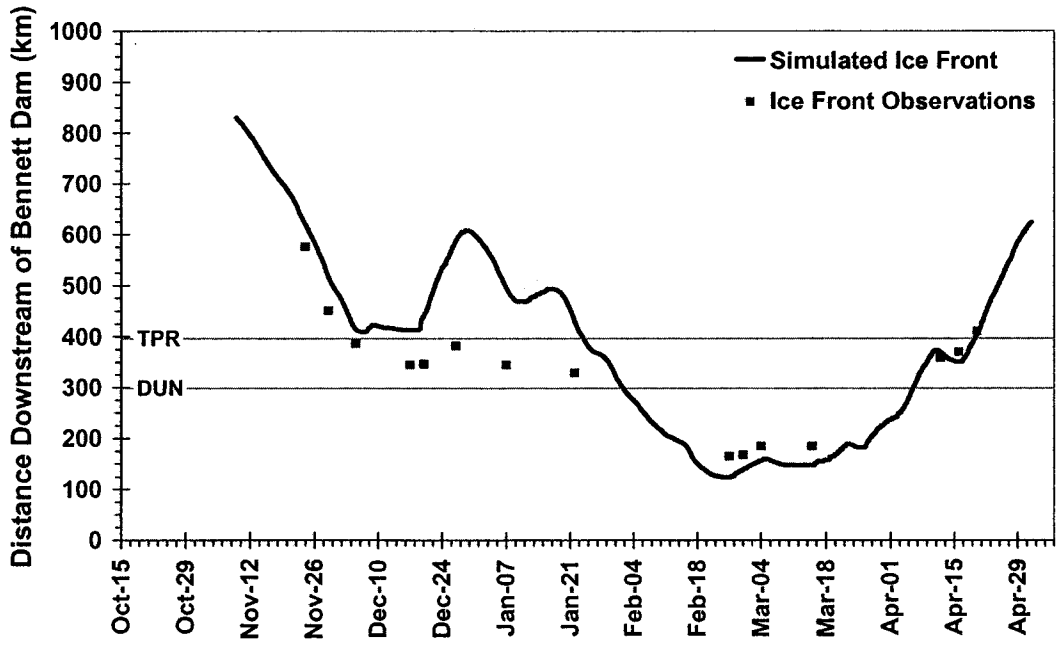

Figure A.19 Ice front profile validation using P_{jux} = 2.5 and 1985/86 ice season data.

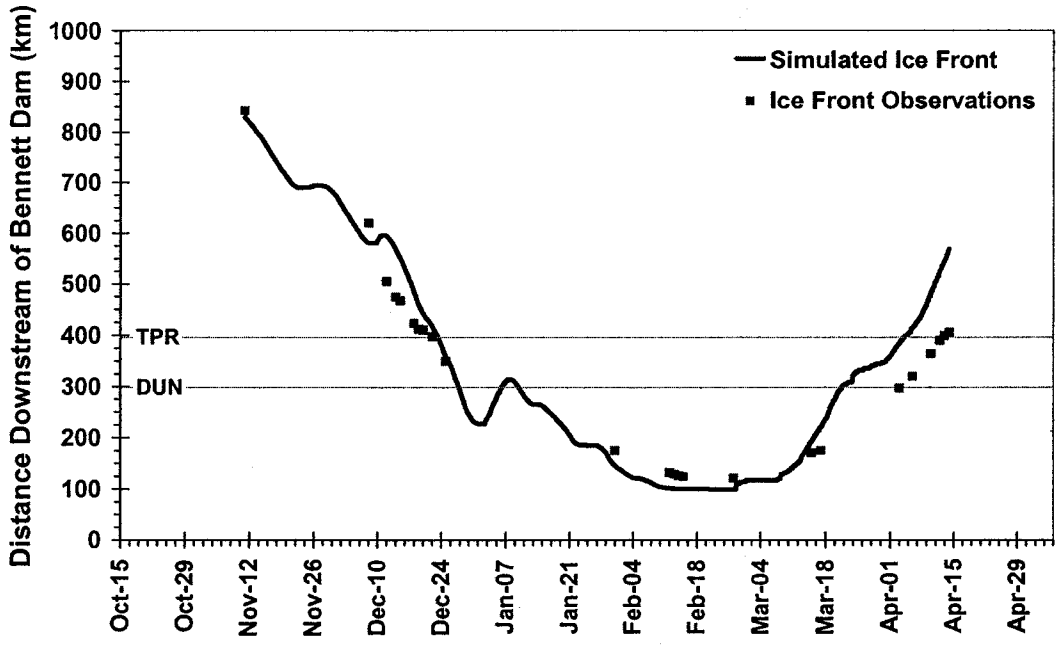

Figure A.20 Ice front profile validation using P_{jux} = 2.5 and 1984/85 ice season data.

– APPENDIX B –

Simulated Future Climate Ice Front Profiles without Adjusted Bridging Date Compared to Historical (1984/85 through 2003/04)

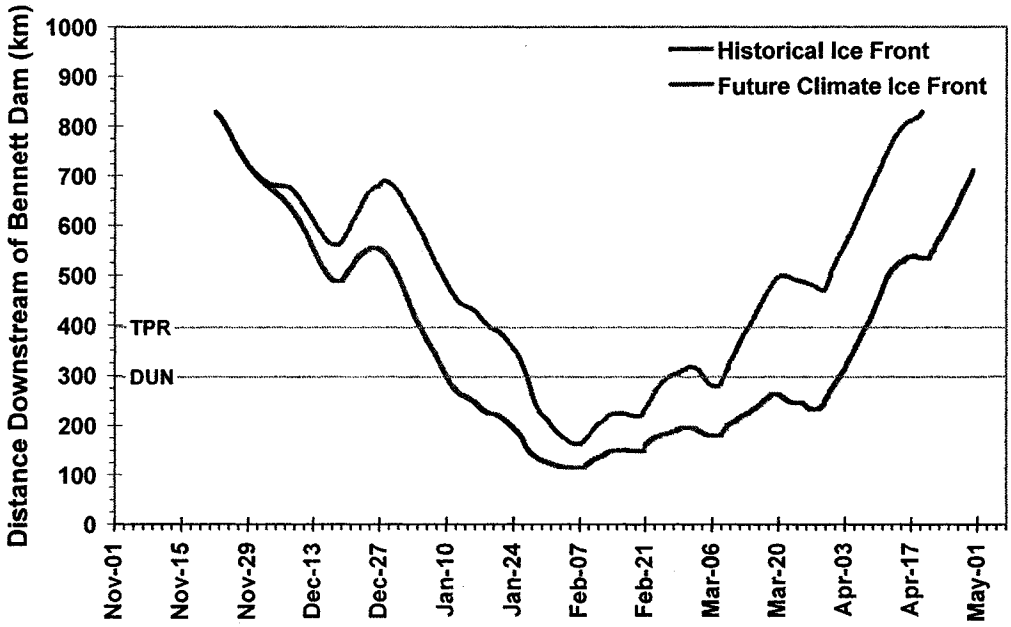

Figure B.1 **Simulated historical and future climate ice front profiles based on 2003/04 ice season data.**

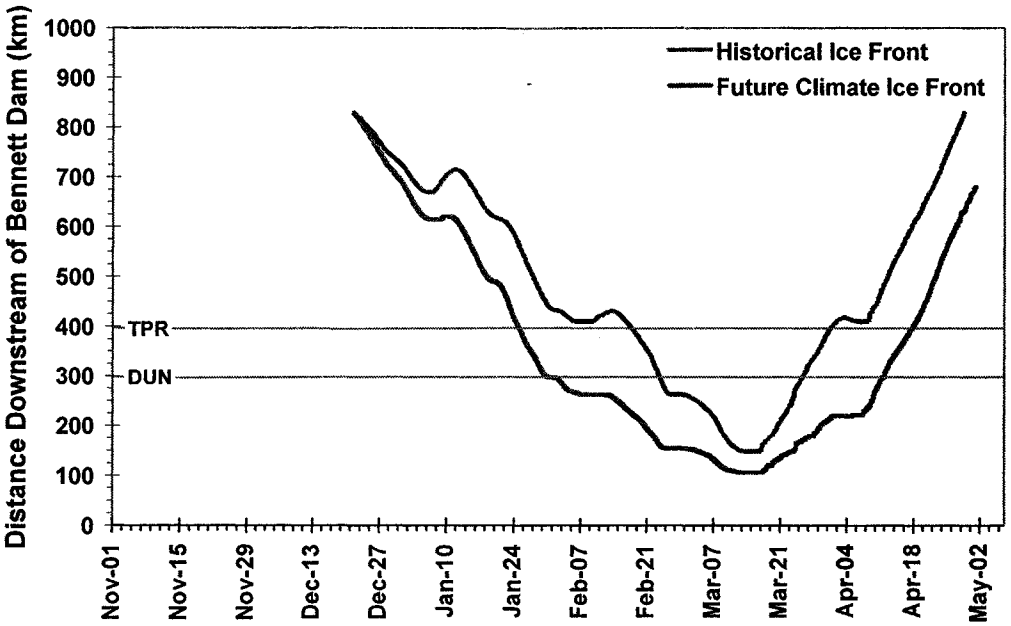

Figure B.2 **Simulated historical and future climate ice front profiles based on 2002/03 ice season data.**

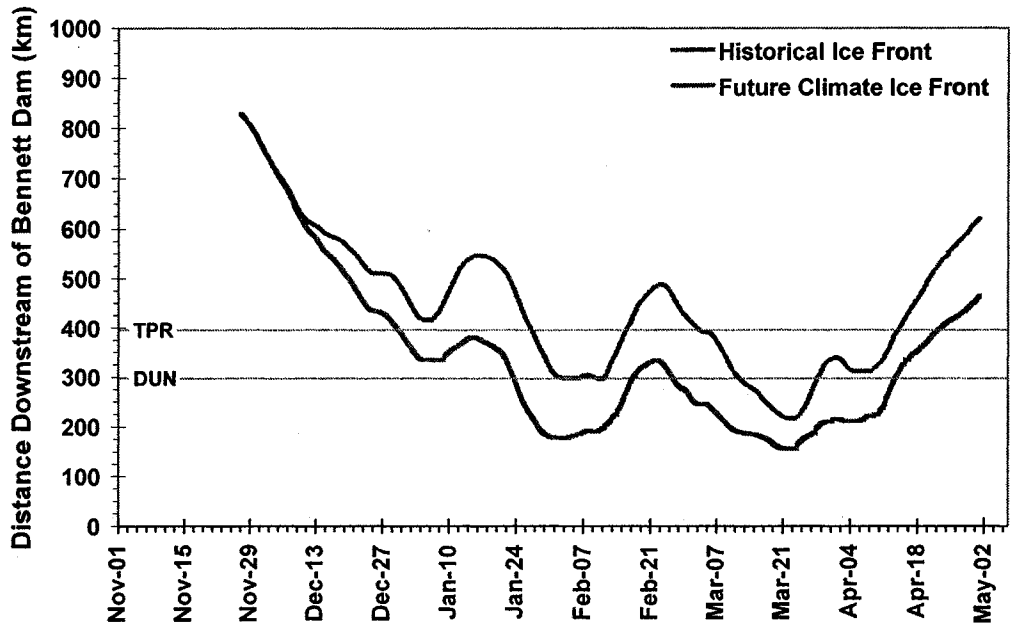

Figure B.3 **Simulated historical and future climate ice front profiles based on 2001/02 ice season data.**

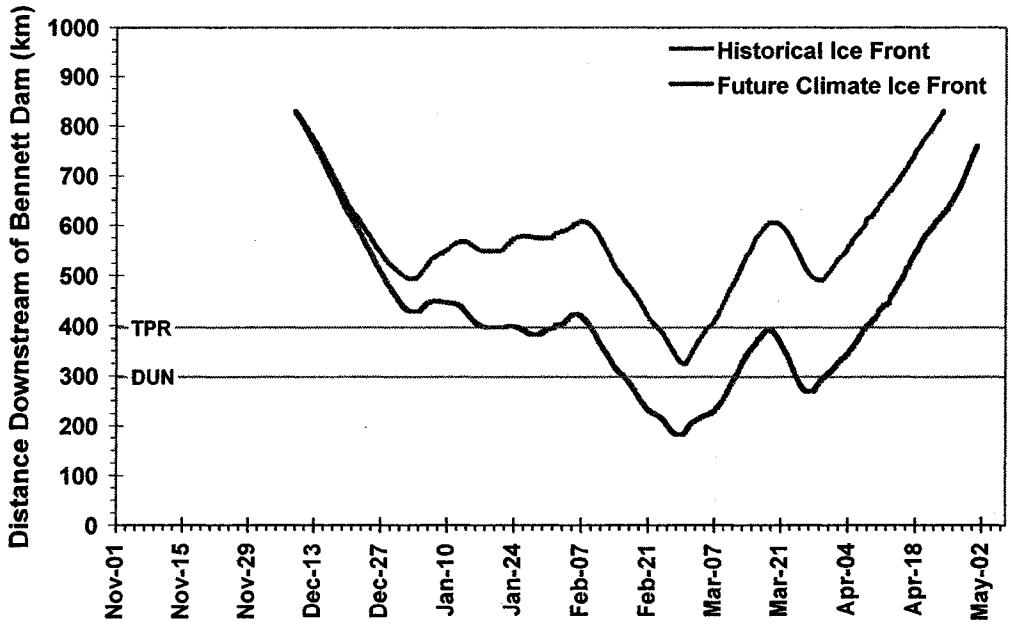

Figure B.4 **Simulated historical and future climate ice front profiles based on 2000/01 ice season data.**

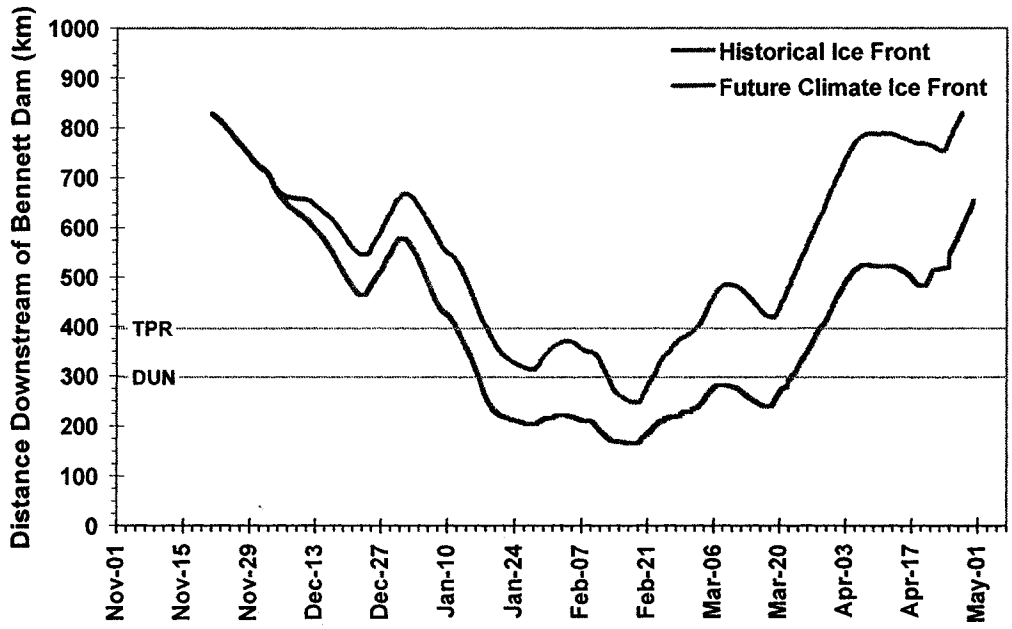

Figure B.5 **Simulated historical and future climate ice front profiles based on 1999/00 ice season data.**

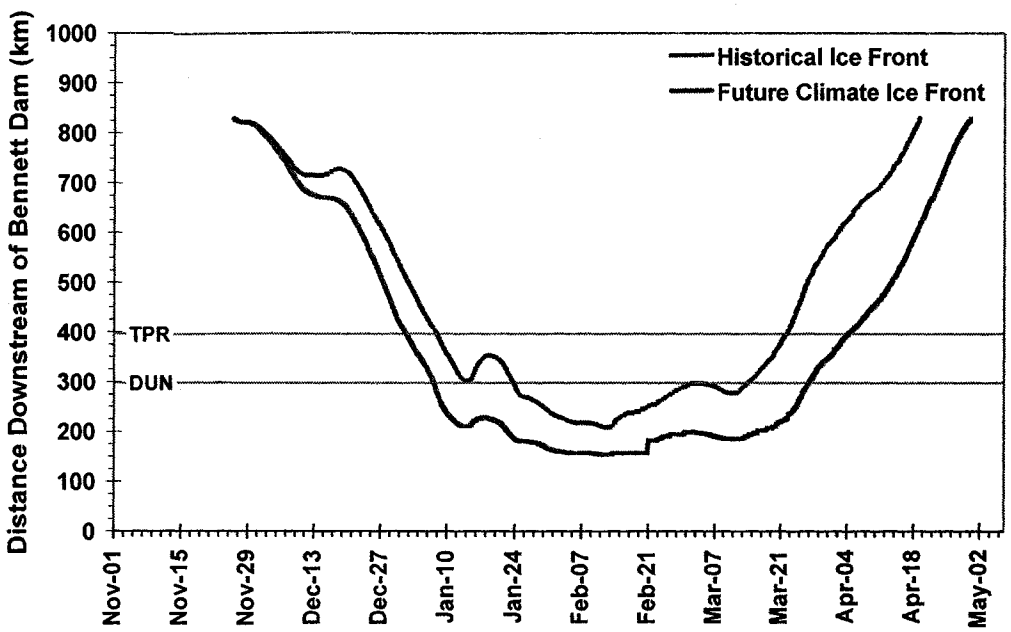

Figure B.6 **Simulated historical and future climate ice front profiles based on 1998/99 ice season data.**

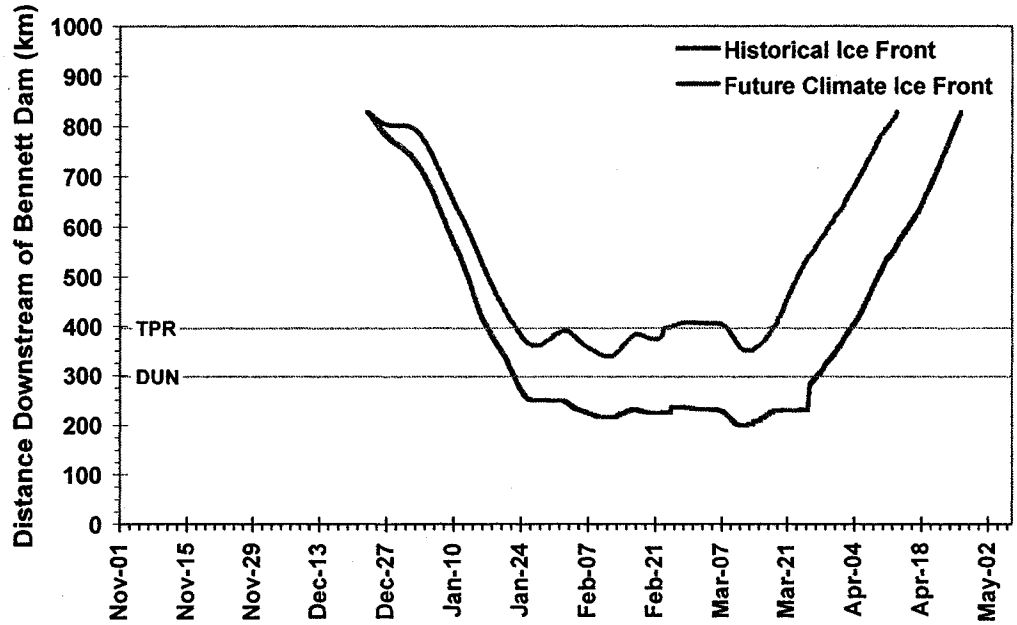

Figure B.7 **Simulated historical and future climate ice front profiles based on 1997/98 ice season data.**

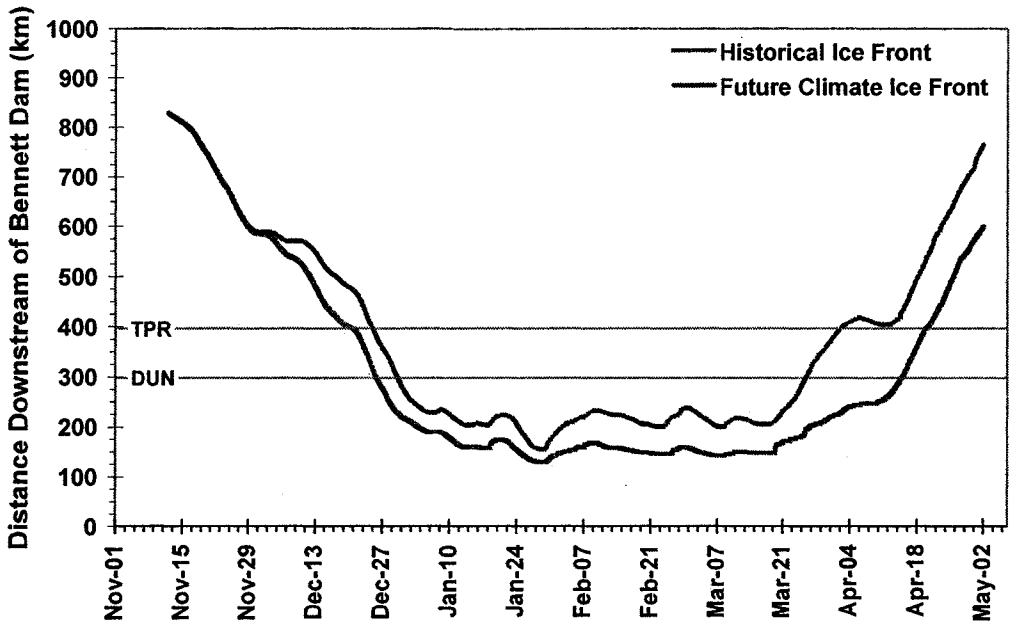

Figure B.8 **Simulated historical and future climate ice front profiles based on 1996/97 ice season data.**

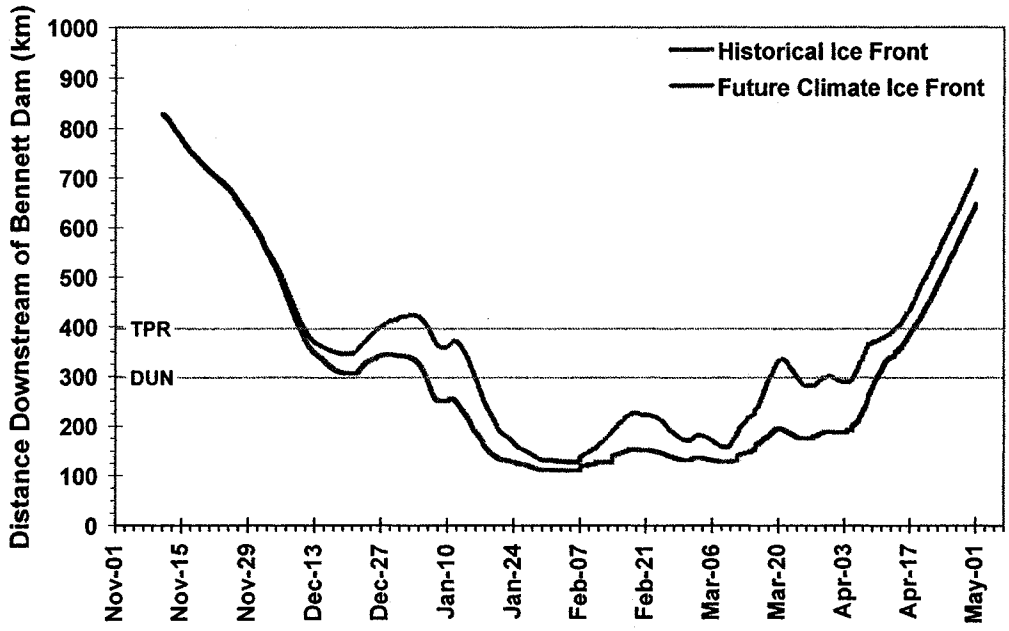

Figure B.9 **Simulated historical and future climate ice front profiles based on 1995/96 ice season data.**

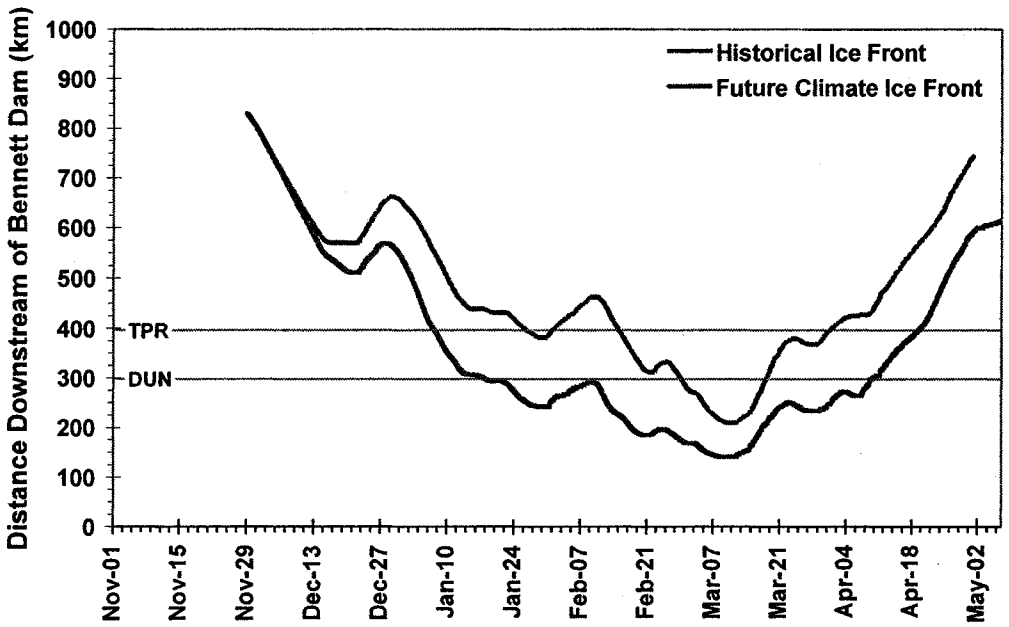

Figure B.10 **Simulated historical and future climate ice front profiles based on 1994/95 ice season data.**

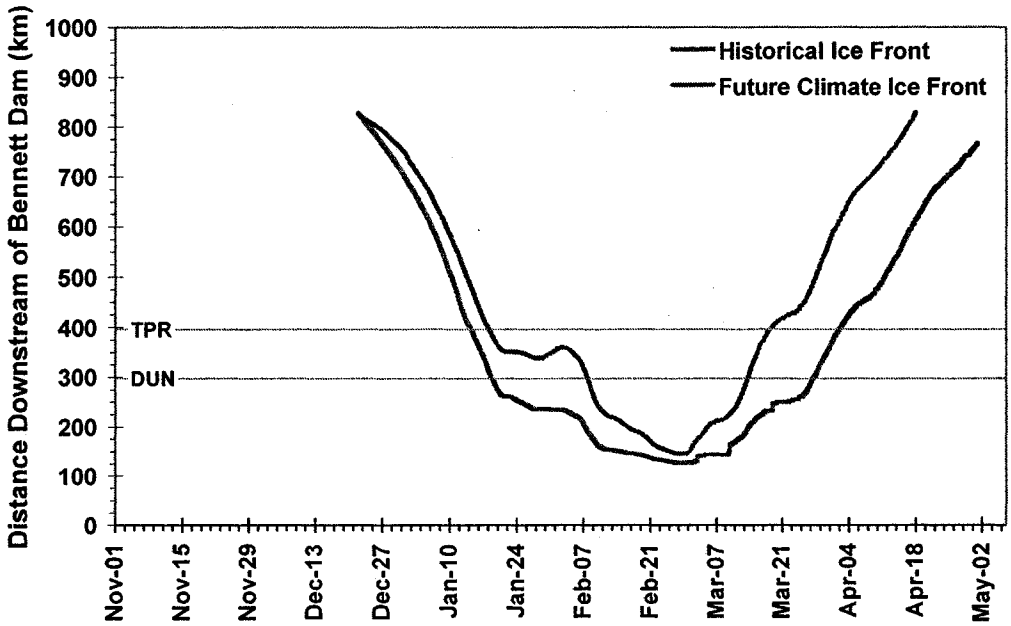

Figure B.11 **Simulated historical and future climate ice front profiles based on 1993/94 ice season data.**

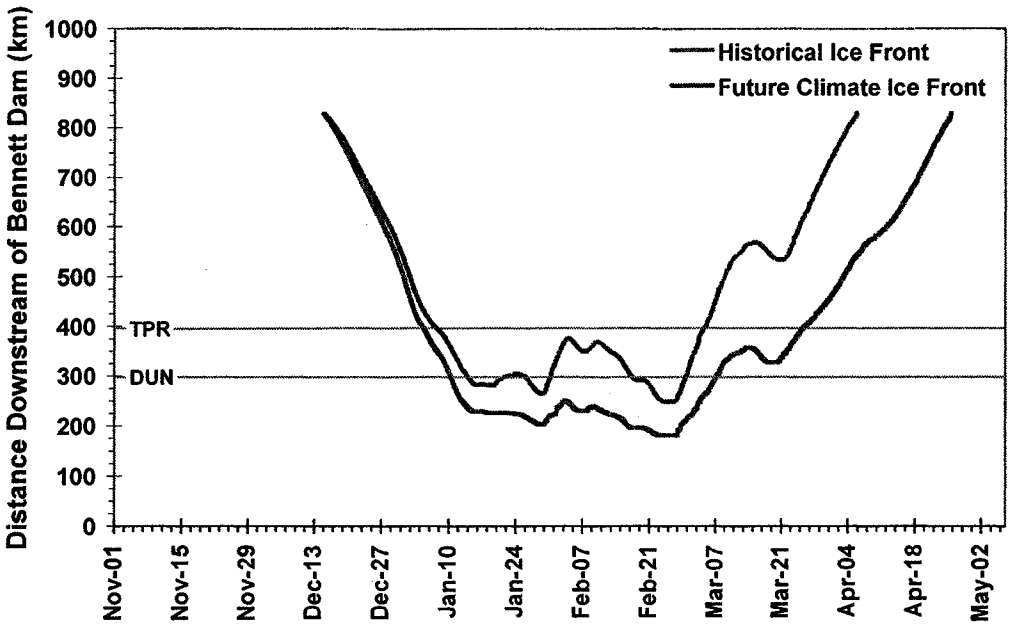

Figure B.12 **Simulated historical and future climate ice front profiles based on 1992/93 ice season data.**

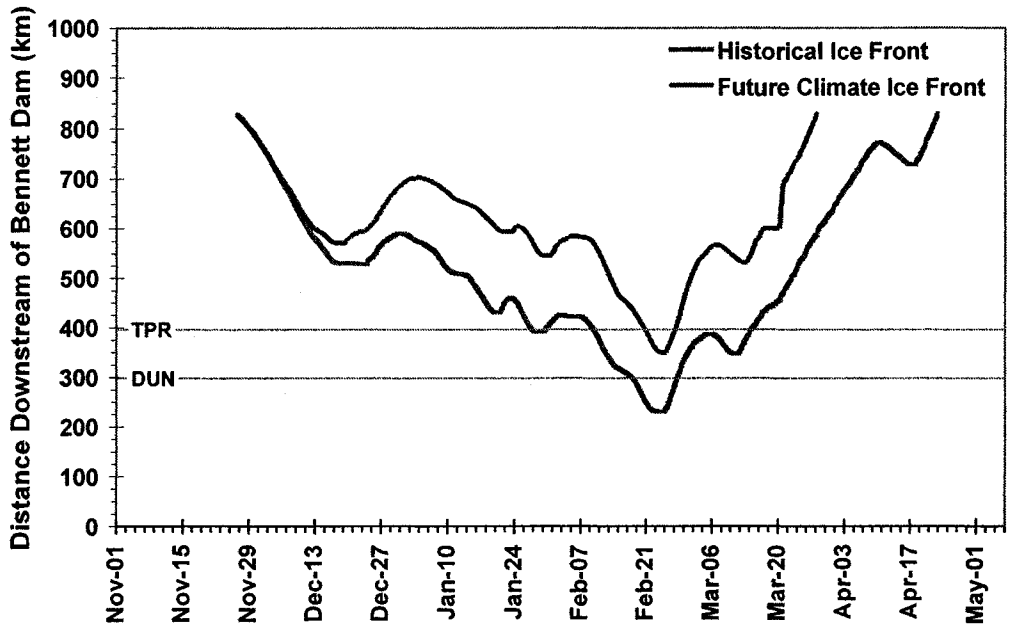

Figure B.13 Simulated historical and future climate ice front profiles based on 1991/92 ice season data.

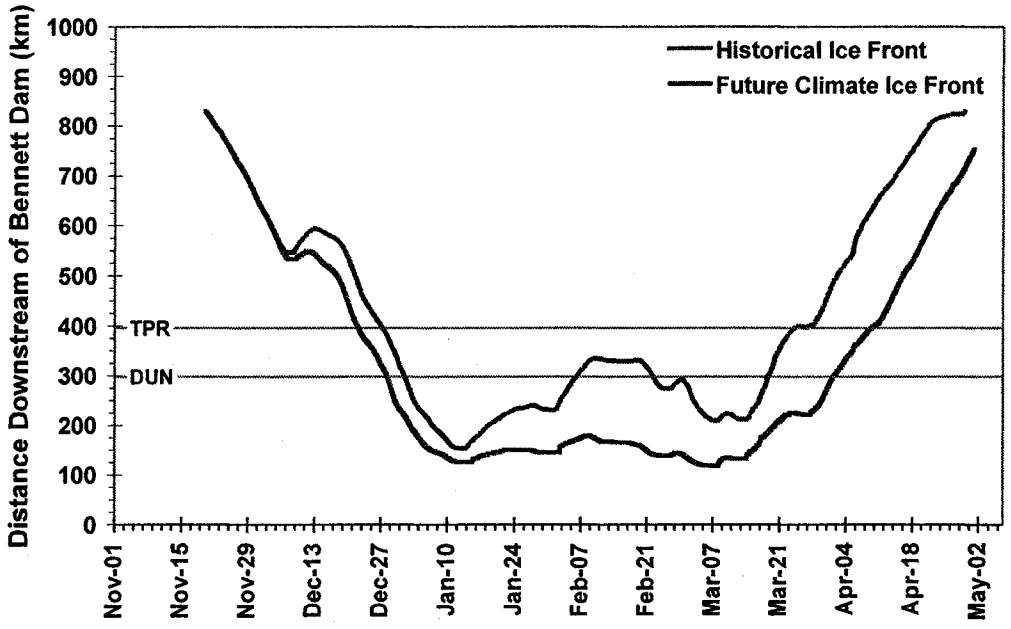

Figure B.14 Simulated historical and future climate ice front profiles based on 1990/91 ice season data.

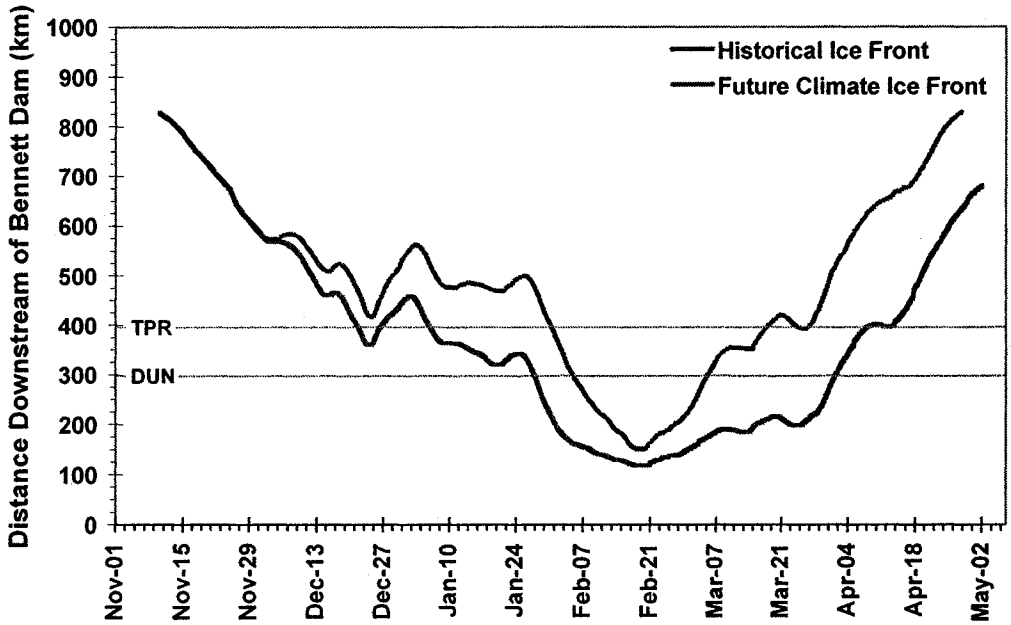

Figure B.15 **Simulated historical and future climate ice front profiles based on 1989/90 ice season data.**

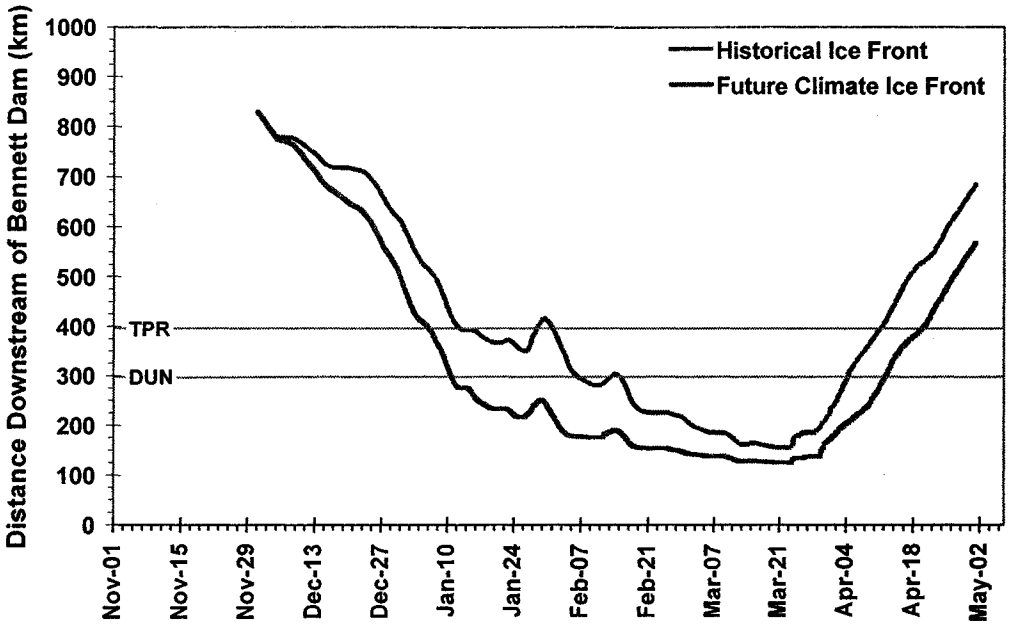

Figure B.16 **Simulated historical and future climate ice front profiles based on 1988/89 ice season data.**

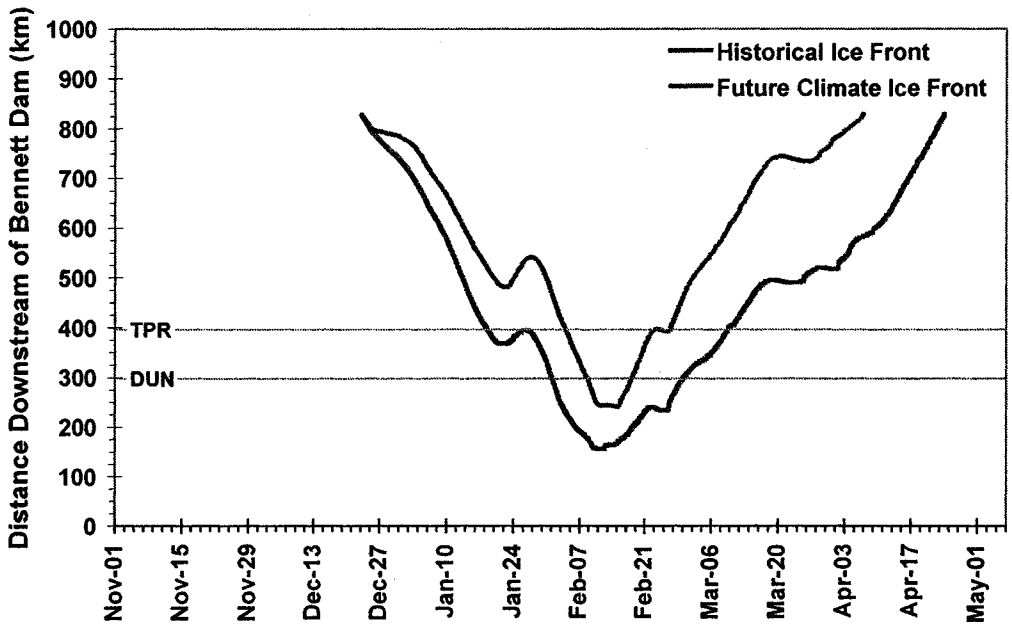

Figure B.17 **Simulated historical and future climate ice front profiles based on 1987/88 ice season data.**

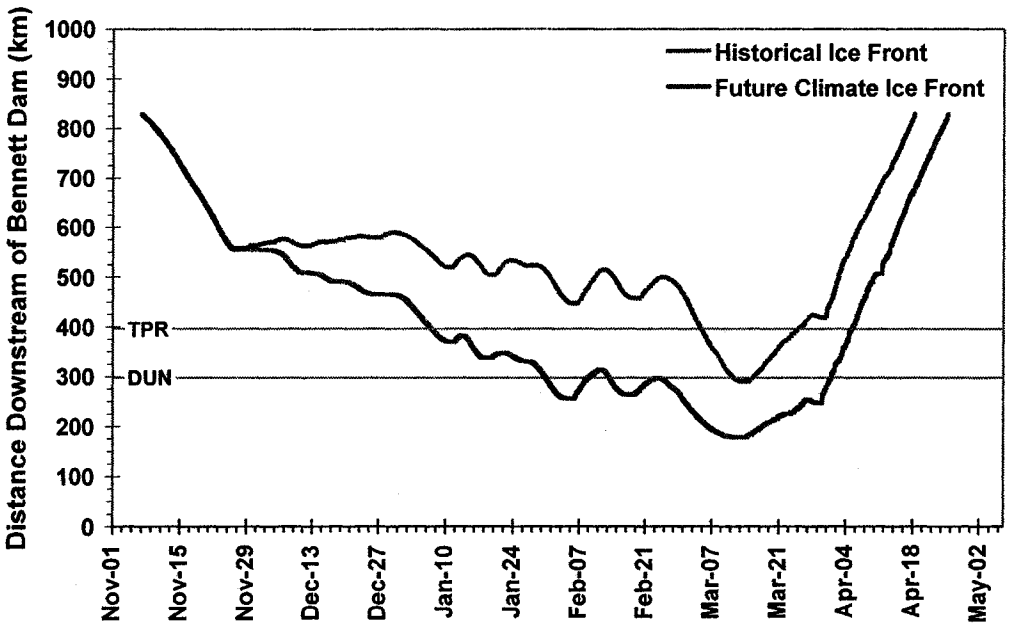

Figure B.18 **Simulated historical and future climate ice front profiles based on 1986/87 ice season data.**

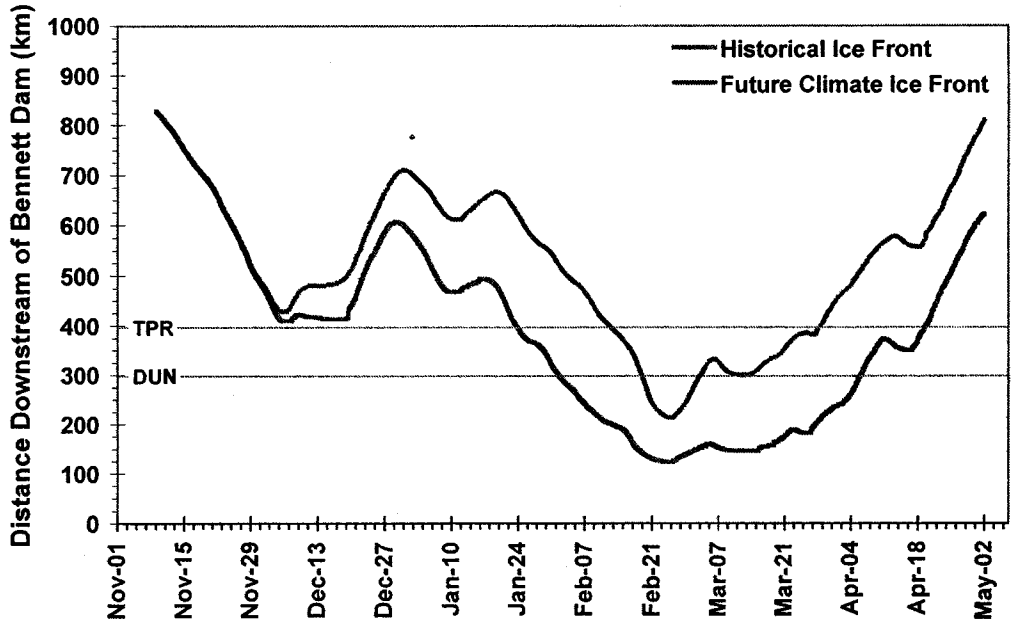

Figure B.19 Simulated historical and future climate ice front profiles based on 1985/86 ice season data.

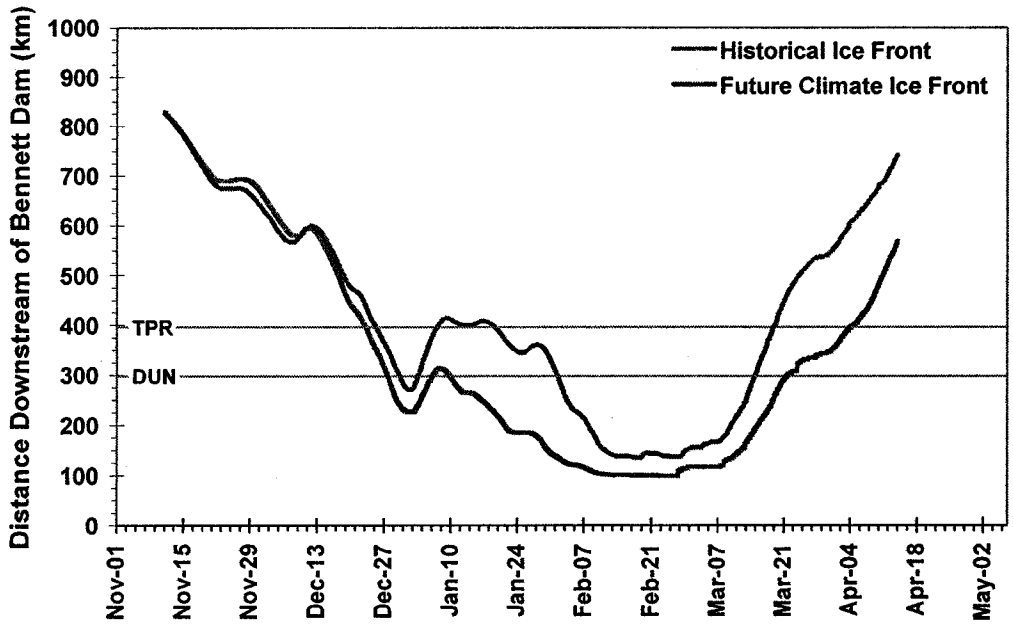

Figure B.20 Simulated historical and future climate ice front profiles based on 1984/85 ice season data.

– APPENDIX C –

A2 Climate Change Scenario Storyline

An excerpt from the Intergovernmental Panel on Climate Change (IPCC) Special Report on Emissions Scenarios (SRES) available online:

http://www.grida.no/climate/ipcc/emission/089.htm

A2 STORYLINE AND SCENARIO FAMILY

The A2 scenario family represents a differentiated world. Compared to the A1 storyline it is characterized by lower trade flows, relatively slow capital stock turnover, and slower technological change. The A2 world "consolidates" into a series of economic regions. Self-reliance in terms of resources and less emphasis on economic, social, and cultural interactions between regions are characteristic for this future. Economic growth is uneven and the income gap between now-industrialized and developing parts of the world does not narrow, unlike in the A1 and B1 scenario families.

The A2 world has less international cooperation than the A1 or B1 worlds. People, ideas, and capital are less mobile so that technology diffuses more slowly than in the other scenario families. International disparities in productivity, and hence income per capita, are largely maintained or increased in absolute terms. With the emphasis on family and community life, fertility rates decline relatively slowly, which makes the A2 population the largest among the storylines (15 billion by 2100). Global average per capita income in A2 is low relative to other storylines (especially A1 and B1), reaching about US$7200 per capita by 2050 and US$16,000 in 2100. By 2100 the global GDP reaches about US$250 trillion. Technological change in the A2 scenario world is also more heterogeneous than that in A1. It is more rapid than average in some regions and slower in others, as industry adjusts to local resource endowments, culture, and education levels. Regions with abundant energy and mineral resources evolve more resource-intensive economies, while those poor in resources place a very high priority on minimizing import dependence through

technological innovation to improve resource efficiency and make use of substitute inputs. The fuel mix in different regions is determined primarily by resource availability. High-income but resource-poor regions shift toward advanced post-fossil technologies (renewables or nuclear), while low-income resource-rich regions generally rely on older fossil technologies. Final energy intensities in A2 decline with a pace of 0.5 to 0.7% per year.

In the A2 world, social and political structures diversify; some regions move toward stronger welfare systems and reduced income inequality, while others move toward "leaner" government and more heterogeneous income distributions. With substantial food requirements, agricultural productivity in the A2 world is one of the main focus areas for innovation and research, development, and deployment (RD&D) efforts, and environmental concerns. Initial high levels of soil erosion and water pollution are eventually eased through the local development of more sustainable high-yield agriculture. Although attention is given to potential local and regional environmental damage, it is not uniform across regions. Global environmental concerns are relatively weak, although attempts are made to bring regional and local pollution under control and to maintain environmental amenities.

As in other SRES storylines, the intention in this storyline is not to imply that the underlying dynamics of A2 are either good or bad. The literature suggests that such a world could have many positive aspects from the current perspective, such as the increasing tendency toward cultural pluralism with mutual acceptance of diversity and fundamental differences. Various scenarios from the literature may be grouped under this scenario family. For example, "New Empires" by Schwartz (1991) is an

example of a society in which most nations protect their threatened cultural identities. Some regions might achieve relative stability while others suffer under civil disorders (Schwartz, 1996). In "European Renaissance" (de Jong and Zalm, 1991; CPB, 1992), economic growth slows down because of a strengthening of protectionist trade blocks. In "Imperial Harmonization" (Lawrence *et al.*, 1997), major economic blocs impose standards and regulations on smaller countries. The Shell scenario "Global Mercantilism" (1989, see Schwartz, 1991) explores the possibility of regional spheres of influence, whereas "Barricades" (Shell, 1993) reflects resistance to globalization and liberalization of markets. Noting the tensions that arise as societies adopt western technology without western culture, Huntington (1996) suggests that conflicts between civilizations rather than globalizing economies may determine the geo-political future of the world.

REFERENCES

CPB (Bureau for Economic Policy Analysis). (1992). "Scanning the Future: A Long-Term Study of the World Economy 1990-2015". Sdu Publishers, The Hague.

De Jong, A. and Zalm, G. (1991). "Scanning the Future: A Long-Term Scenario Study of the World Economy 1990-2015". In Long-term Prospects of the World Economy, OECD, Paris, 27-74.

Huntington, S.P. (1996). "The Clash of Civilizations and the Remaking of World Order". Simon and Schuster, New York, NY.

Lawrence, R.Z., Bressand, A. and Ito, T. (1997). "A Vision for the World Economy - Openness, Diversity, and Cohesion". The Brookings Institution, Washington, DC.

Schwartz, P. (1991). "The Art of the Longview: Three Global Scenarios to 2005". Doubleday Publications, New York, NY.

Schwartz, P. (1996). "The New World Disorder". WIRED Special Edition 1.10. (See also: Global Business Network. (http://www.gbn.org/scenarios).

Shell. (1993). "Global Scenarios 1992-2020". PL-93-S-04, Group Planning, Shell International, London.

– APPENDIX D –

Peace River Ice Modeling Database (CD-ROM)